NASA CONTRACTOR REPORT

NASA CR-2833

NASA CR-2833

FORCE AND PRESSURE TESTS OF THE GA(W)-1 AIRFOIL WITH A 20% AILERON AND PRESSURE TESTS WITH A 30% FOWLER FLAP

W. H. Wentz, Jr., H. C. Seetharam, and K. A. Fiscko

Prepared by
WICHITA STATE UNIVERSITY
Wichita, Kans. 67208
for Langley Research Center

NATIONAL AERONAUTICS AND SPACE ADMINISTRATION • WASHINGTON, D. C. • JUNE 1977

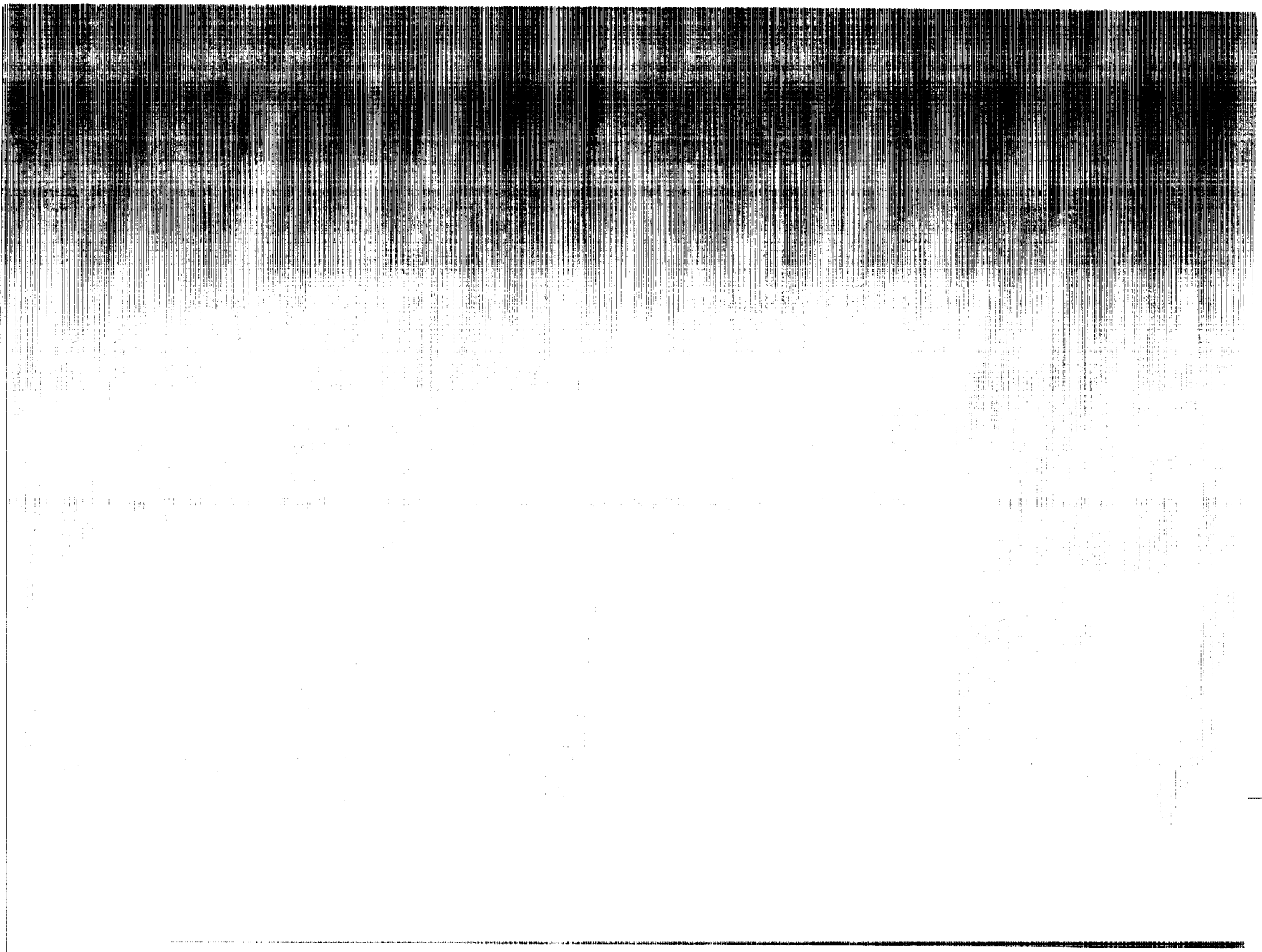

1. Report No.	2. Government Accession No.	3. Recipient's Catalog No.
NASA CR-2833		

4. Title and Subtitle	5. Report Date
FORCE AND PRESSURE TESTS OF THE GA(W)-1 AIRFOIL WITH A 20% AILERON AND PRESSURE TESTS WITH A 30% FOWLER FLAP	June 1977
	6. Performing Organization Code

7. Author(s)	8. Performing Organization Report No.
W. H. Wentz, Jr , H. C. Seetharam, and K. A. Fiscko	WSU AR 76-1
	10. Work Unit No. 505-06-33-10
9. Performing Organization Name and Address Wichita State University Wichita, KS 67208	11. Contract or Grant No. NSG-1165
	13. Type of Report and Period Covered Contractor Report
12. Sponsoring Agency Name and Address National Aeronautics & Space Administration Washington, DC 20546	14. Sponsoring Agency Code

15. Supplementary Notes
Topical report
Langley technical monitor: Robert J. McGhee

16. Abstract

Wind-tunnel force and pressure tests have been conducted for the GA(W)-1 airfoil equipped with a 20% aileron, and pressure tests have been conducted with a 30% Fowler flap. All tests were conducted at a Reynolds number of 2.2×10^6 and a Mach number of 0.13. The aileron provides control effectiveness similar to ailerons applied to more conventional airfoils. Effects of aileron gaps from 0% to 2% chord were evaluated, as well as hinge moment characteristics. The aft camber of the GA(W)-1 section results in a substantial up-aileron moment, but the hinge moments associated with aileron deflection are similar to other configurations.

Fowler flap pressure distributions indicate that unseparated flow is achieved for flap settings up to 40°, over a limited angle-of-attack range. Theoretical pressure distributions compare favorable with experiment for low flap deflections, but show substantial errors at large deflections.

17. Key Words (Suggested by Author(s))	18. Distribution Statement
Airfoil Flap Aileron Pressure distributions	Unclassified - Unlimited Subject Category 02

19. Security Classif. (of this report)	20. Security Classif. (of this page)	21. No. of Pages	22. Price*
Unclassified	Unclassified	94	$5.00

*For sale by the National Technical Information Service, Springfield, Virginia 22161

SUMMARY

Wind tunnel force and pressure tests have been conducted for the GA(W)-1 airfoil equipped with a 20% aileron, and pressure tests have been conducted with a 30% Fowler flap. All tests were conducted at a Reynolds number of 2.2×10^6 and a Mach number of 0.13. The aileron provides control effectiveness similar to ailerons applied to more conventional airfoils. Effects of aileron gaps from 0% to 2% chord were evaluated, as well as hinge moment characteristics. The aft camber of the GA(W)-1 section results in a substantial up-aileron moment, but the hinge moments associated with aileron deflection are similar to other configurations.

Fowler flap pressure distributions indicate that unseparated flow is achieved for flap settings up to 40°, over a limited angle of attack range Theoretical pressure distributions compare favorably with experiment for low flap deflections, but show substantial errors at large deflections.

INTRODUCTION

The high performance possible with the new GA(W)-1 airfoil and airfoil-flap combinations has been reported earlier (Refs. 1,2,3). The present report documents force and pressure tests of the airfoil fitted with a 20% aileron, and pressure studies of the airfoil with a 30% Fowler flap.

All experimental tests reported herein were conducted in the Walter Beech Memorial Wind Tunnel at Wichita State University.

SYMBOLS

The force and moment data have been referred to the .25c location on the flap-nested airfoil. Dimensional quantities are given in both International (SI) Units and U.S. Customary Units. Measurements were made in U.S. Customary Units. Conversion factors between the various units may be found in reference 4. The symbols used in the present report are defined as follows:

c	Airfoil reference chord (flap-nested)
c_d	Airfoil section drag coefficient, section drag/(dynamic pressure x chord)
c_f	Flap chord
c_h	Control surface hinge moment coefficient, section moment/(dynamic pressure x control surface reference chord^2)
c_ℓ	Airfoil section lift coefficient, section lift/(dynamic pressure x chord)
c_m	Airfoil section pitching moment coefficient with respect to the .25c location, section moment/(dynamic pressure x chord^2)
c_n	Airfoil or flap normal force coefficient, section normal force/(dynamic pressure x chord)
c_p	Coefficient of pressure, $(p-p_\infty)$/dynamic pressure
ℓ_c	Cove length
p	Static pressure
x	Coordinate parallel to airfoil chord
z	Coordinate normal to airfoil chord
α	Angle of attack, degrees
Δ	Increment
δ	Rotation of surface from nested position, degrees

Subscripts:

a Aileron

f Flap

p Pivot

∞ Remote free-stream value

APPARATUS AND TEST METHODS

Model Description

The GA(W)-1 airfoil is a 17% maximum thickness section developed at the NASA Langley Research Center (Ref. 1). For tests in the WSU two-dimensional facility, models are sized with a 91.4 cm (36 inch) span and 61.0 cm (24 inch) chord. The forward section of the model was fabricated from laminated mahogany bonded to a 2.5 cm x 34.8 cm (1 inch x 13.7 inch) aluminum spar. Wing trailing sections to match each flap and aileron were fabricated from solid aluminum as were the flaps and ailerons. Airfoil and flap or aileron are mounted on 107 cm (42 inch) diameter end plates. A set of external brackets permit positioning of flap or aileron without disturbing the flow over the model. Models are fitted with flush tubes for static pressure surveys. Geometric contour details are given in figure 1.

As shown, the 20% aileron model has inserts to permit tests with leading edge gaps of 2%, 1%, and 0.5% chord. Tests were made with zero gap by sealing the slot with cloth-backed adhesive tape applied to the airfoil lower surface.

The Fowler flap has 30% chord with full Fowler action possible as shown in figure 1(b). The force characteristics and optimization of this airfoil-flap combination have been reported in reference 2. Performance with spoilers has been reported in references 3 and 5. The purpose of the present research is to provide surface pressure distribution and flap loads information for optimum flap settings.

All tests were conducted with transition fixed by 2.5 mm (0.10 inch) wide strips of #80 carborundum grit located at 5% chord on upper and lower surfaces.

Instrumentation

Pressure studies are conducted by multiplexing as many as 96 pressure ports through four pressure transducers by means of a set

of pressure scanning switches. The tunnel is equipped with a semi-automated data system which converts analog force and pressure output signals to digital form, and records the data on punch cards. Computational analysis and computer graphics are done through the University Digital Computing Center.

Test Procedure

All tests were conducted at a Reynolds number of 2.2×10^6 and Mach number of 0.13. Lift, drag and pitching moment data are obtained by direct load cell measurements from the tunnel main balance. Drag data are corrected for end plate tare drag based upon wake survey drag measurements conducted with the unflapped airfoil.

Wind Tunnel

The WSU Walter Beech Tunnel is a closed return tunnel with atmospheric test section static pressure. The test section with two-dimensional inserts is 0.91 m x 2.13 m (3 feet x 7 feet). Complete description of the insert and calibration details are given in reference 6.

TEST RESULTS

Force Tests with 20% Aileron

Results of three-component force measurements are shown in figures 2 through 4 for 0%, 0.5%, 1% and 2% aileron gaps. Crossplots of important incremental effects of aileron deflection are shown in figures 5 through 7.

These data show that the aileron provides positive control response for deflections from -60° to +60° throughout the angle of attack range prior to stall.

From the c_ℓ vs. alpha curves, it is observed that down aileron results in early stalling, and conversely for up aileron. This means that control reversal occurs at post-stall angles of attack. While this is not a desirable characteristic, it is typical aileron behavior, and is not peculiar to the GA(W)-1 airfoil.

Pitching moment data reflect a nose-down tendency for downward aileron deflections. Drag data reflect a tendency toward greater

drag increase for down aileron than for up aileron. This drag difference will produce adverse yawing moments on a finite span wing. It must be remembered, however, that the principal contribution to aileron adverse yaw is induced drag.

Effects of aileron slot gap opening are illustrated by comparing the various figures. Figures 5(a) through 5(d) show that opening the gap from 0% to 2.0% results in only very slight degradation of control authority. Close examination of figures 3(a) through 3(d) shows that the most significant effect of gap opening is to increase the basic section drag with zero aileron deflection. This effect becomes more pronounced as lift coefficient is increased. Gaps of 0.5% and 1% actually increase $c_{\ell max}$ slightly, evidently as a result of the boundary layer energization provided. A gap of 0.5% would seem to be a good compromise, providing adequate clearance with minimal penalty.

Pressure Tests with 20% Aileron

Pressure surveys were conducted for -10° to +10° aileron with zero gap to determine whether gap sealing had any significant influence (figure 8). Because of the extensive time required to obtain pressure data, complete pressure surveys were conducted only for the 0.5% gap configuration (figure 9). Comparison of figures 8 and 9 shows that the gap has little effect on overall pressure distributions.

Aileron hinge moment data with respect to the 80% chord hingeline location were obtained by numerical integration of the surface pressure data. Results of this analysis are shown in figure 10. The data show that the hinge moment variation is nearly linear with aileron deflection. The 0.5% gap has negligible effect on hinge moment. The aileron is subjected to large up-aileron moments with zero deflection at high angles of attack. This is attributed to the relatively large camber near the trailing edge which characterizes the GA(W)-1 airfoil section.

Pressure Tests with 30% Fowler Flap

Optimum settings for the 30% Fowler flap were determined from force tests reported earlier (Ref. 2). Subsequent to those tests,

a slightly modified 40° flap setting was developed to simplify flap track design. The c_ℓ vs. α performance with original and modified flap settings is essentially the same, as shown in figure 11. The pressure data presented here were obtained with the modified setting for 40° flap, and original settings for all other flap deflections. Experimental pressure distributions are presented in figure 12.

The flap cove on this model has a fairly abrupt entry. Theoretical analysis of the airfoil-flap combination (using the method of reference 7) with the true cove shape invariably results in a computer prediction of flow separation at the cove entry. It was experimentally observed that the flow does separate in the region, but reattachment occurs ahead of the slot exit. Since the present theoretical techniques do not account for flow reattachment, it was decided that the effective airfoil contour should be modified in the cove region to approximate the separation and reattachment. Figure 13 compares results of analyses using three cove contours with an experimental pressure distribution for 30° flap at 10.3° angle of attack.

Based upon these results, a decision was made to approximate the effective shape of the free streamline within the cove by a straight line from the cove entrance to the 75% assumed reattachment location. It is seen that this modification results in considerable improvement in the prediction of pressures near the airfoil trailing edge. Two additional difficulties arise in utilizing the theoretical computing routine. First, the computational program may indicate flow separation. If separation is present at 0.95c or further aft, little change in pressure distribution is expected, and the program results are probably valid. However, if a substantial region of separation is present, large changes in pressures are expected. Calculation of separated flow cases is beyond the capability of the present computer program, and therefore computer-predicted pressure distributions are probably invalid for these cases.

The second computational difficulty involves analysis of the confluence of the flap and airfoil boundary layers. In a number

of cases the program prints a "confluent boundary layer error" message, indicating that slot flow velocity and outer flow velocity are not within limits specified in the program. No means for obtaining proper convergence for these cases are presently provided by the program.

Figures 14 through 17 compare theoretical pressure distributions with experimental distributions for a number of cases. Normal force coefficients for airfoil and flap obtained from integration of surface pressures are also compared with theory in these figures. The agreement is generally quite good for flap deflections up to 30° and angles of attack below stall. For 40° flap, the theory consistently over-predicts the flap upper surface pressures, indicating that the flap boundary layer is thicker than the theoretical prediction.

Unfortunately predictions of separation are inconsistent, and frequent confluent boundary layer errors were encountered.

CONCLUSIONS

1. Force and pressure tests have shown that aileron characteristics for the GA(W)-1 airfoil are not unlike airfoils with more conventional camber and thickness distributions. The airfoil provides excellent aileron control effectiveness.

2. Hinge moment characteristics of an aileron applied to the GA(W)-1 airfoil are reasonably linear and of expected magnitudes. The airfoil aft camber inherent to this section does result in rather large up-aileron moments, particularly at large angles of attack.

3. Pressure distributions for a 30% Fowler flap applied to the GA(W)-1 airfoil indicate that with proper gap and overlap, attached flow can be provided for flap deflections up to 40°, at least for a limited angle of attack range. Present viscous flow computational modeling is inadequate for many practical flap cove designs in which flow separation and reattachment occur.

Aeronautical Engineering Department
Wichita State University
Wichita, Kansas 67208
August 1976

REFERENCES

1. McGhee, R.J. and Beasley, W.D.: Low-Speed Aerodynamic Characteristics of a 17-Percent Thick Airfoil Section Designed for General Aviation Applications. NASA TN D-7428, 1973.

2. Wentz, W.H. and Seetharam, H.C.: Development of a Fowler Flap System for a High Performance General Aviation Airfoil. NASA CR-2443, 1974.

3. Wentz, W.H.: Effectiveness of Spoilers on the GA(W)-1 Airfoil with a High-Performance Fowler Flap. NASA CR-2538, 1975.

4. Mechtly, E.A.: The International System of Units - Physical Constants and Conversion Factors (Revised) NASA SP-7012, 1969.

5. Wentz, W.H. and Volk, C.G.: Reflection-Plane Tests of Spoilers on an Advanced Technology Wing with a Large Fowler Flap. NASA CR-2696, 1976.

6. Siew, R.: Calibration of a Two-Dimensional Insert for the WSU 7' x 10' Wind Tunnel. WSU AR 73-2, 1973.

7. Stevens, W.A., Goradia, S.H. and Braden, J.A.: Mathematical Model for Two-Dimensional Multi-Component Airfoils in Viscous Flow. NASA CR-1843, 1971.

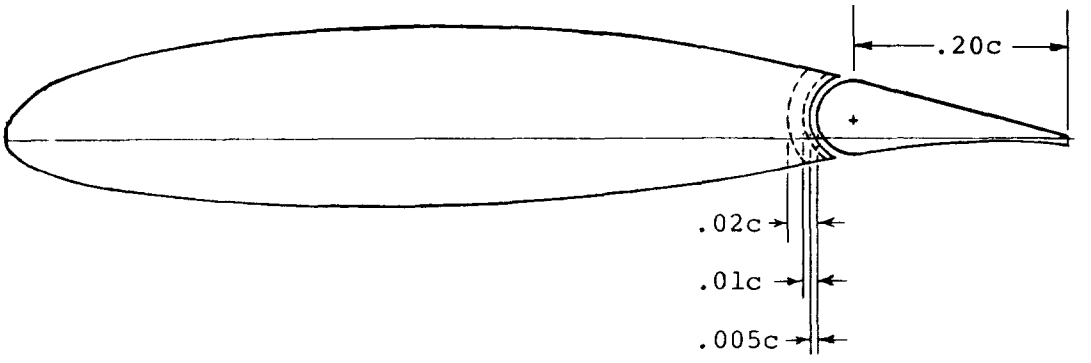

20%c Aileron Coordinates

Upper Surface		Lower Surface	
x_a/c	z_a/c	x_a/c	z_a/c
.000	.01960	.000	.01960
.005	.03750	.005	.00375
.017	.05000	.017	-.01040
.035	.05286	.035	-.01600
.060	.04646	.060	-.01200
.085	.03988	.085	-.00860
.110	.03315	.110	-.00580
.135	.02639	.135	-.00360
.160	.01961	.160	-.00250
.185	.01287	.185	-.00260
.210	.00609	.210	-.00400
.235	-.00070	.235	-.00800

L.E. Radius = 0.03443c

(a) 20% Aileron.

Figure 1 - Model Geometry.

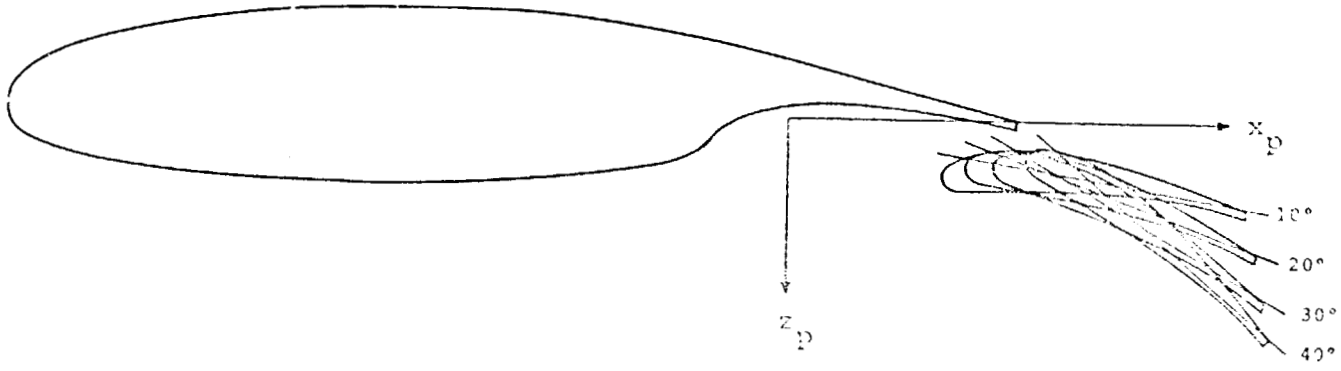

30% Fowler Flap Coordinates

Upper Surface		Lower Surface	
x_f/c	z_f/c	x_f/c	z_f/c
.000	-.01920	.000	-.01920
.025	.00250	.025	-.02940
.050	.01100	.050	-.02490
.075	.01630	.075	-.02040
.100	.01900	.100	-.01600
.125	.01950	.125	-.01200
.150	.01820	.150	-.00860
.175	.01670	.175	-.00580
.200	.01330	.200	-.00360
.225	.00950	.225	-.00250
.250	.00530	.250	-.00260
.275	.00100	.275	-.00400
.300	-.00435	.300	-.00800

L.E. Radius = 0.0122c

Flap Pivot Point Locations

δ_f	x_p/c	z_p/c	gap/c	overlap/c
0°	0.0	0.0	0.0	0.300
10°	.232	.046	.025	.071
20°	.256	.050	.025	.047
30°	.280	.058	.025	.022
40°	.306	.062	.030	.000

Note: Pivot point is at $0.25c_f$ on the wing chord line.

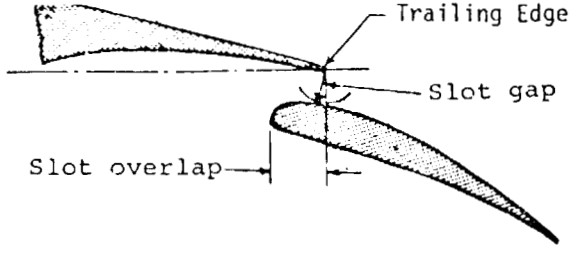

Definitions of gap and overlap.

(b) 30% Fowler Flap.

Figure 1 - Concluded.

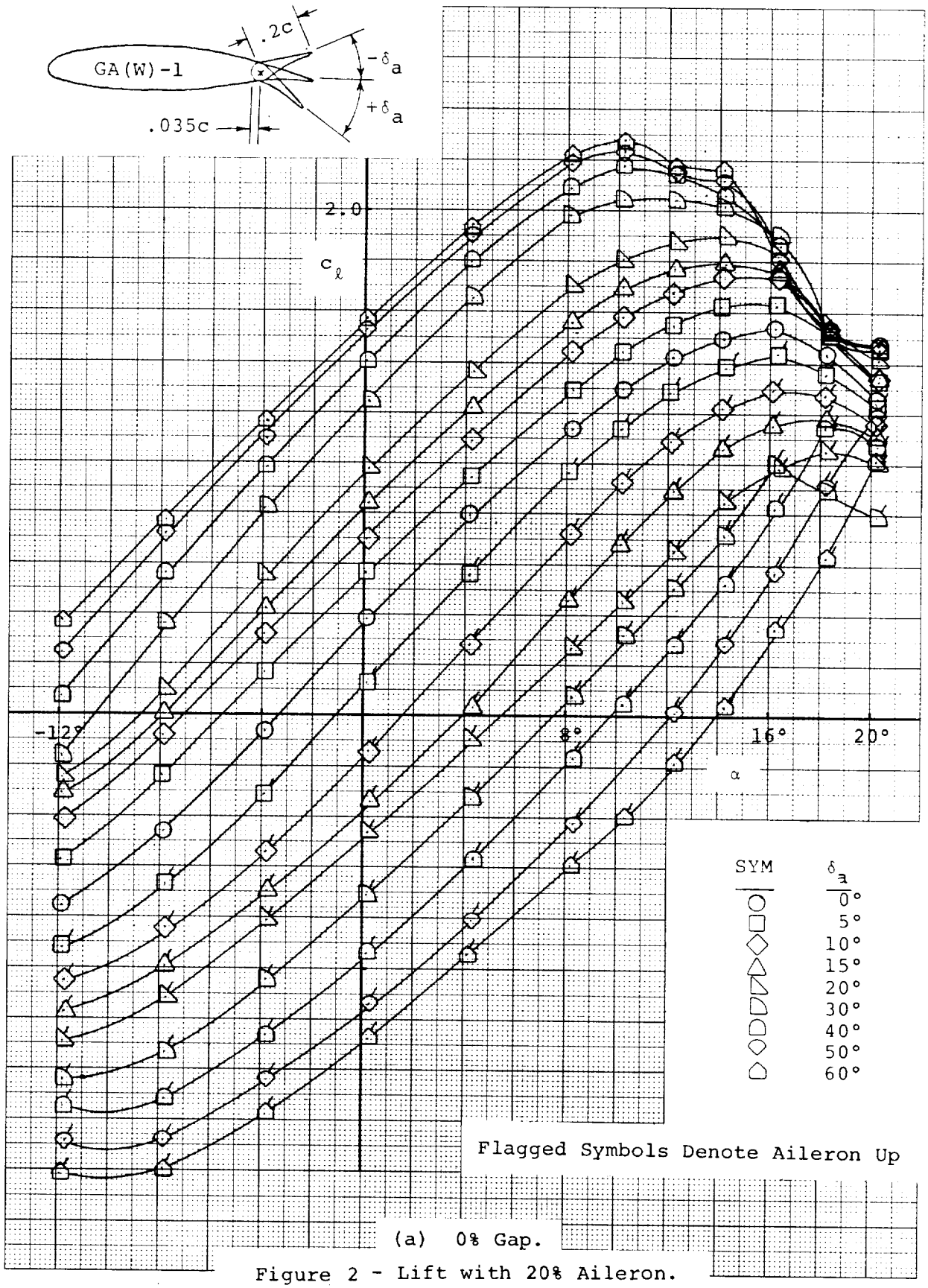

(a) 0% Gap.

Figure 2 - Lift with 20% Aileron.

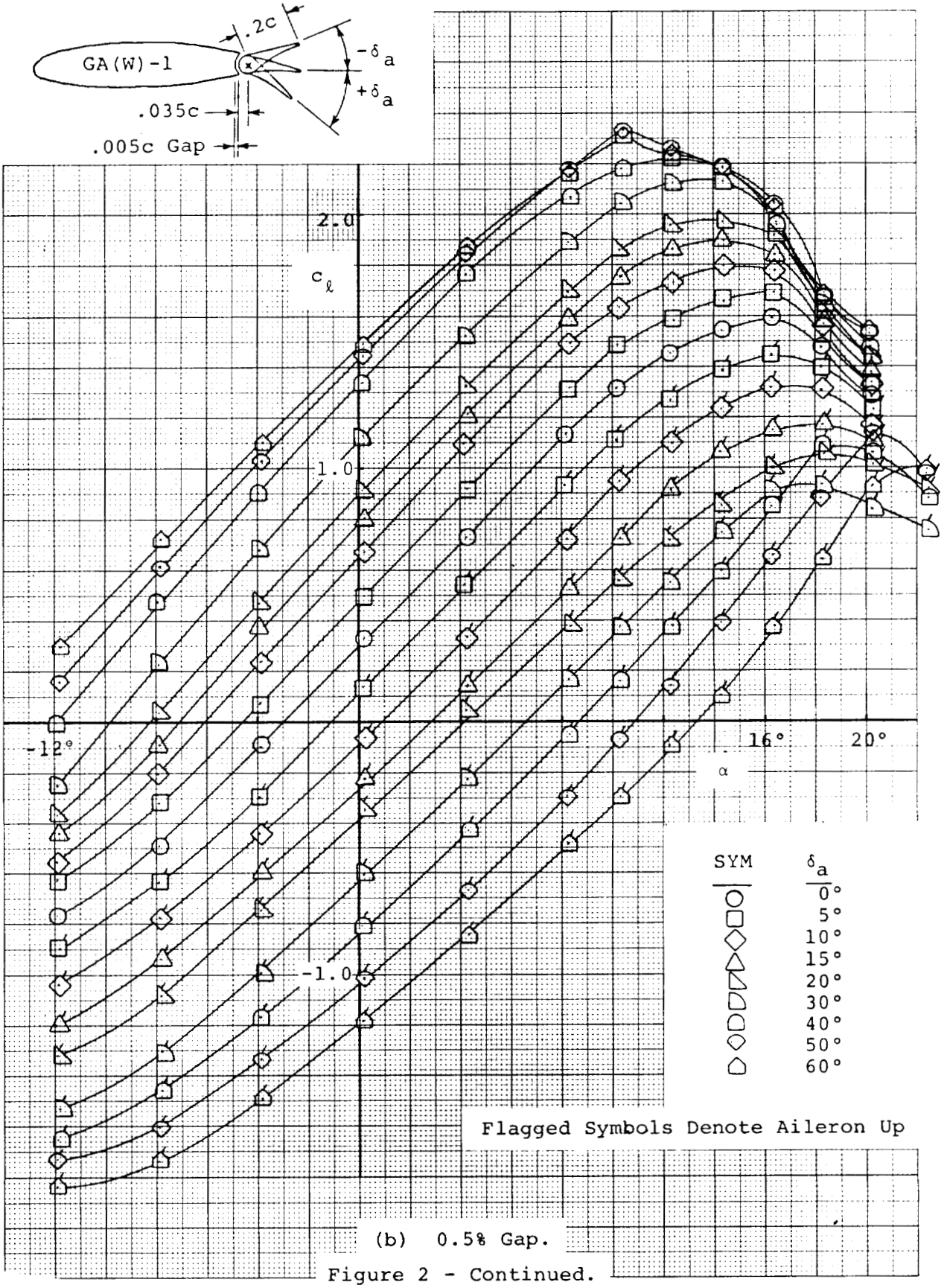

(b) 0.5% Gap.

Figure 2 - Continued.

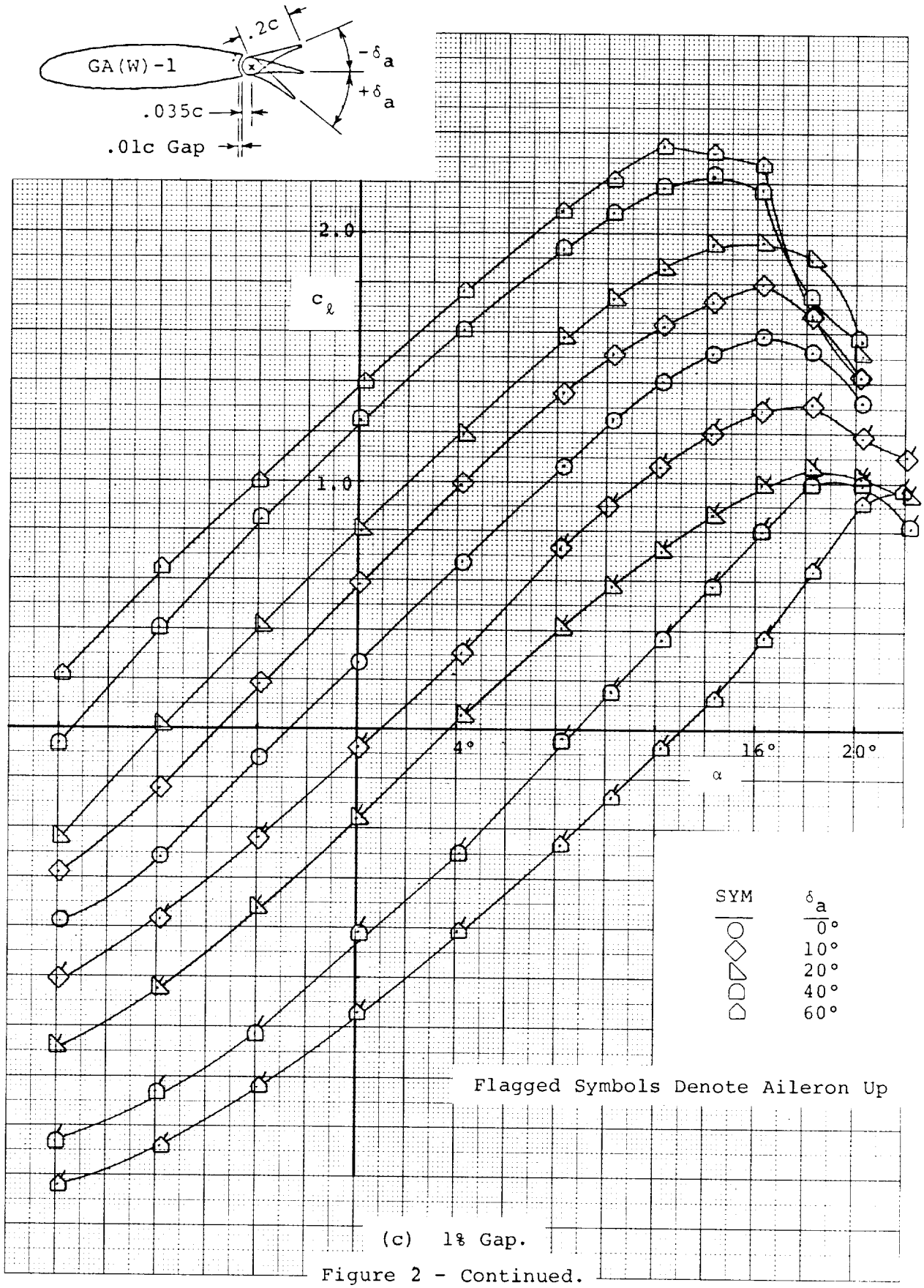

(c) 1% Gap.

Figure 2 - Continued.

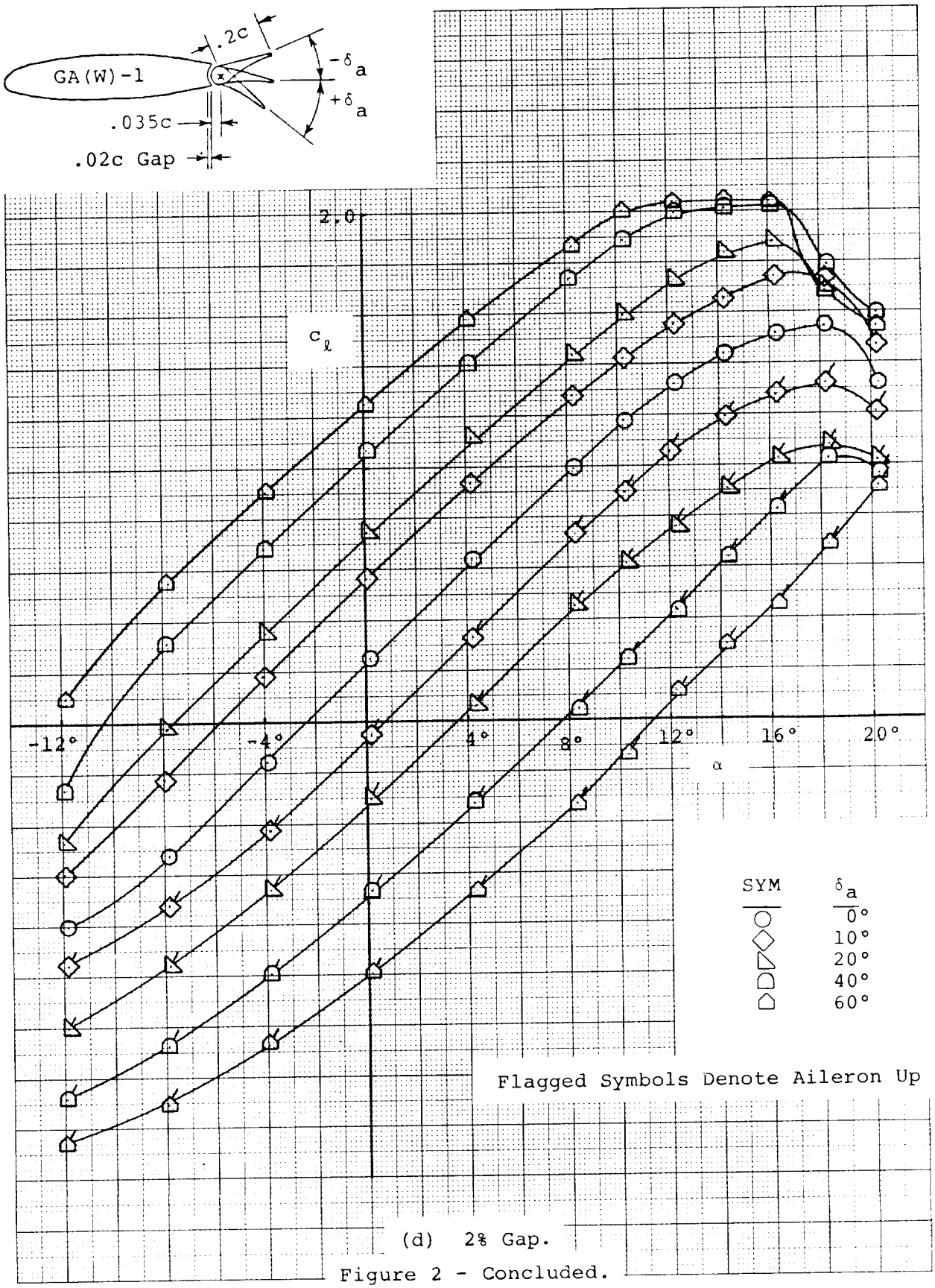

(d) 2% Gap.

Figure 2 - Concluded.

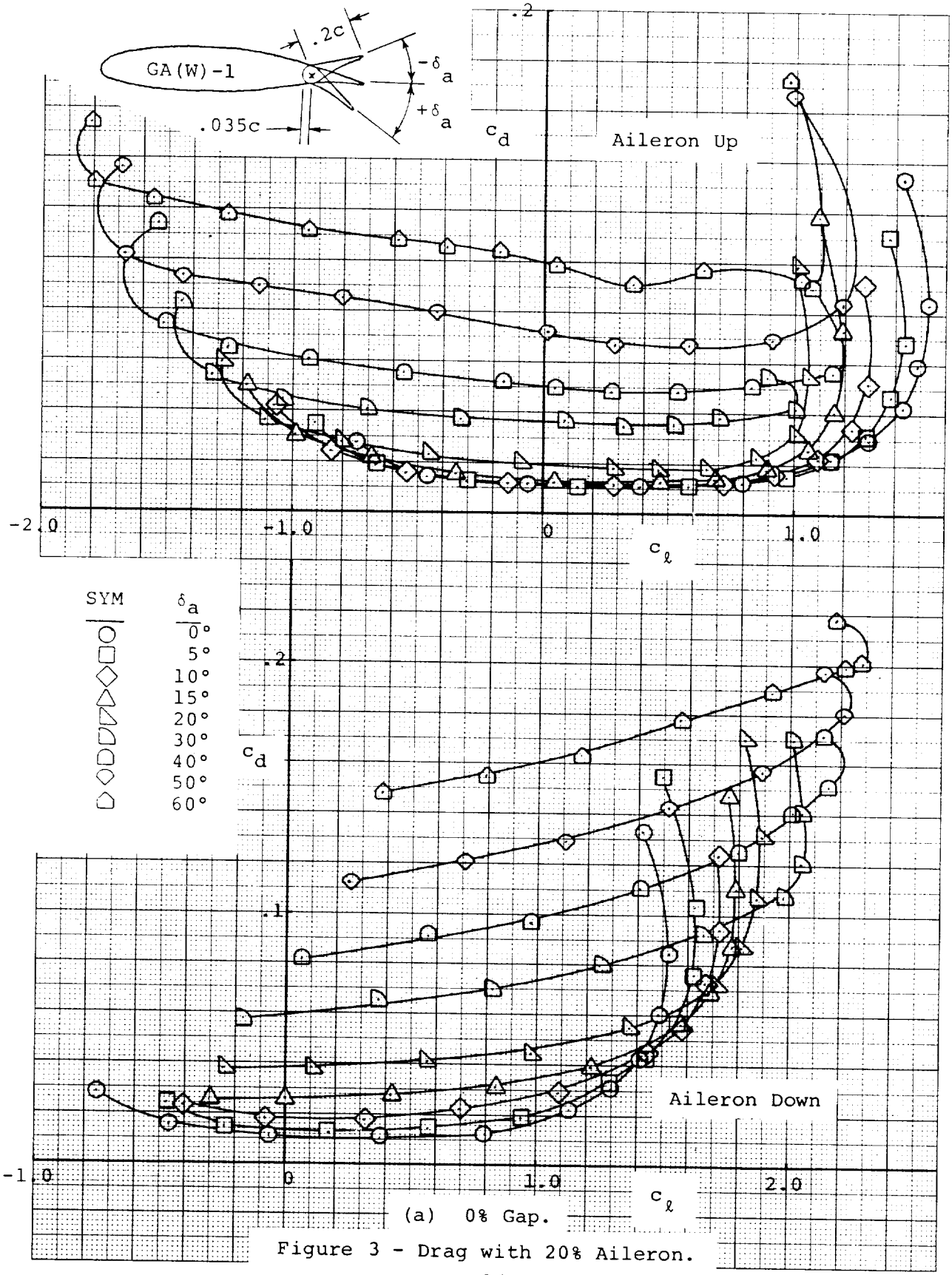

(a) 0% Gap.

Figure 3 - Drag with 20% Aileron.

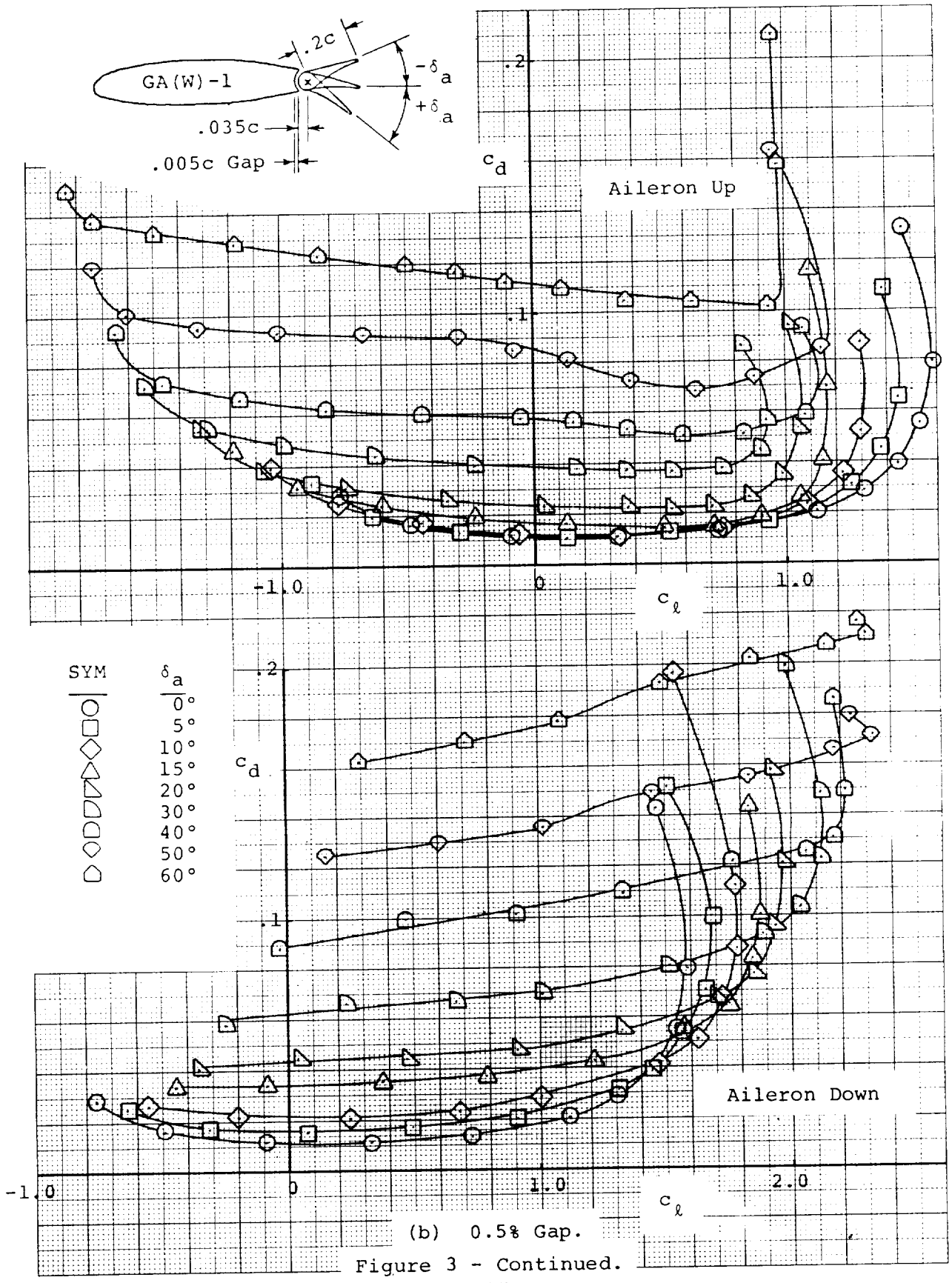

(b) 0.5% Gap.

Figure 3 - Continued.

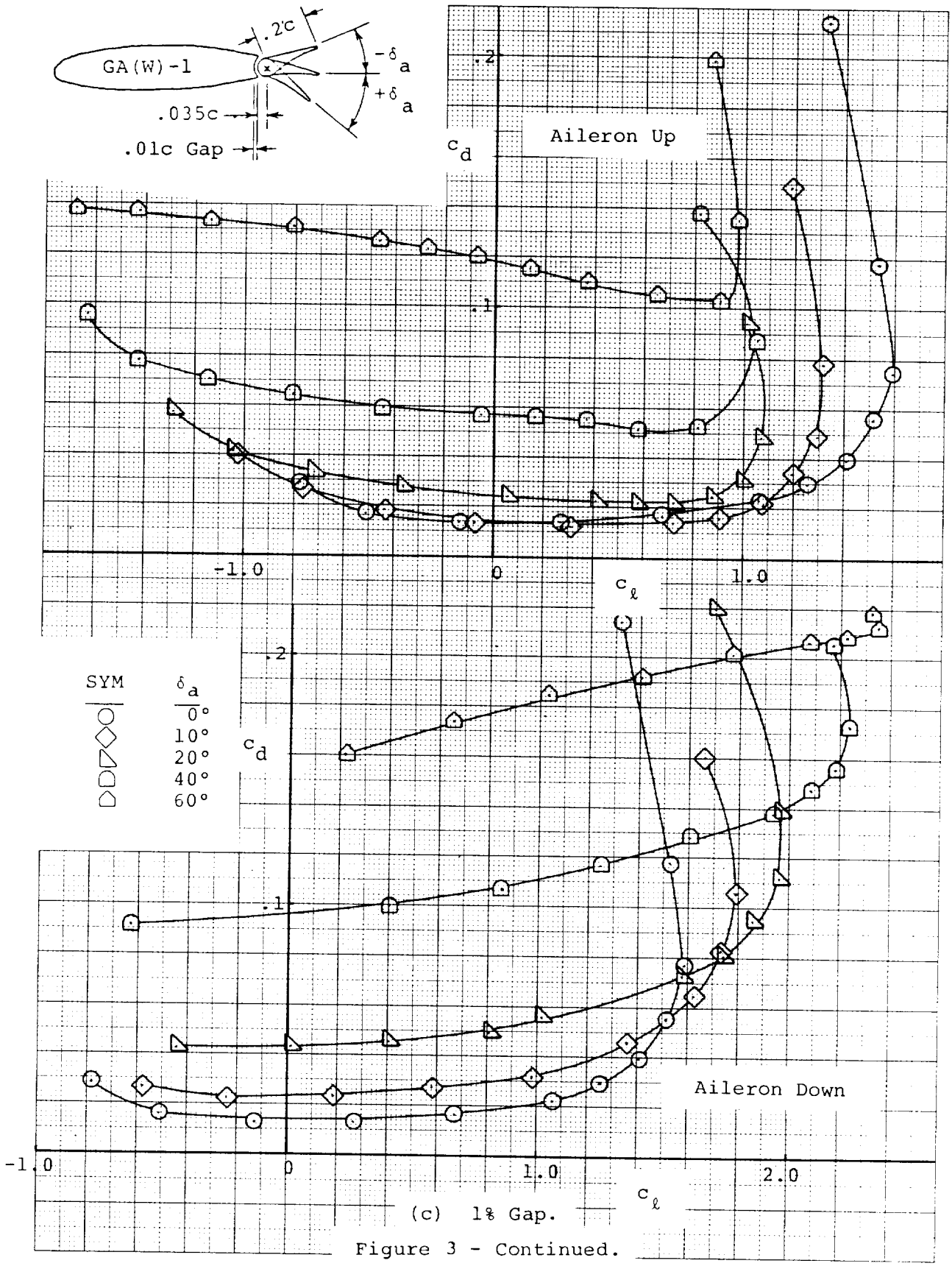

(c) 1% Gap.

Figure 3 - Continued.

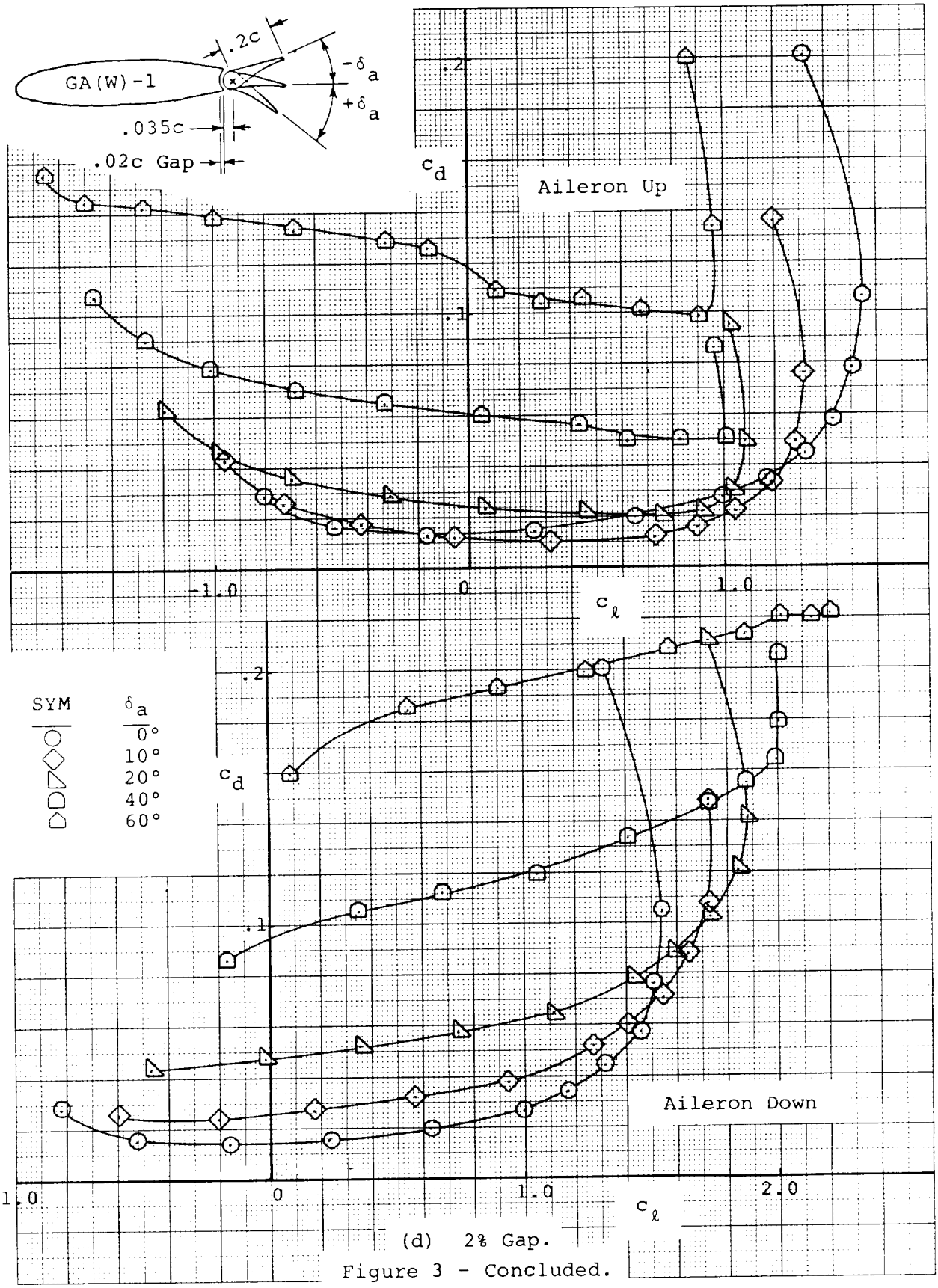

(d) 2% Gap.

Figure 3 - Concluded.

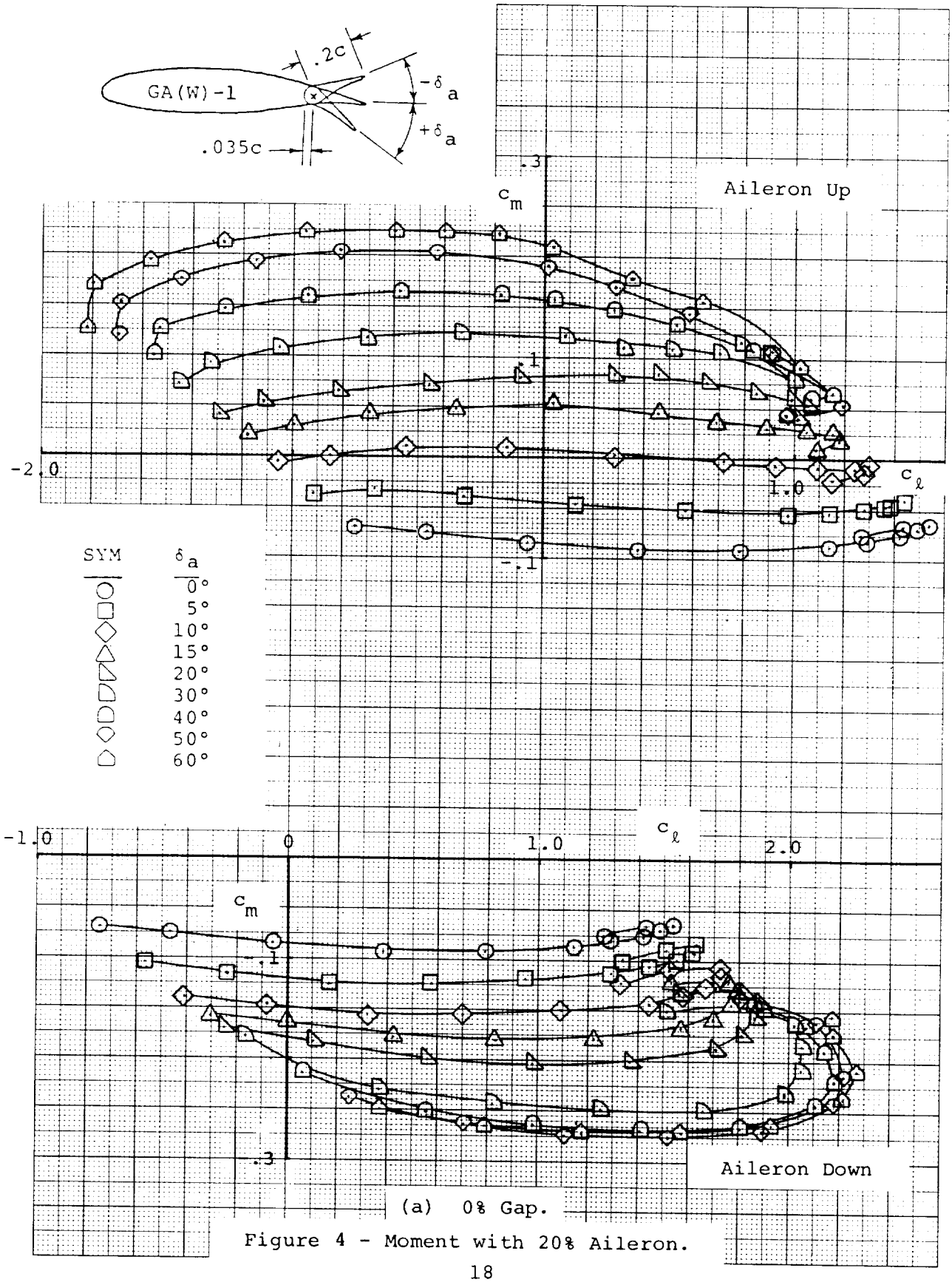

(a) 0% Gap.

Figure 4 - Moment with 20% Aileron.

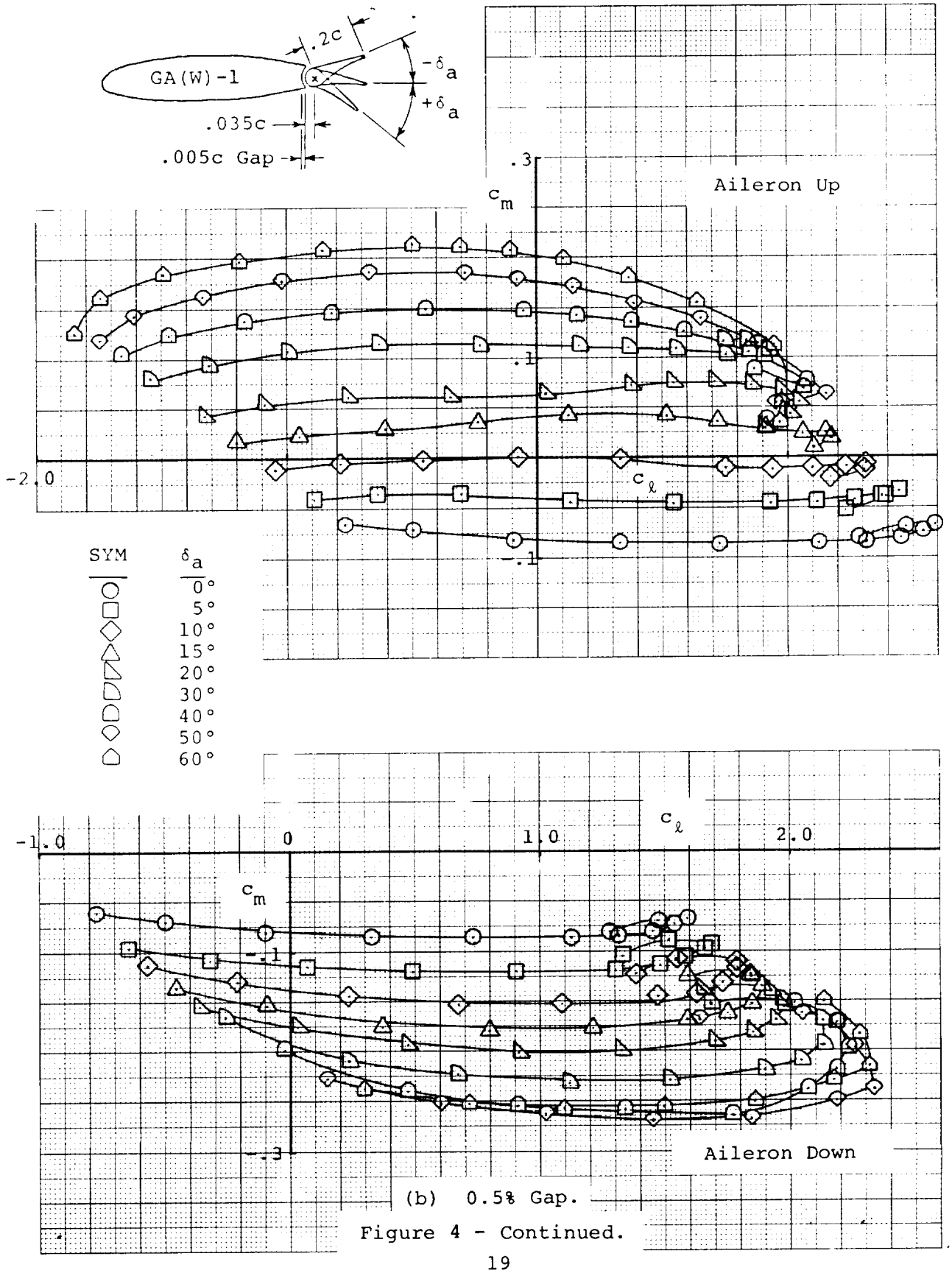

(b) 0.5% Gap.

Figure 4 - Continued.

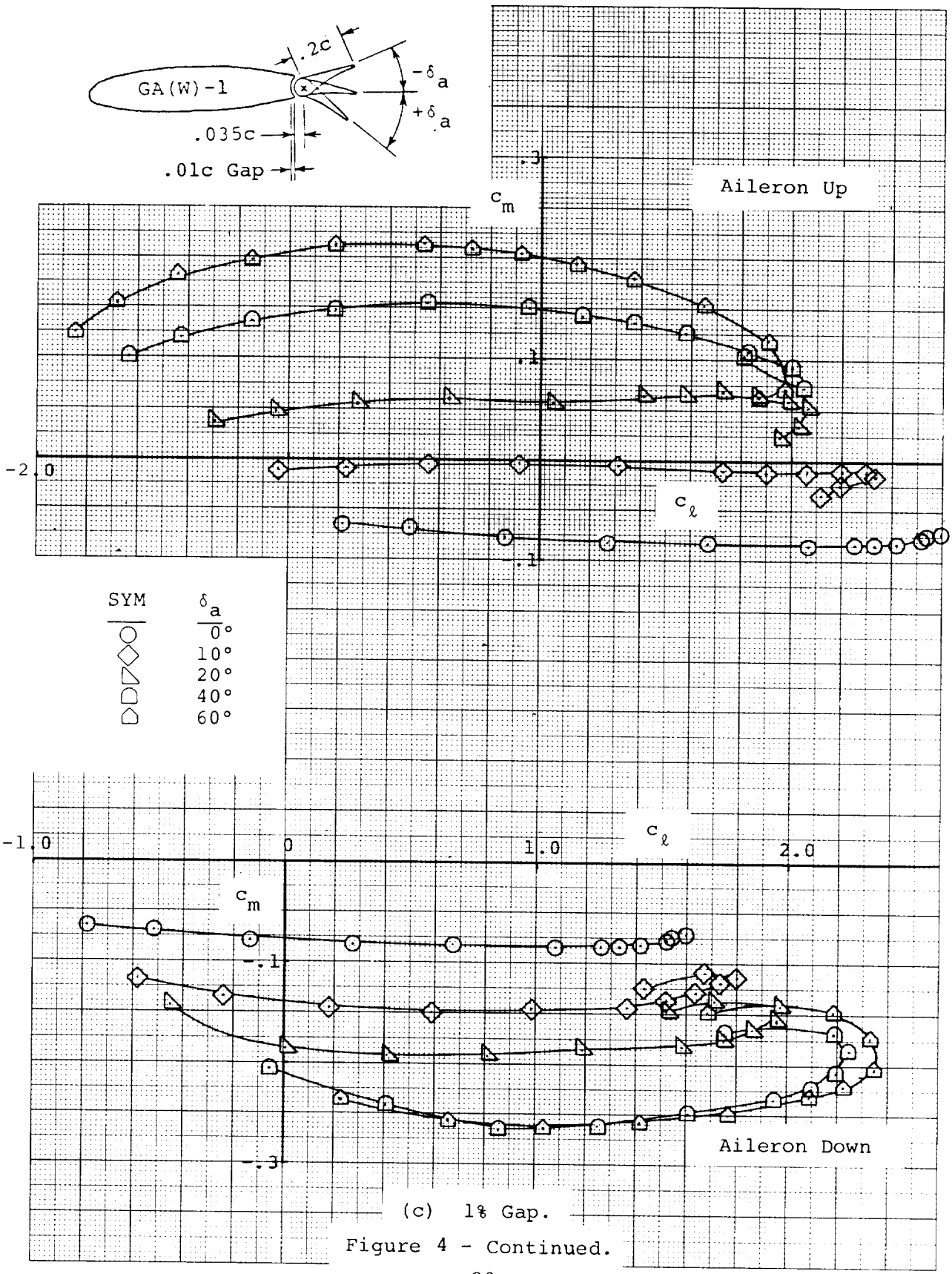

(c) 1% Gap.

Figure 4 - Continued.

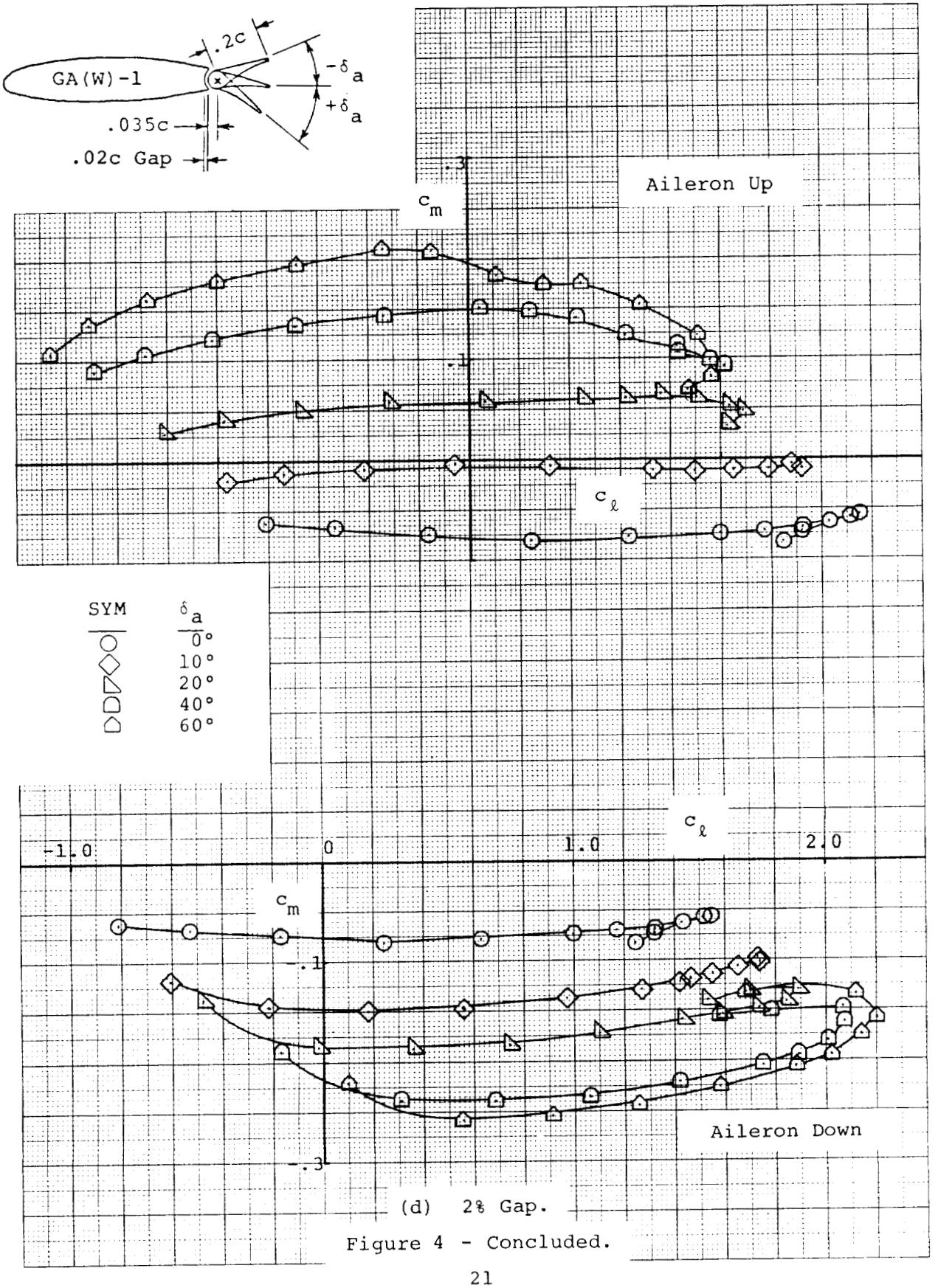

(d) 2% Gap.

Figure 4 - Concluded.

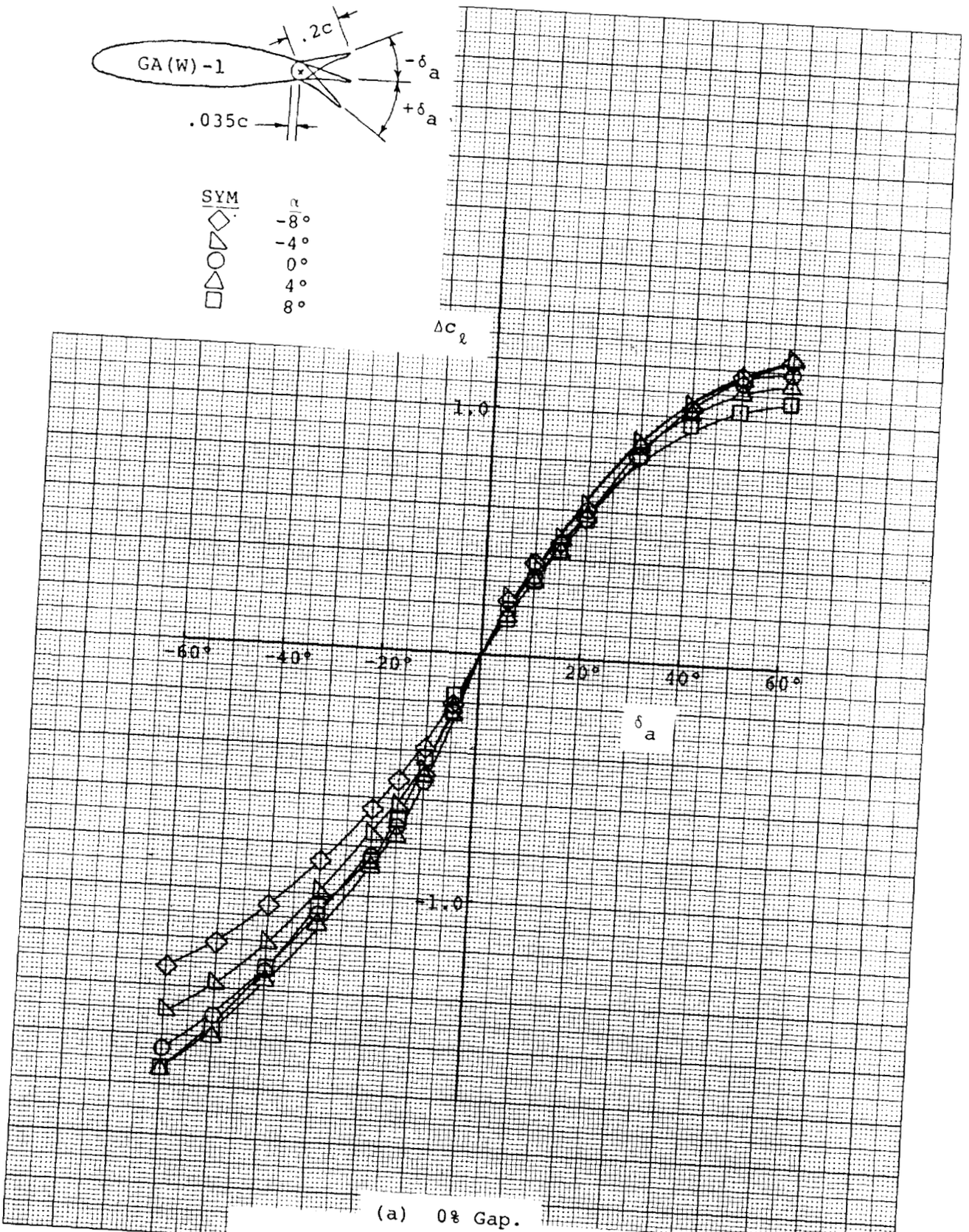

(a) 0% Gap.

Figure 5 - Aileron Effectiveness.

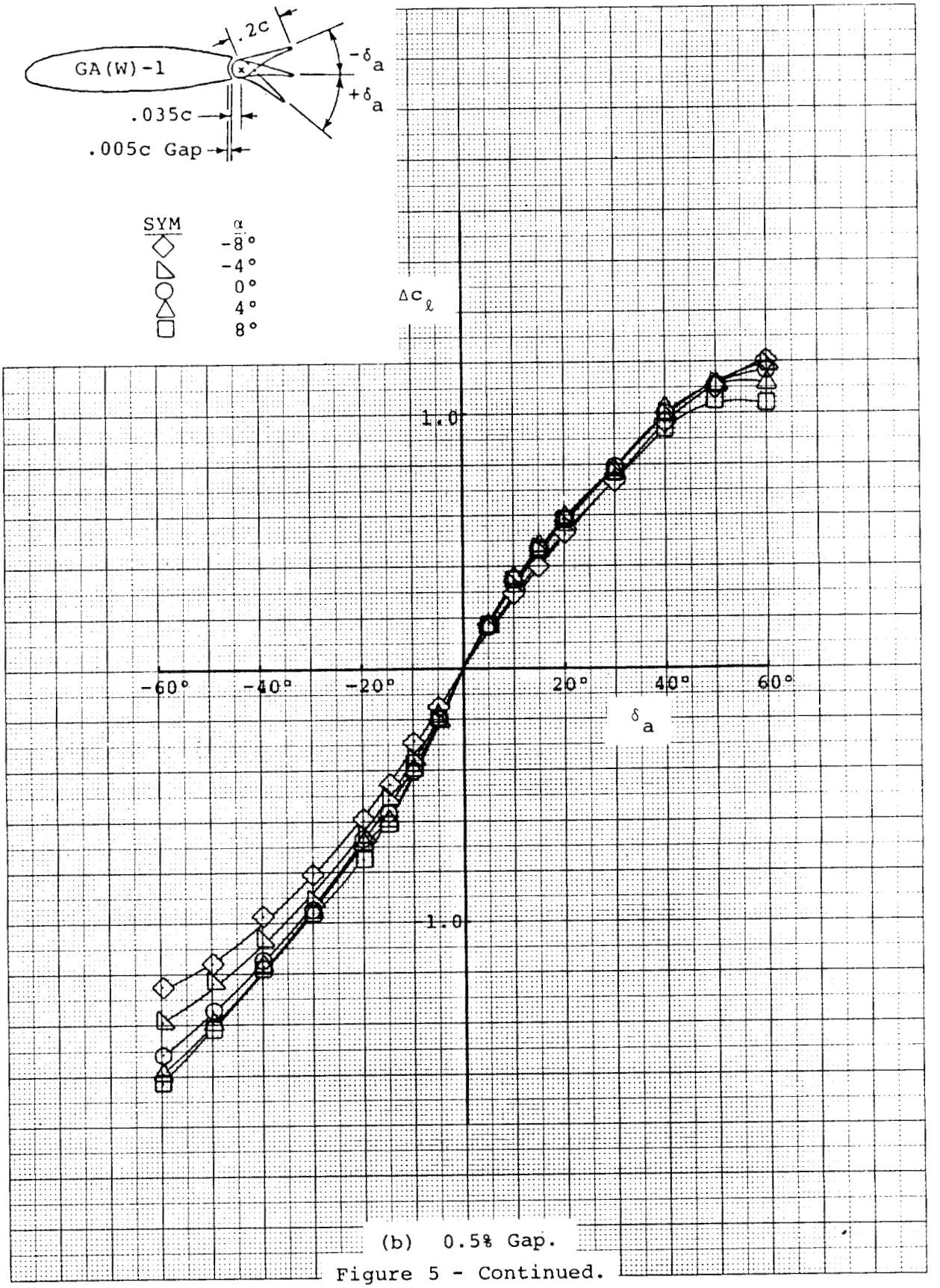

(b) 0.5% Gap.

Figure 5 - Continued.

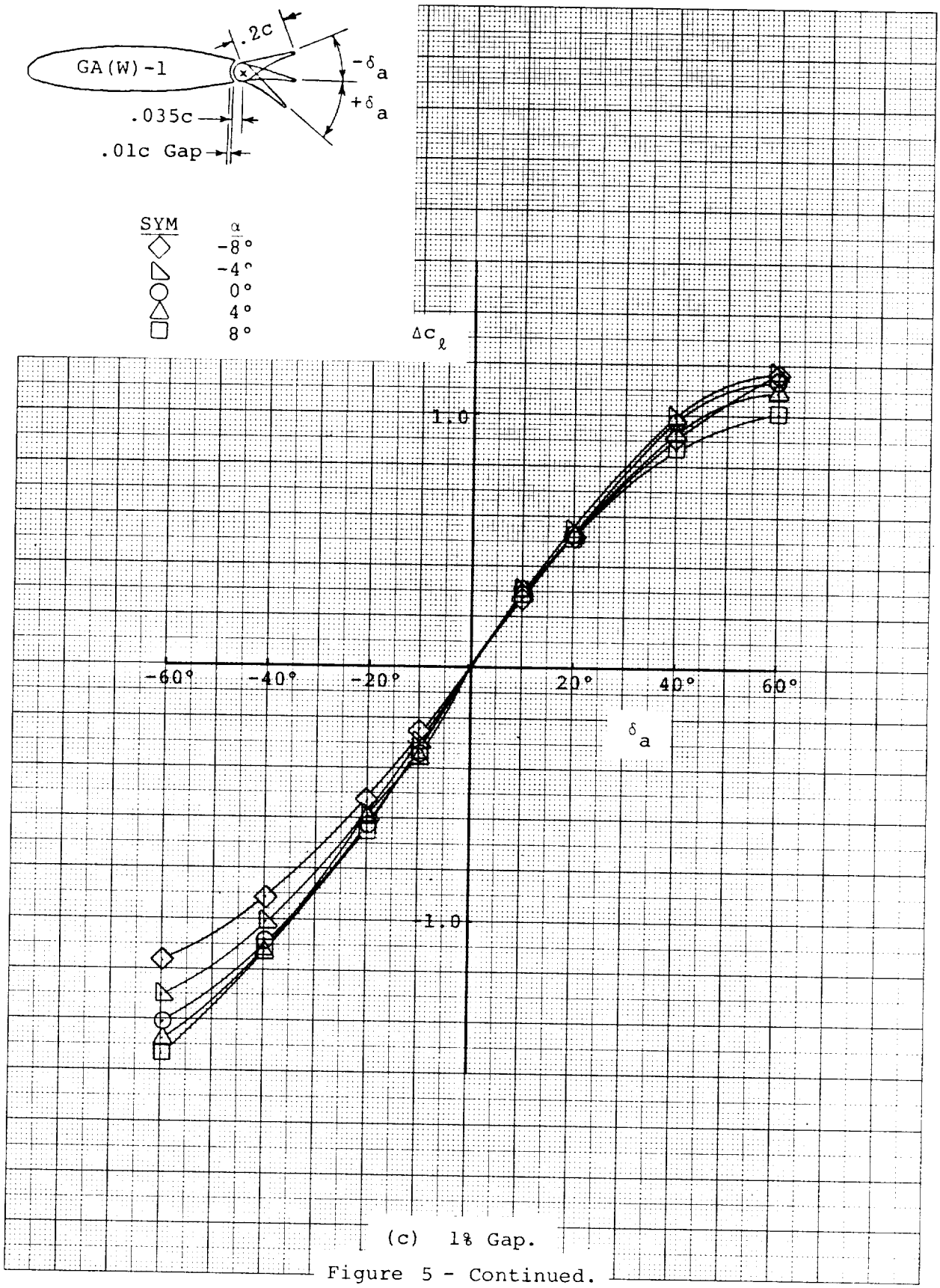

(c) 1% Gap.

Figure 5 - Continued.

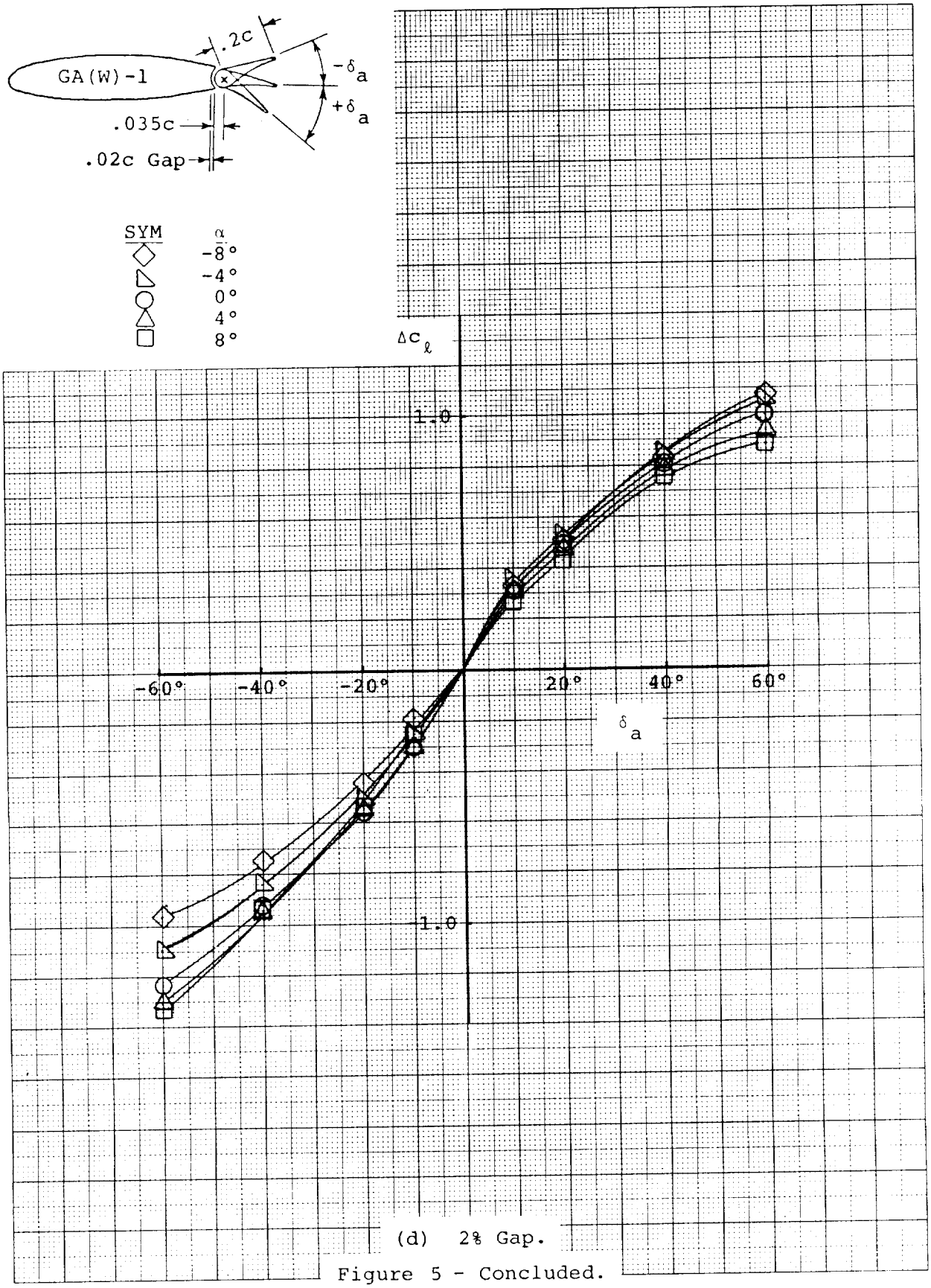

(d) 2% Gap.

Figure 5 - Concluded.

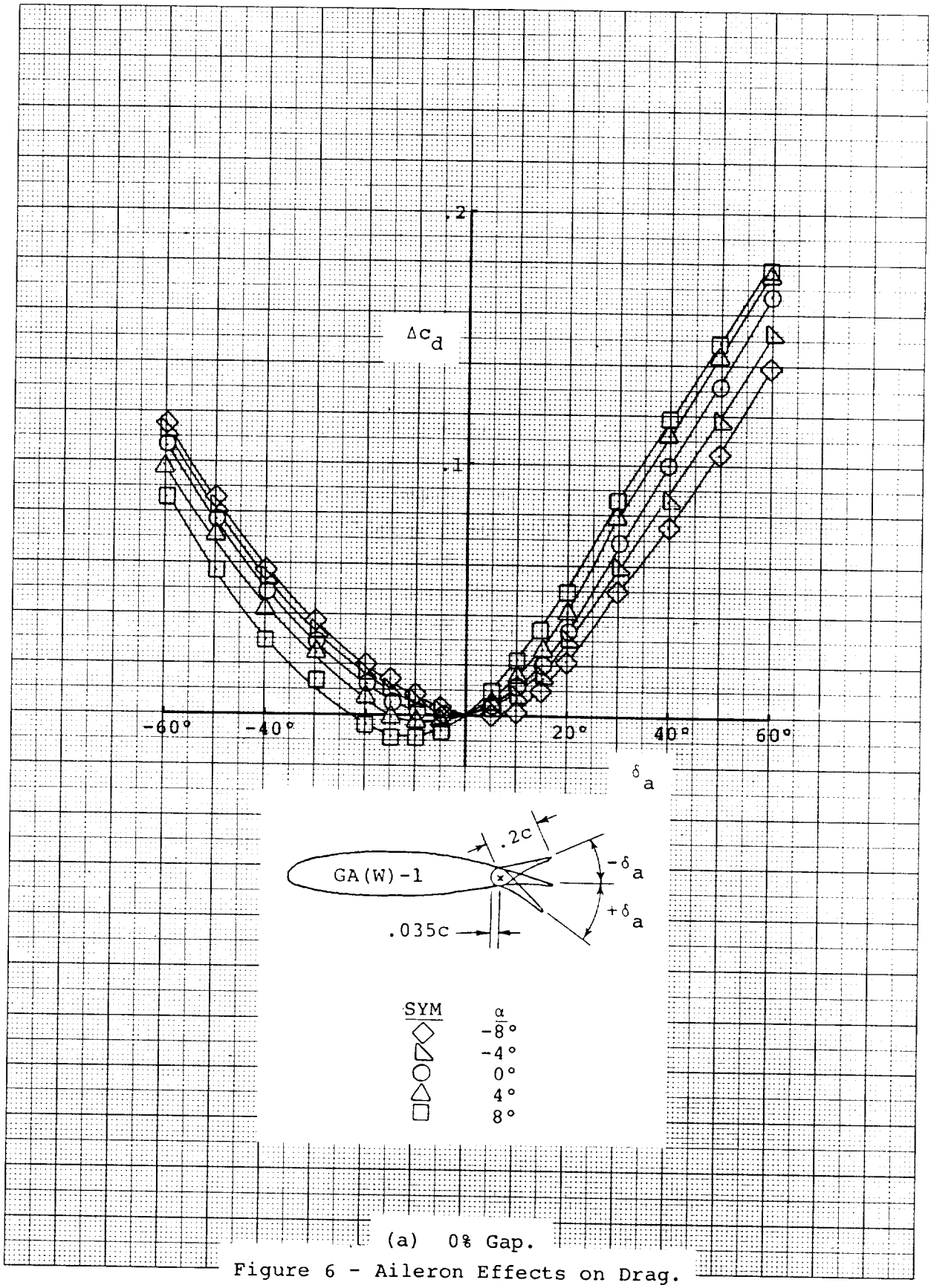

(a) 0% Gap.

Figure 6 - Aileron Effects on Drag.

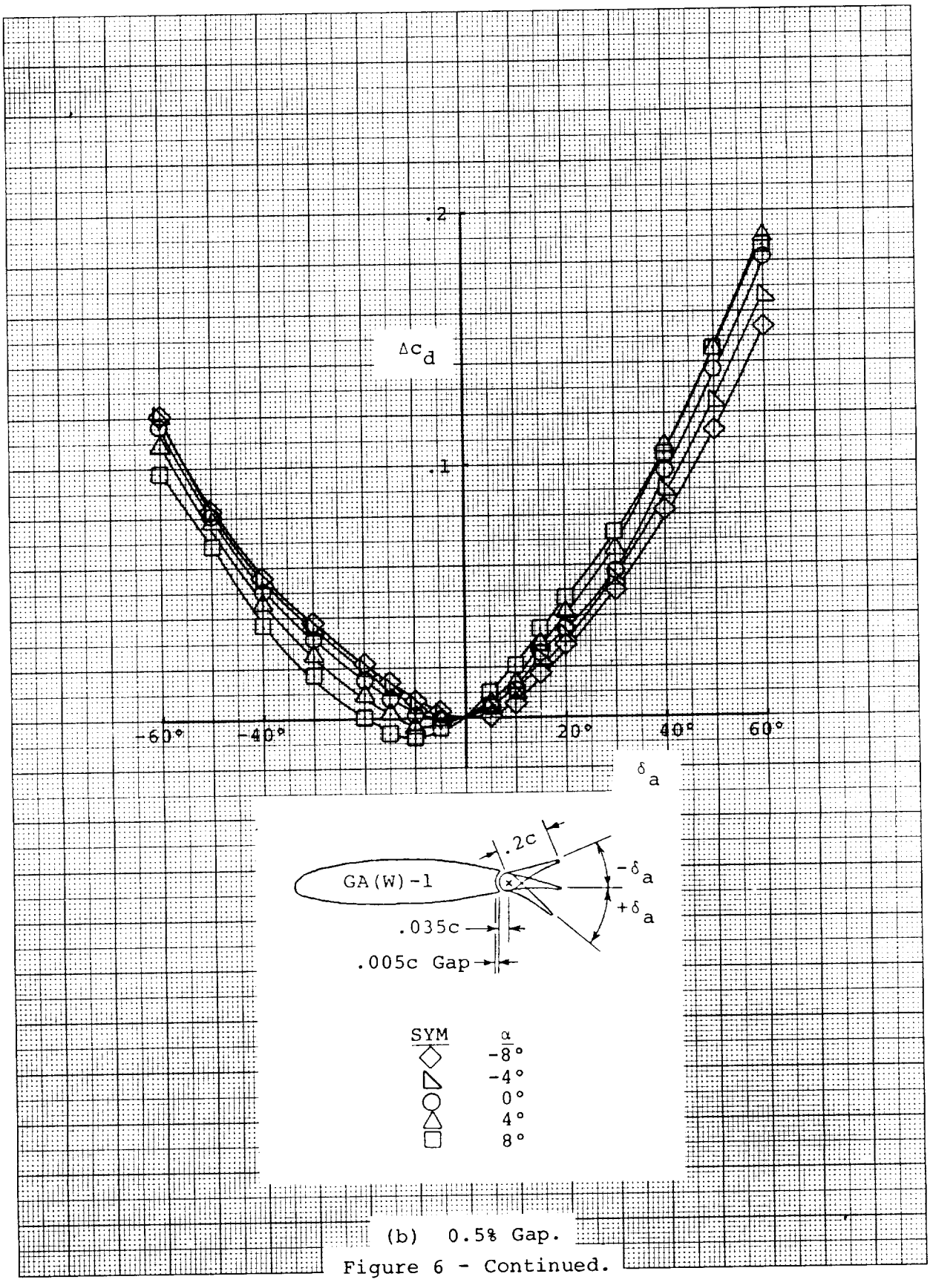

(b) 0.5% Gap.

Figure 6 - Continued.

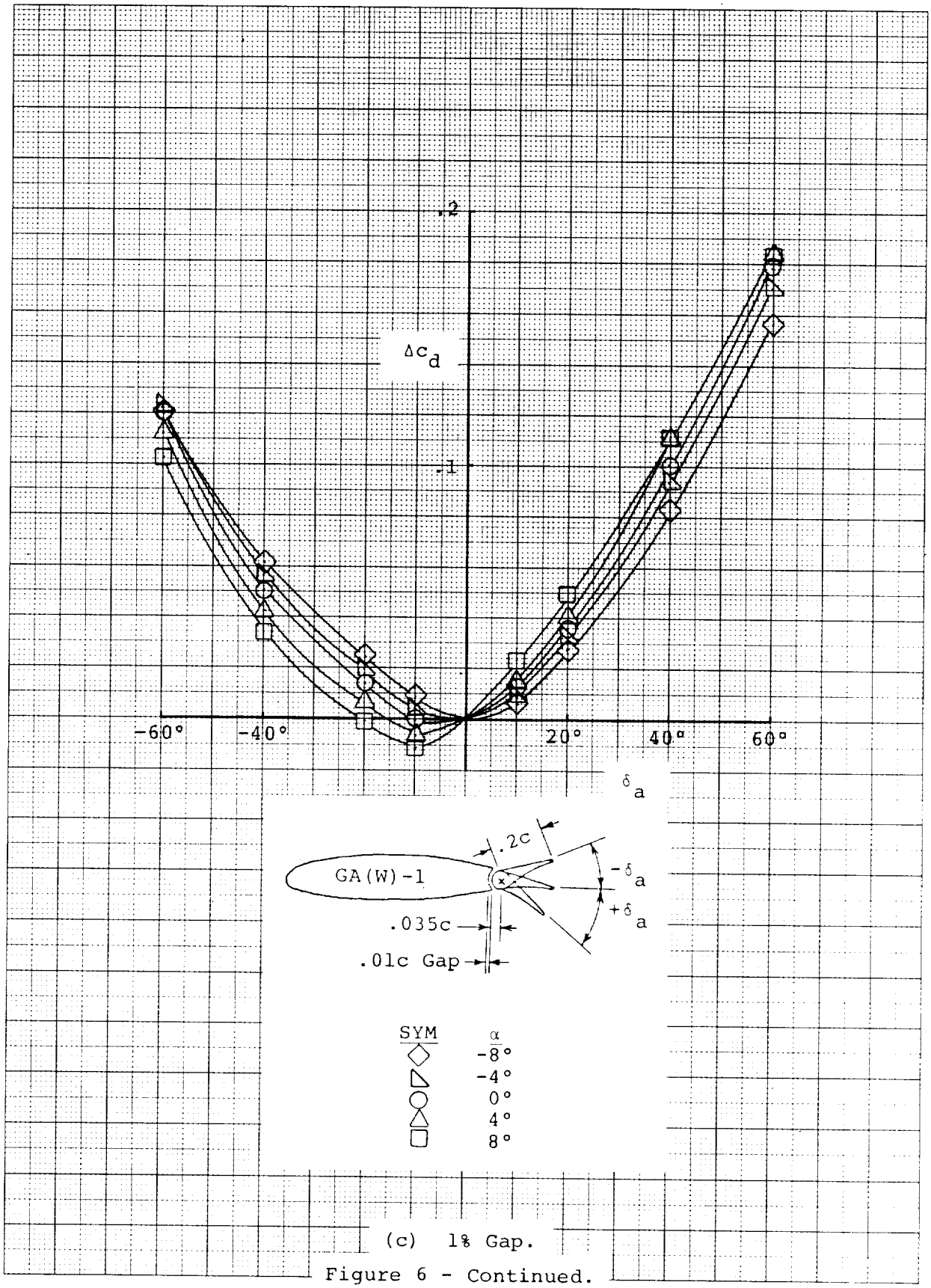

(c) 1% Gap.

Figure 6 - Continued.

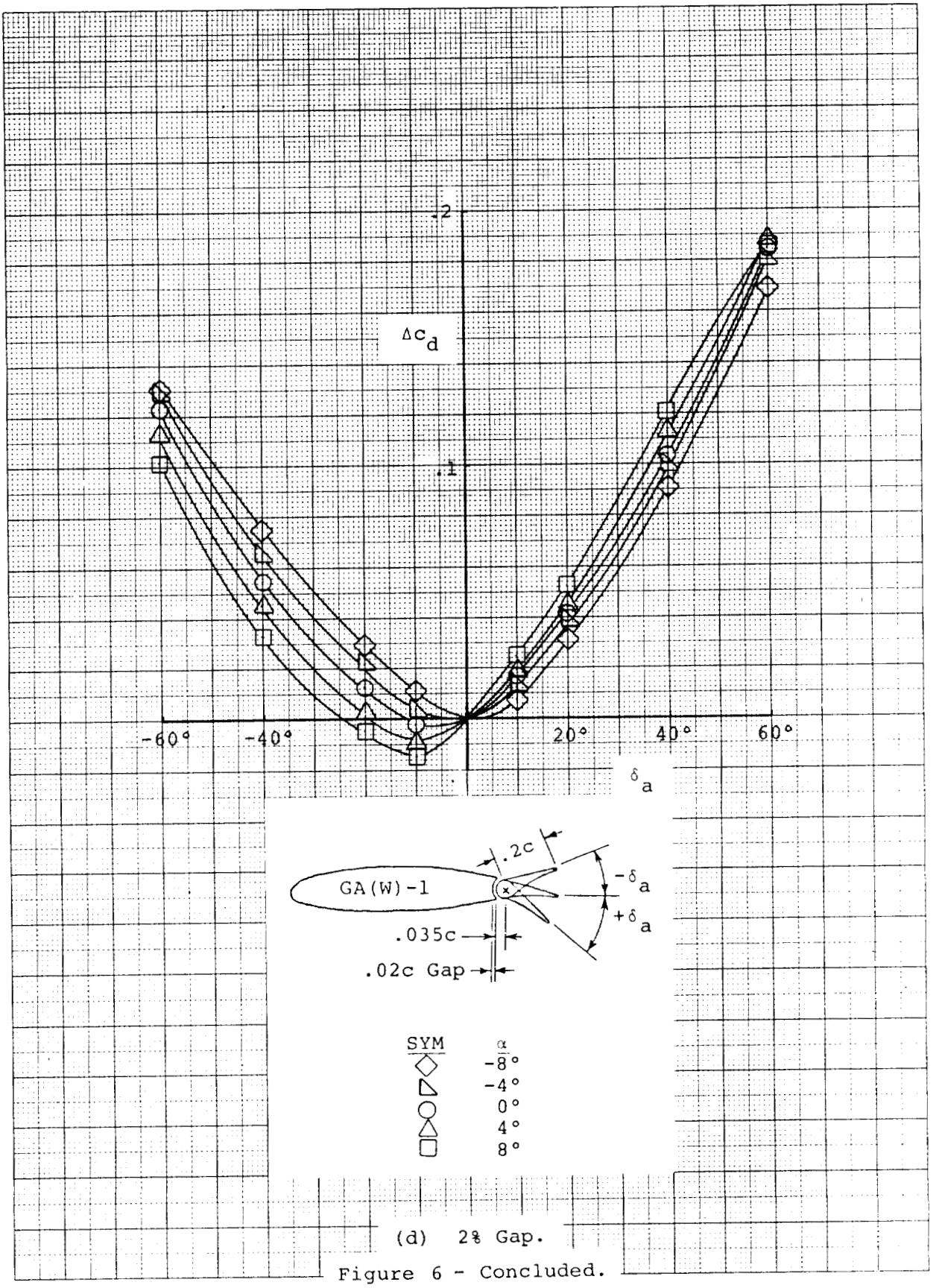

(d) 2% Gap.

Figure 6 - Concluded.

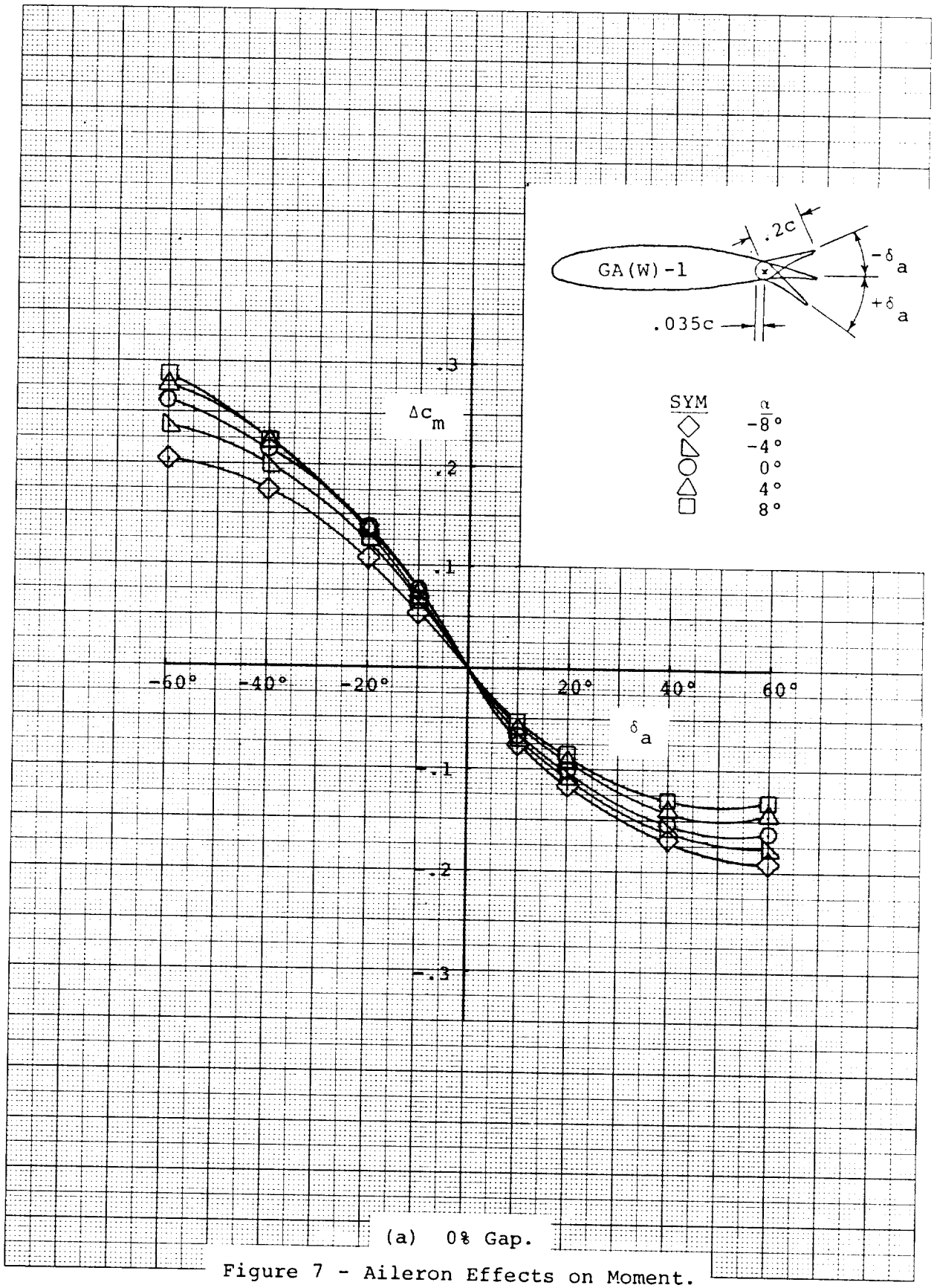

(a) 0% Gap.

Figure 7 - Aileron Effects on Moment.

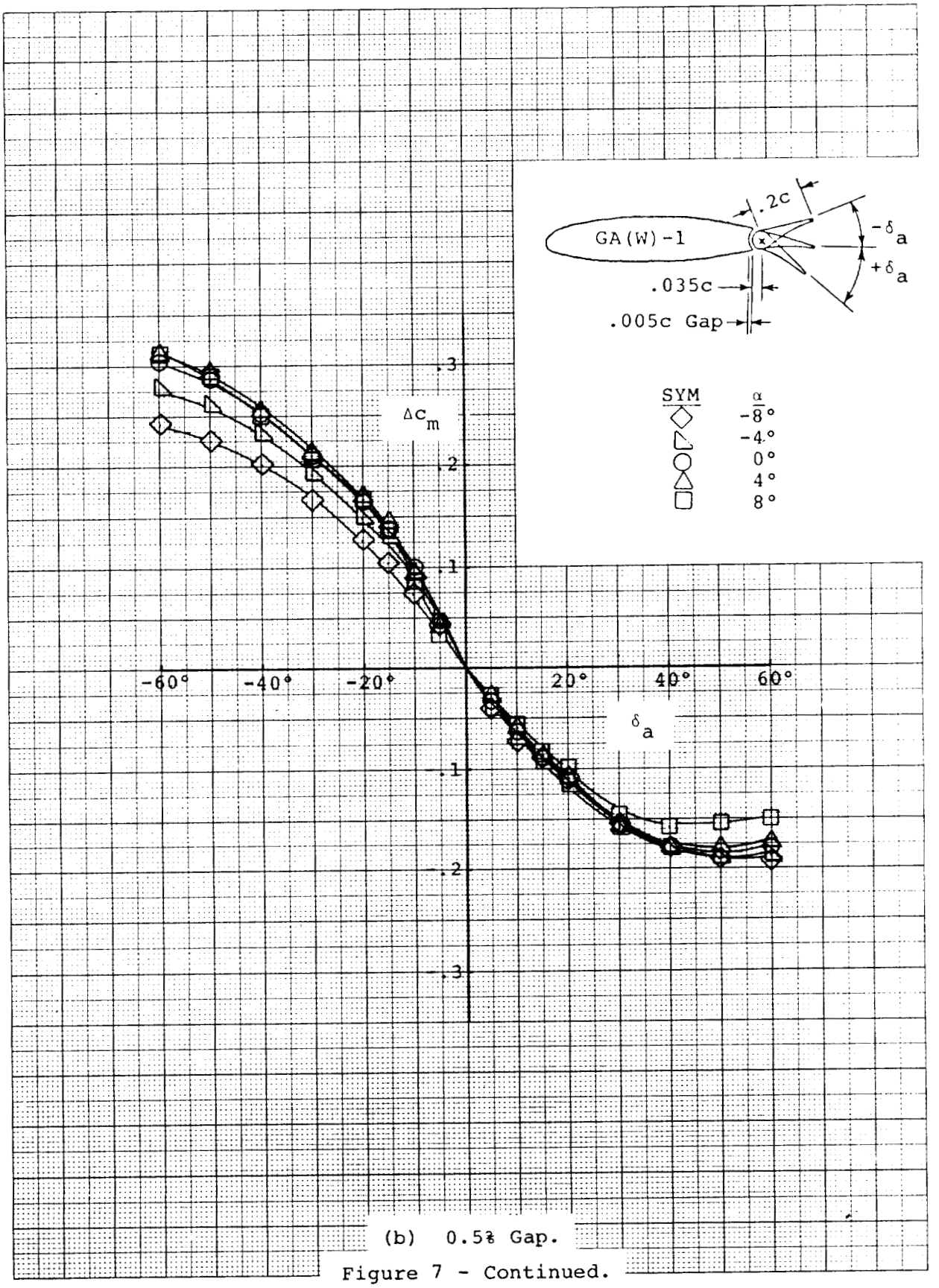

(b) 0.5% Gap.

Figure 7 - Continued.

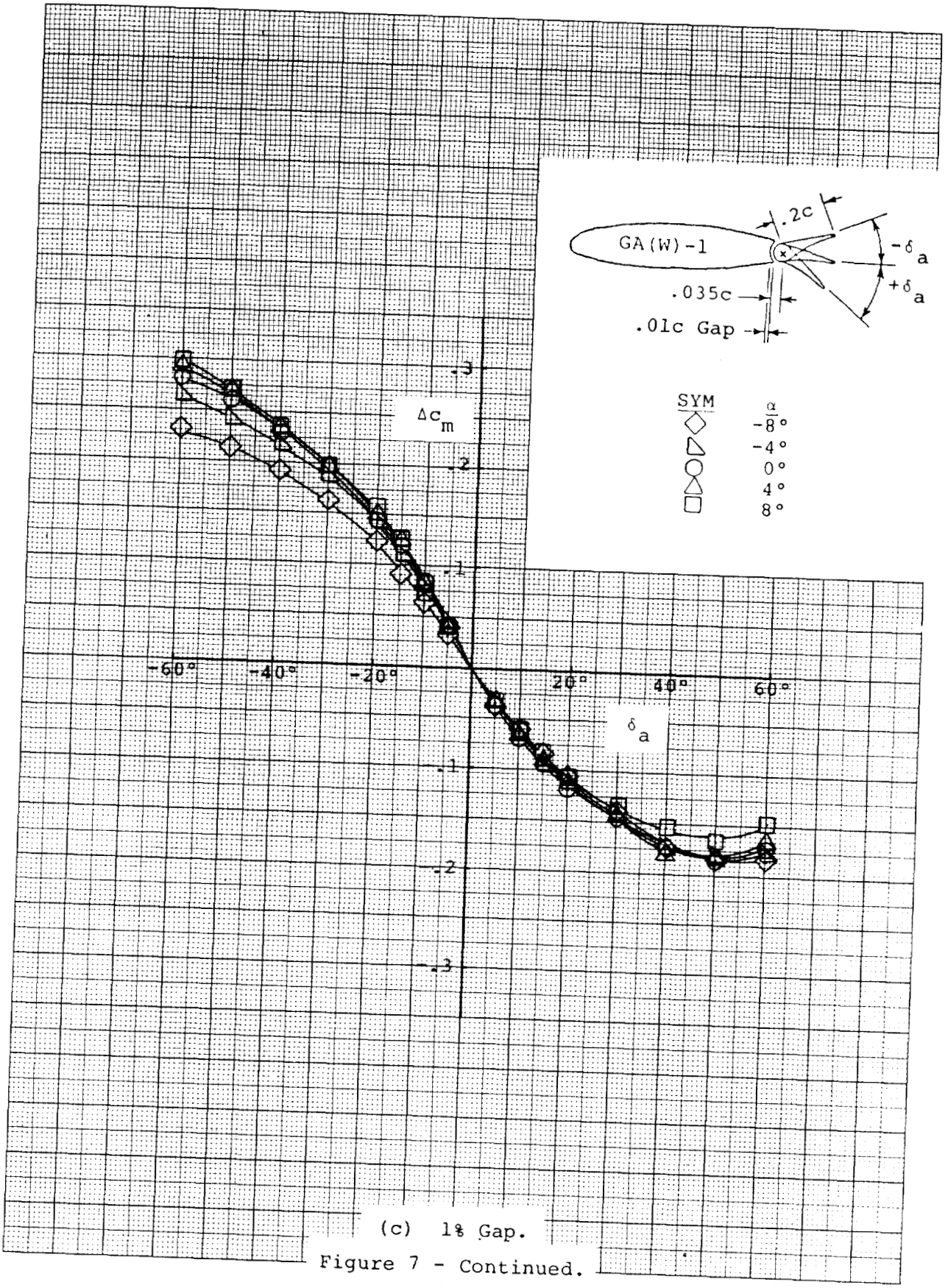

(c) 1% Gap.

Figure 7 - Continued.

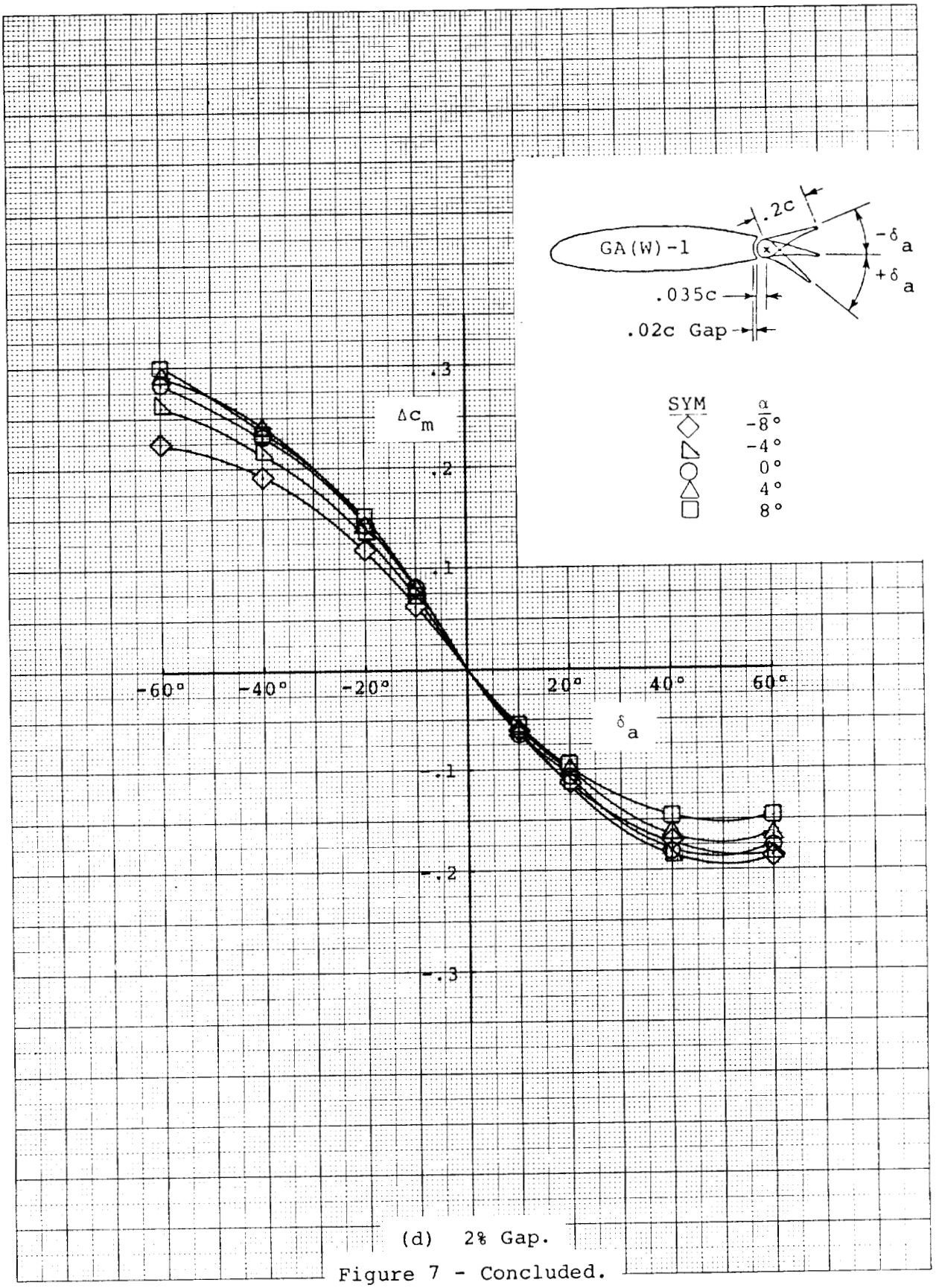

(d) 2% Gap.

Figure 7 - Concluded.

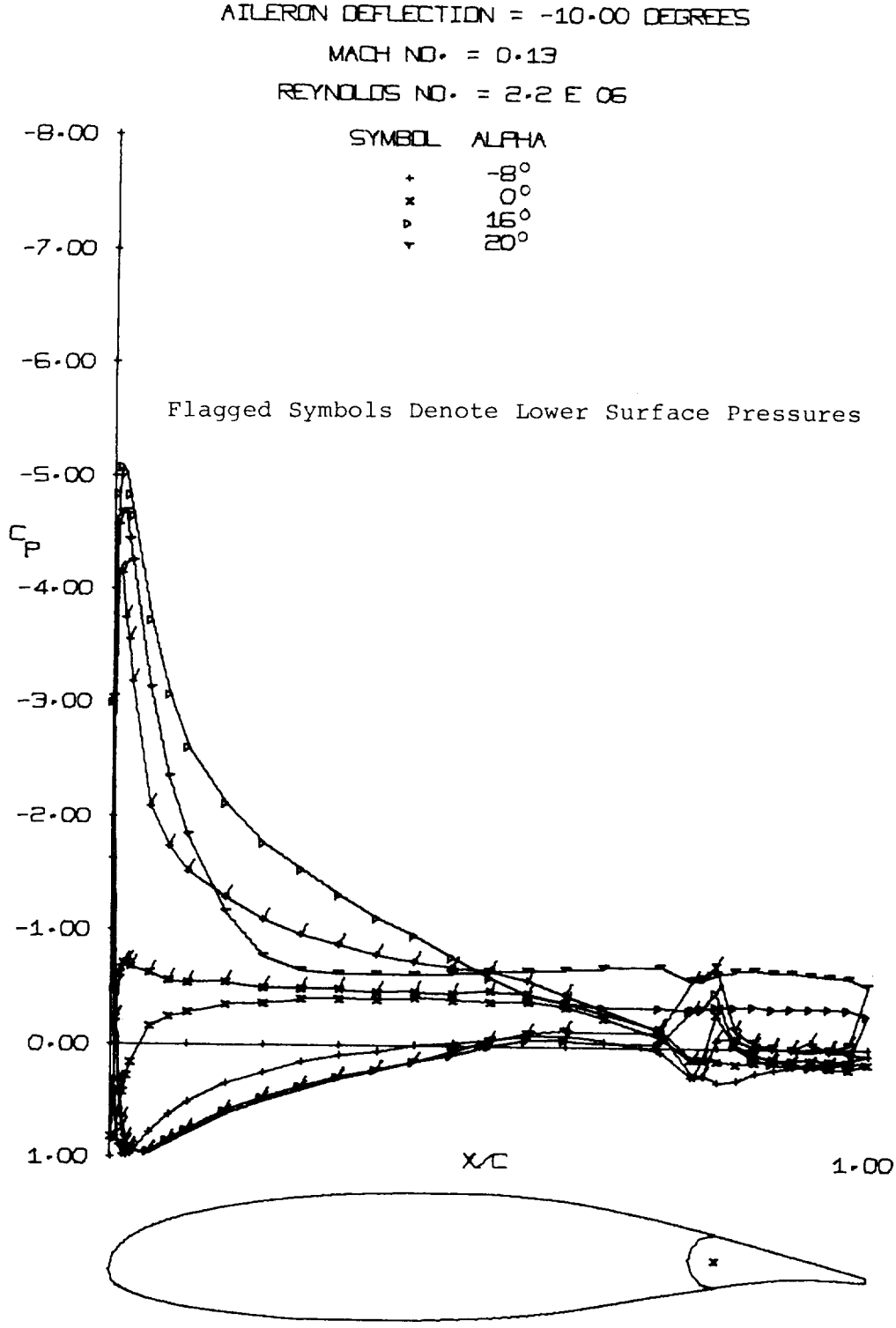

(a) -10° Aileron, Large α's.

Figure 8 - Pressure Distributions with 0% Gap.

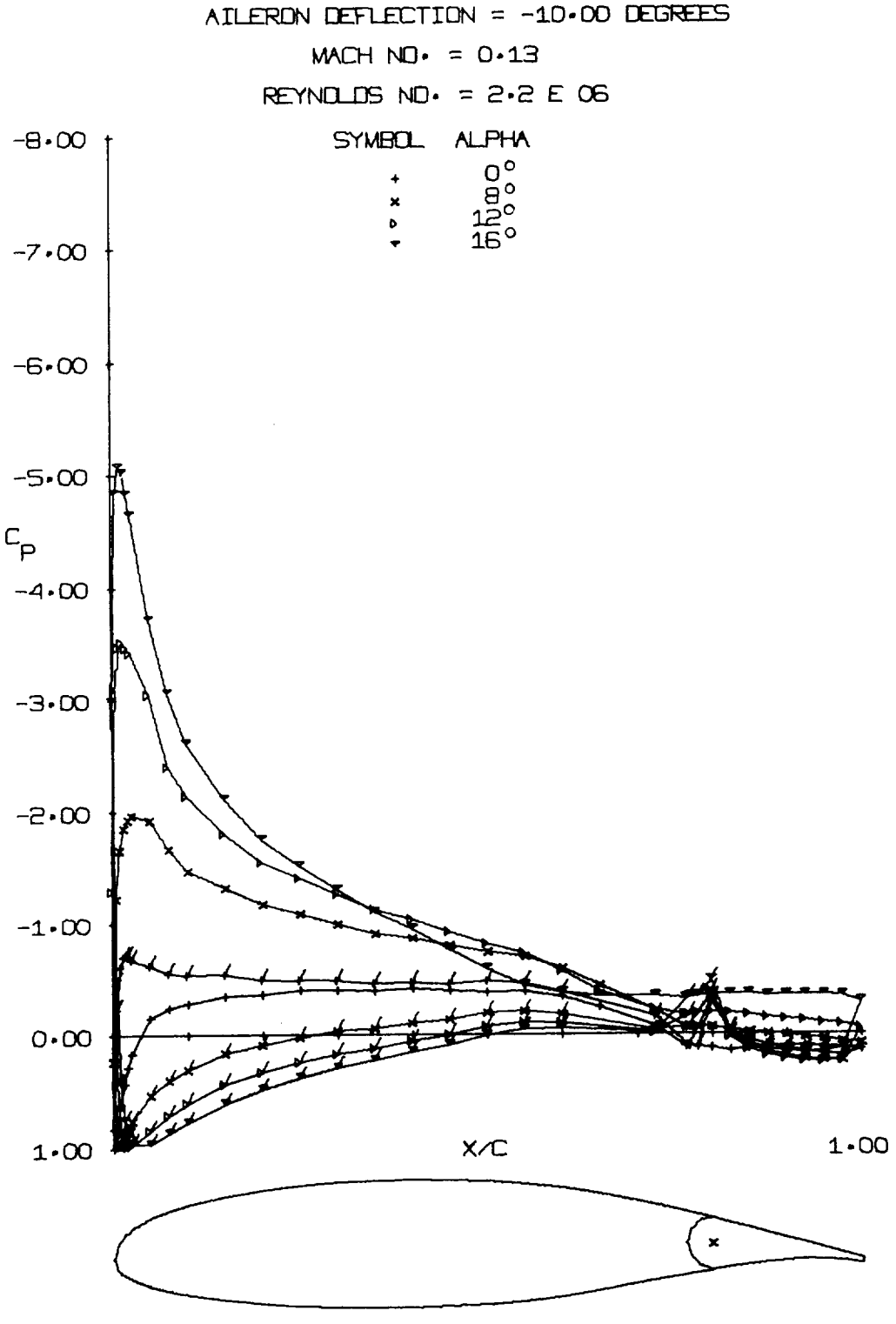

(b) -10° Aileron, Moderate α's.

Figure 8 - Continued.

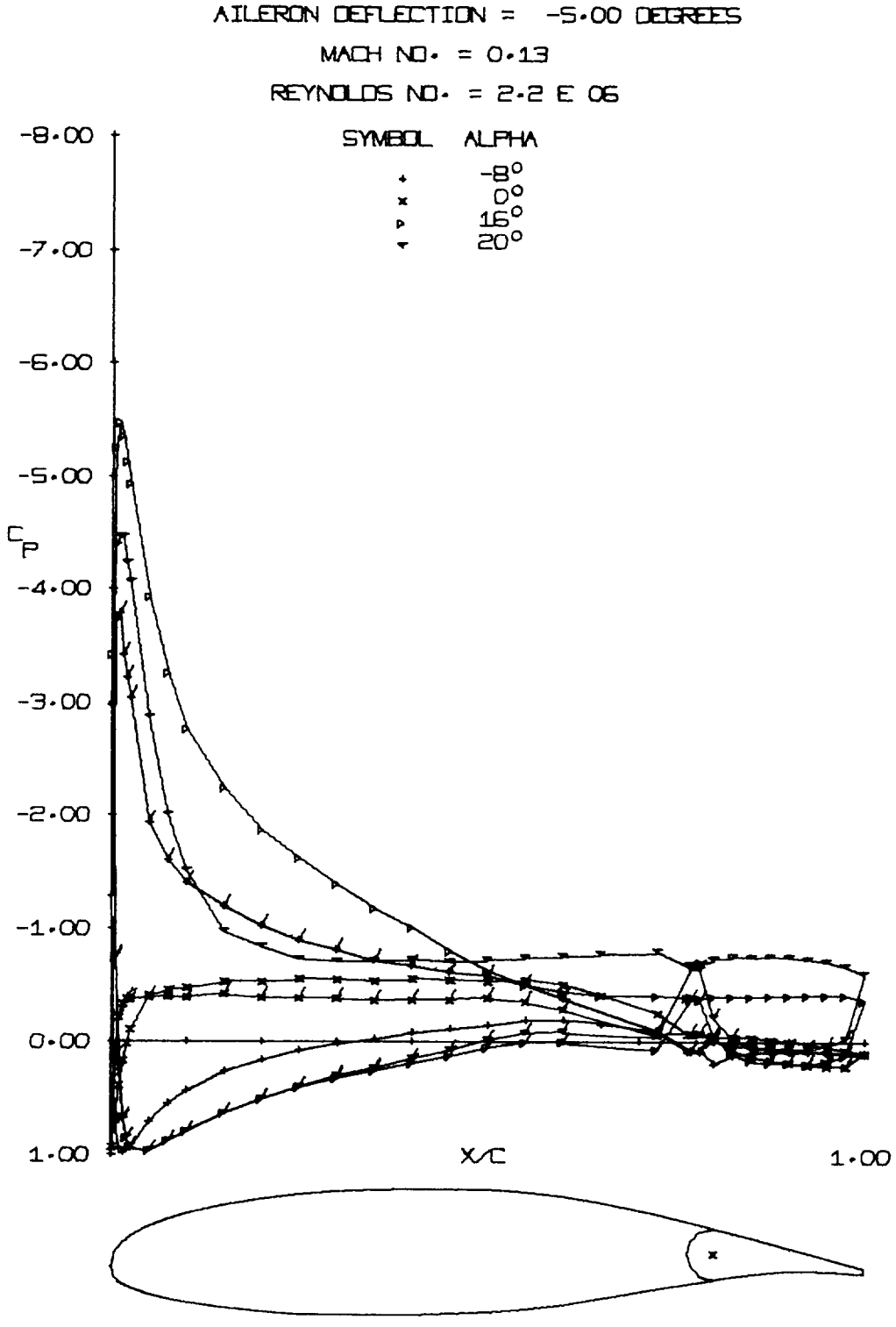

(c) -5° Aileron, Large α's.

Figure 8 - Continued.

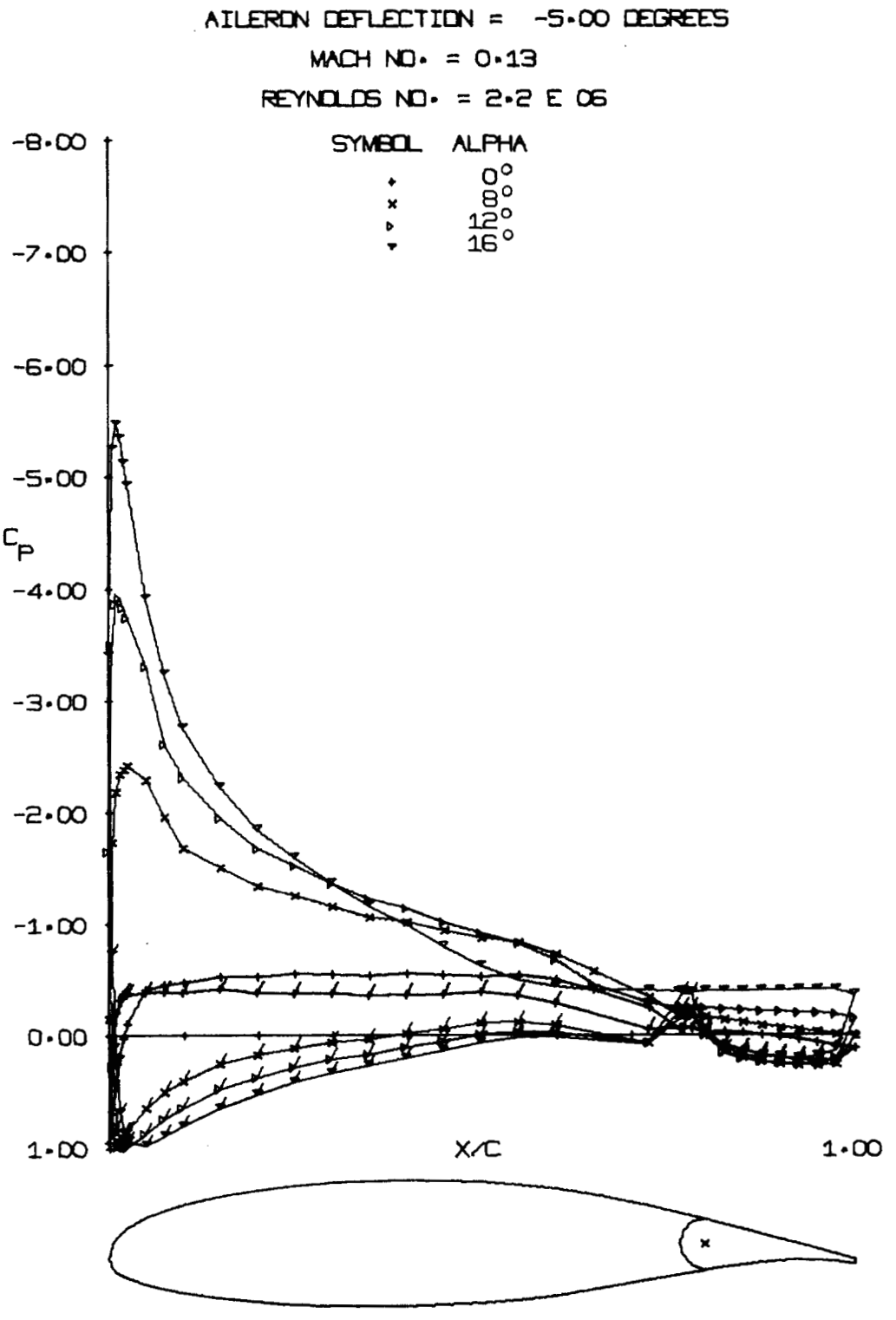

(d) -5° Aileron, Moderate α's.

Figure 8 - Continued.

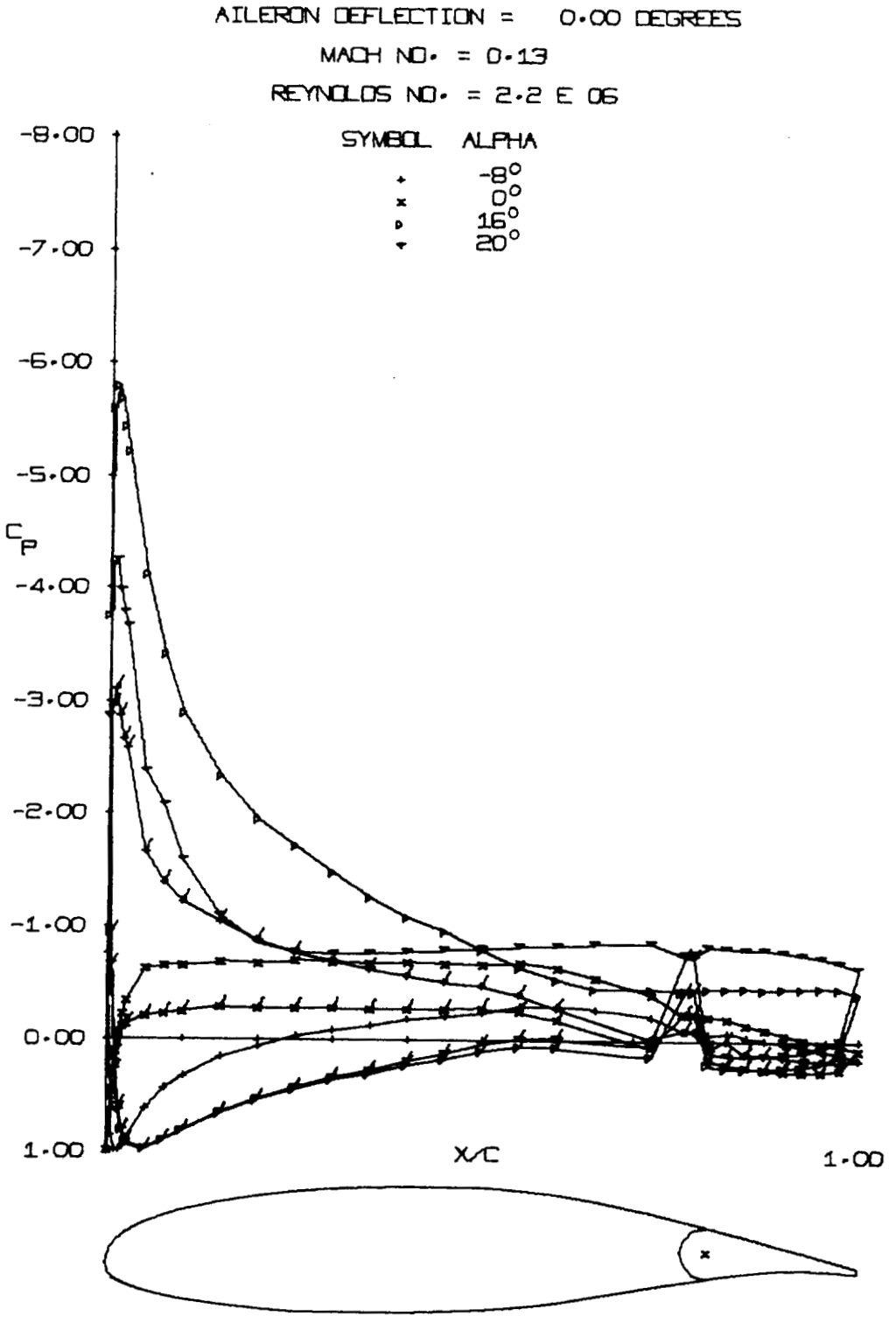

(e) 0° Aileron, Large α's.

Figure 8 - Continued.

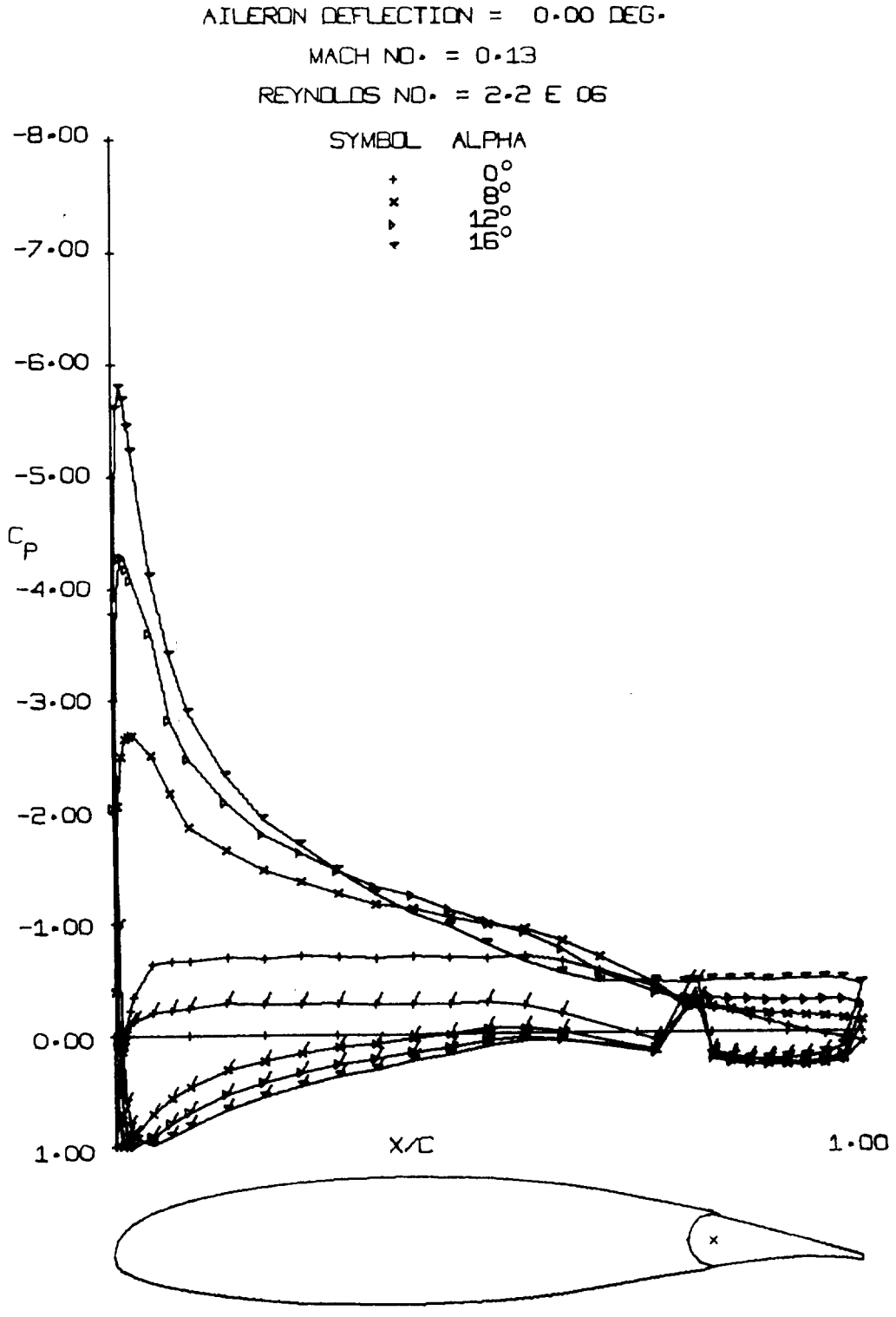

(f) 0° Aileron, Moderate α's.

Figure 8 - Continued.

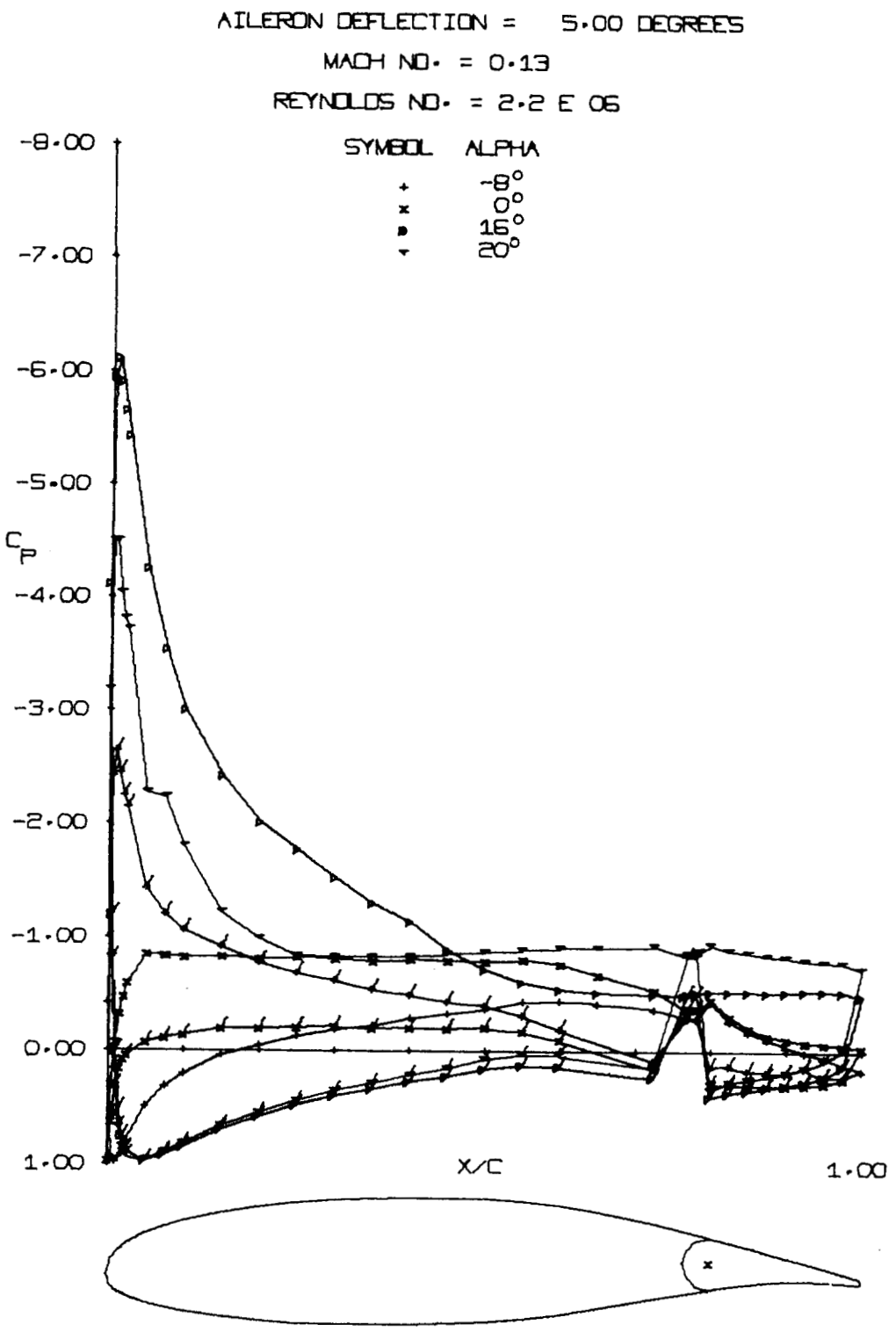

(g) +5° Aileron, Large α's.

Figure 8 - Continued.

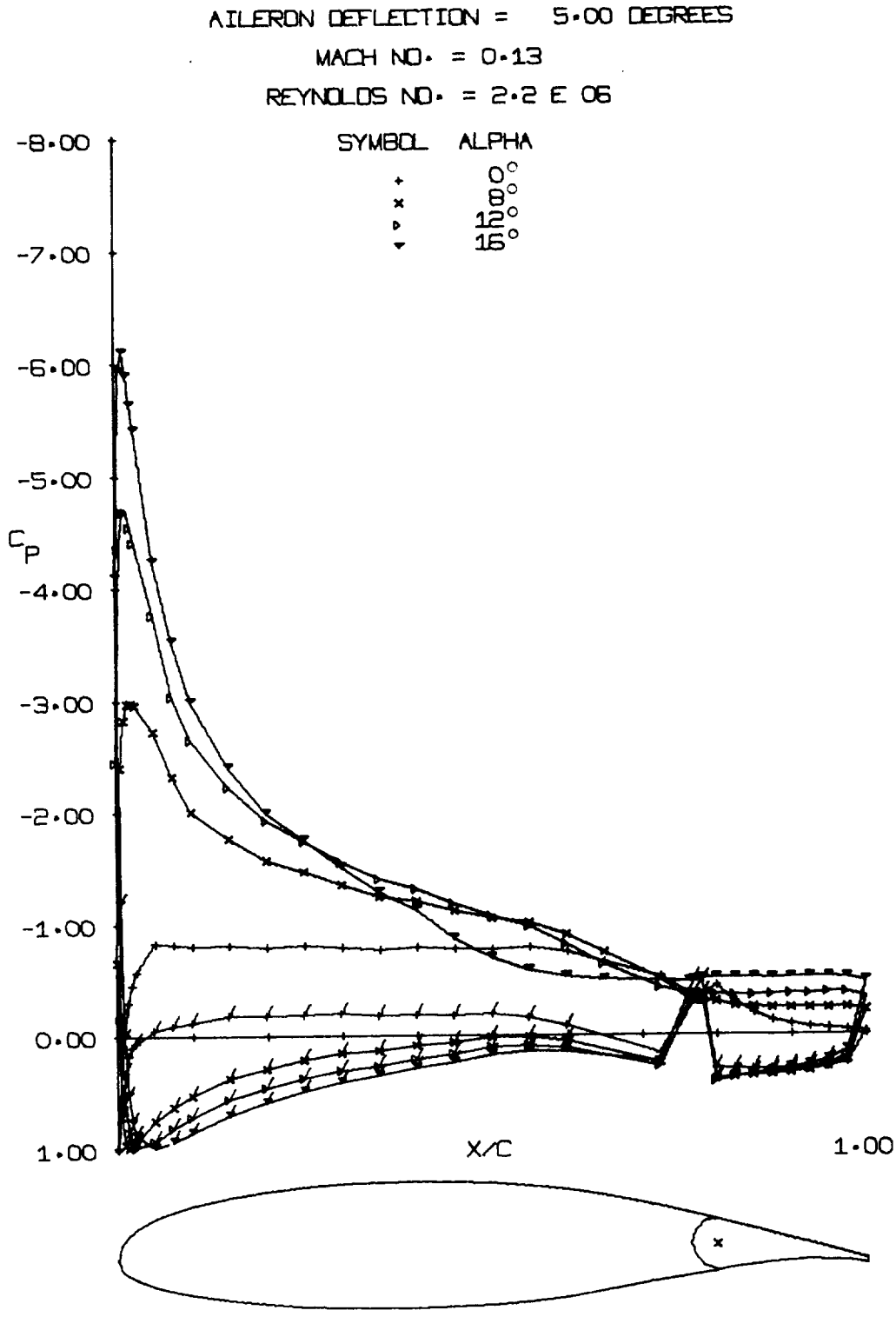

(h) +5° Aileron, Moderate α's.

Figure 8 - Continued.

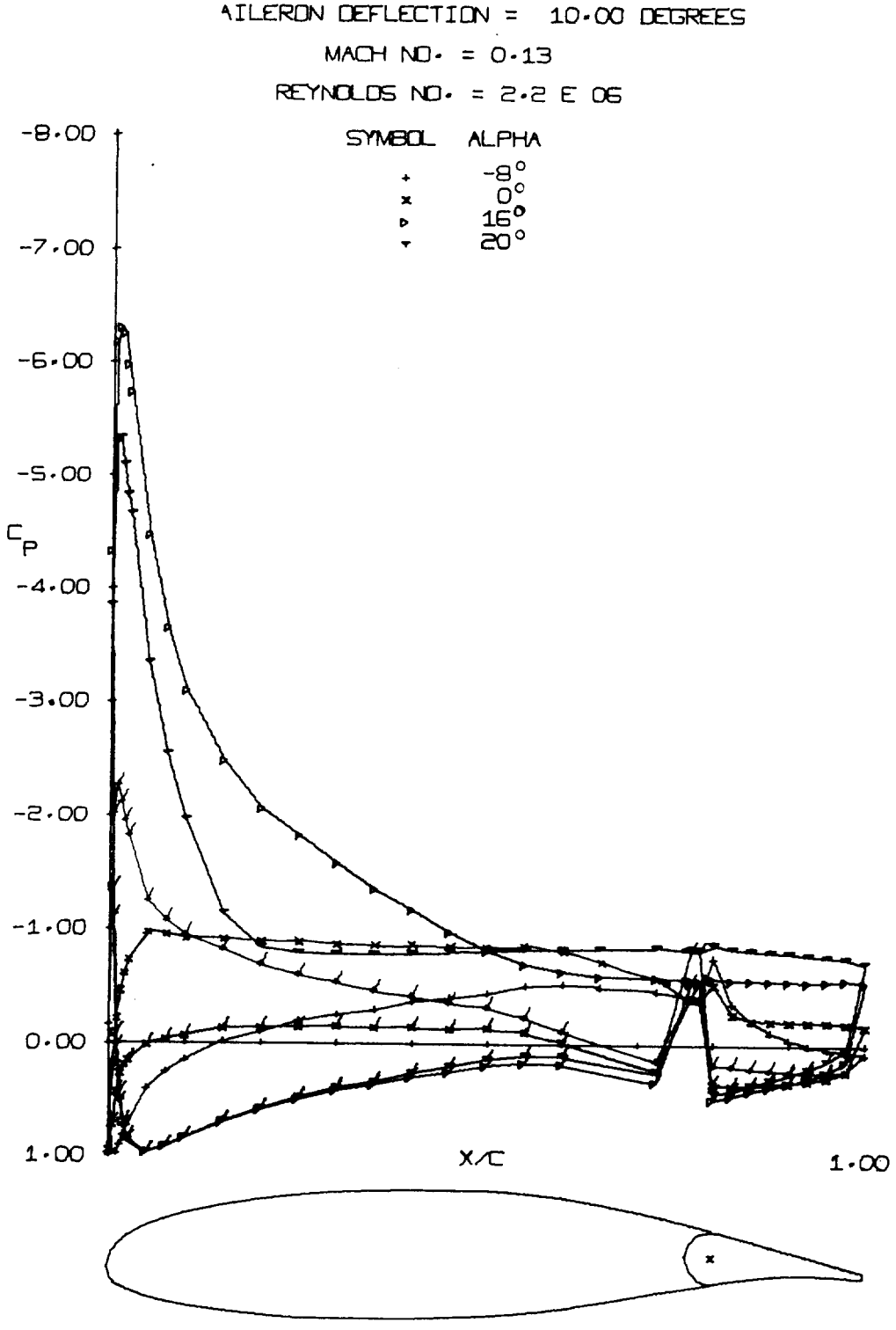

(i) +10° Aileron, Large α's.

Figure 8 - Continued.

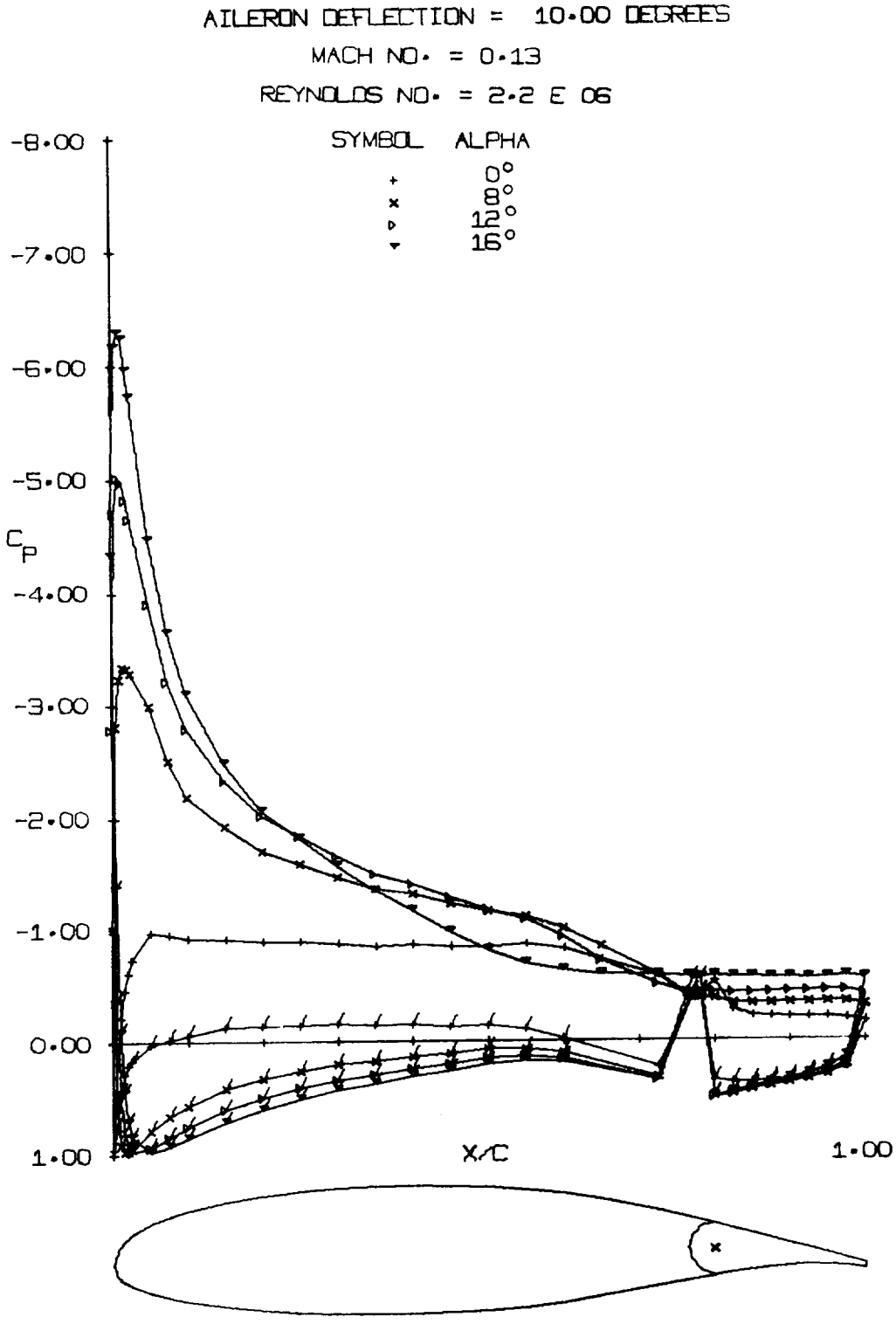

(j) +10° Aileron, Moderate α's.

Figure 8 - Concluded.

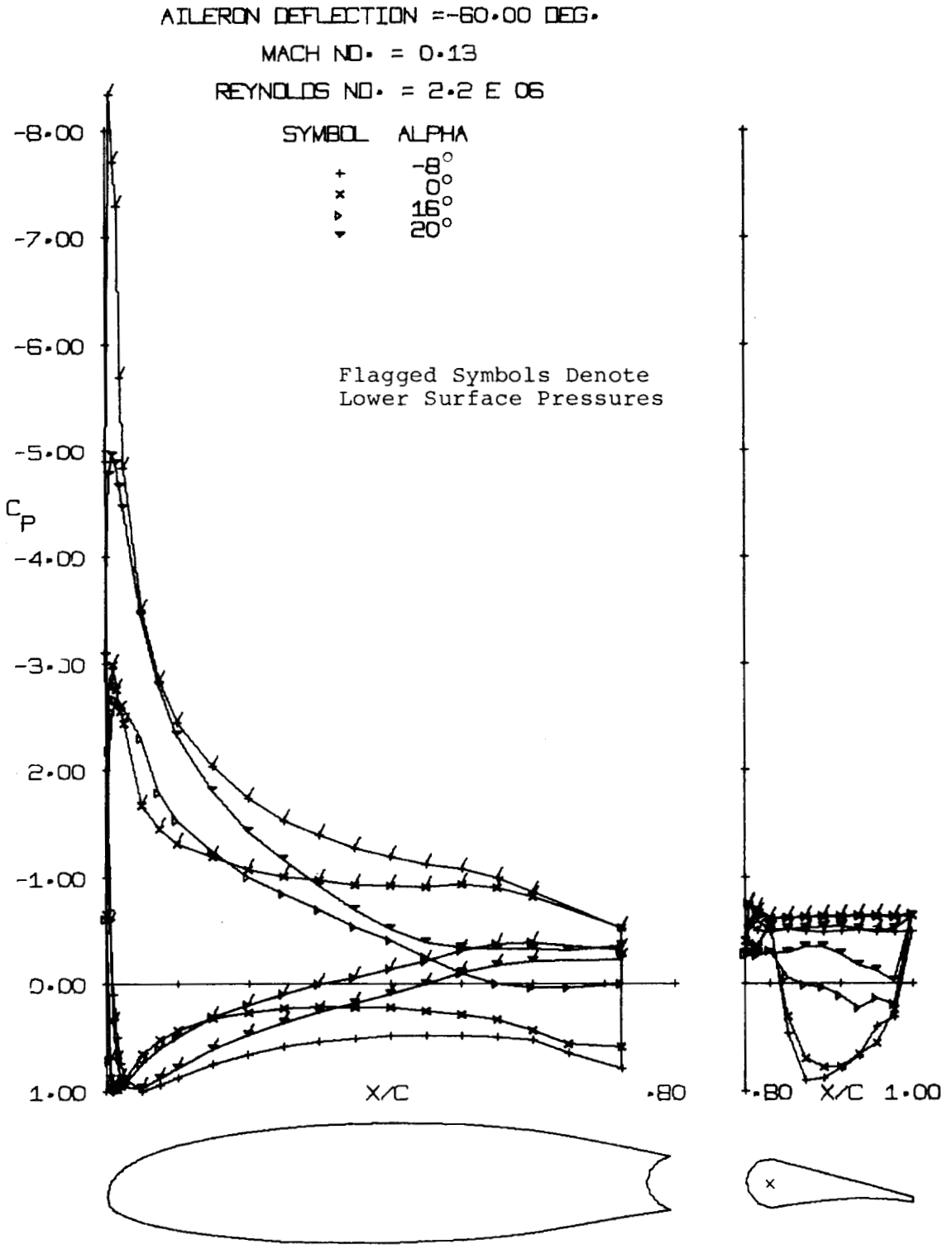

(a) -60° Aileron, Large α's

Figure 9 - Pressure Distributions with 0.5% Gap.

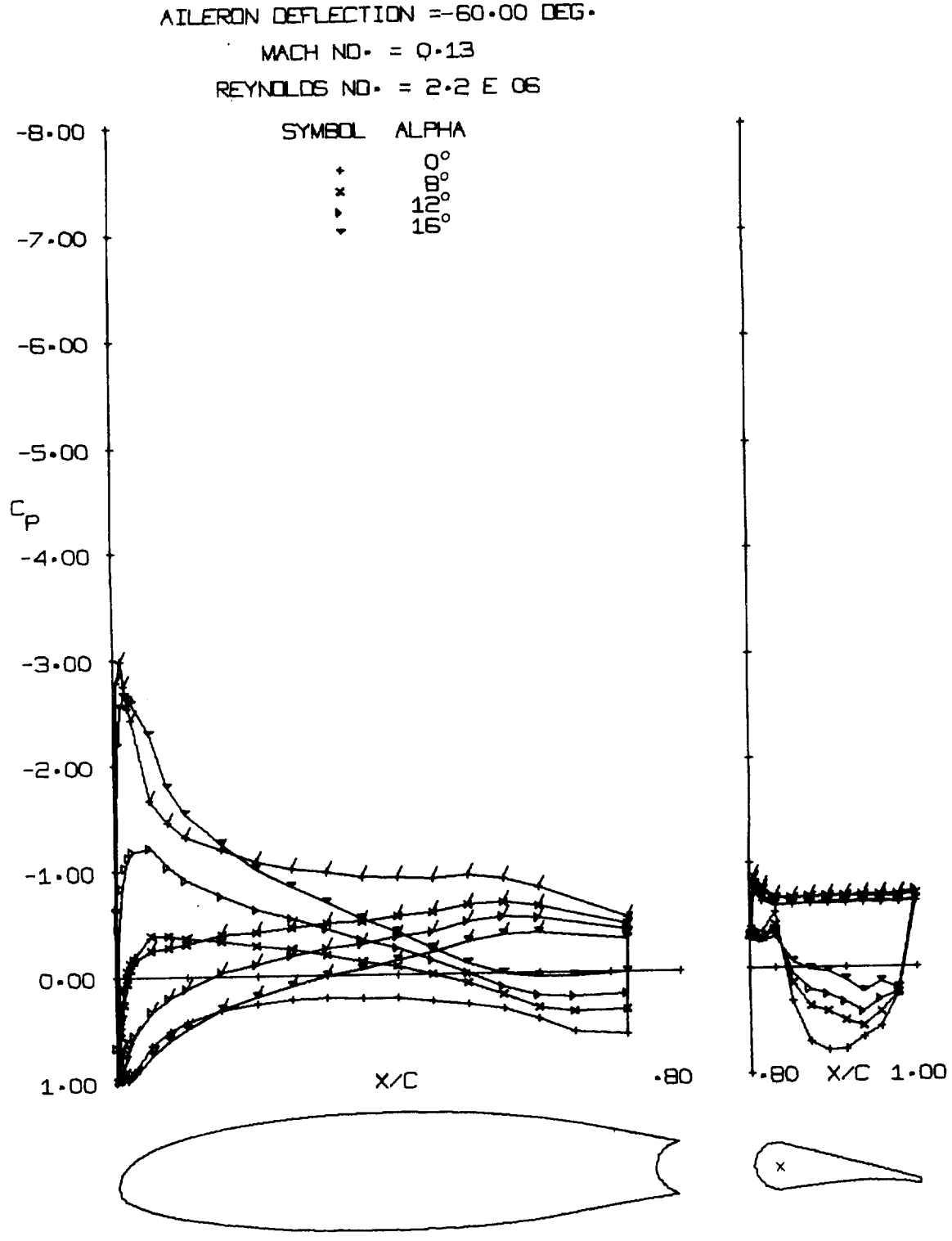

(b) -60° Aileron, Moderate α's.

Figure 9 - Continued.

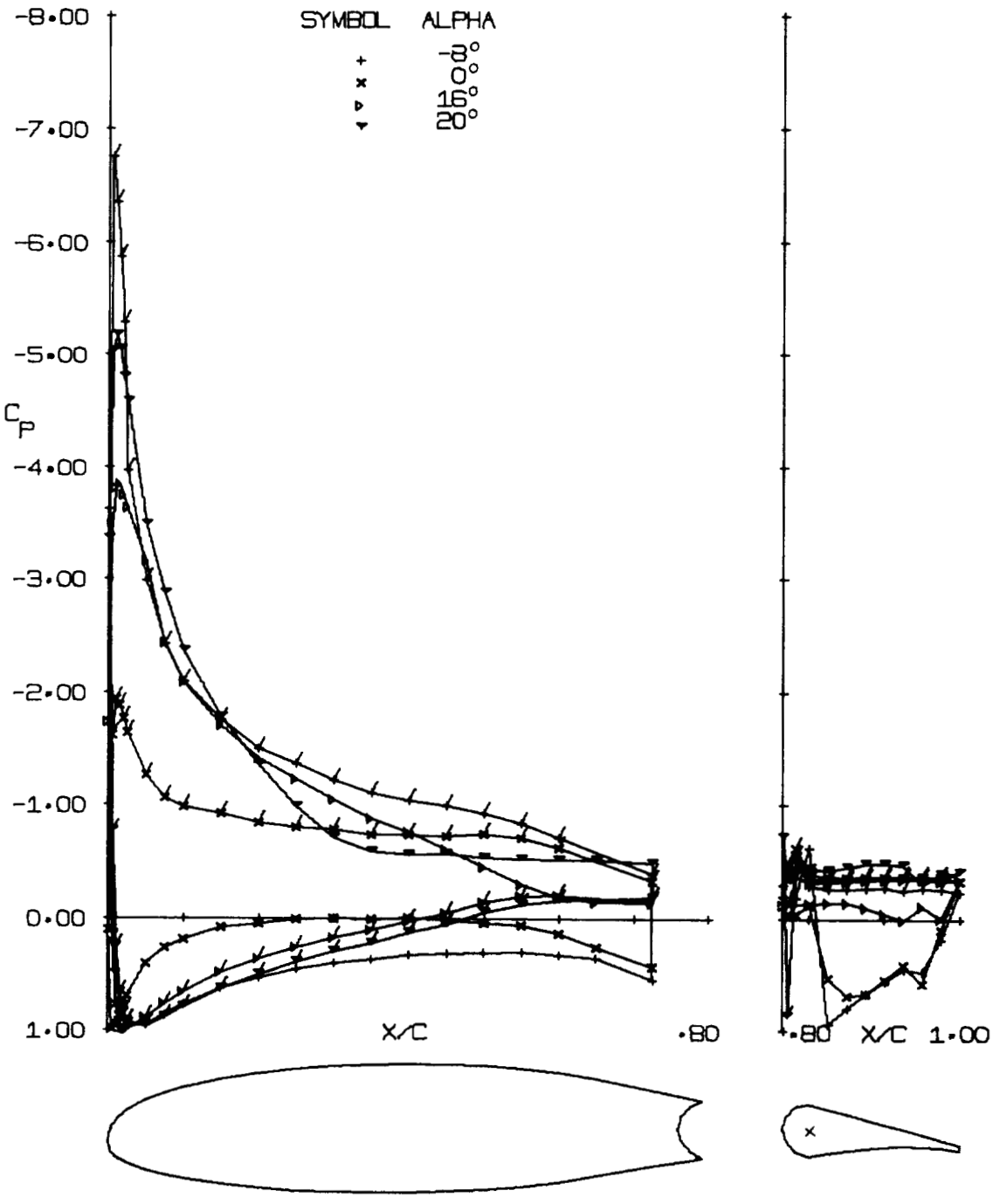

(c) -40° Aileron, Large α's.

Figure 9 - Continued.

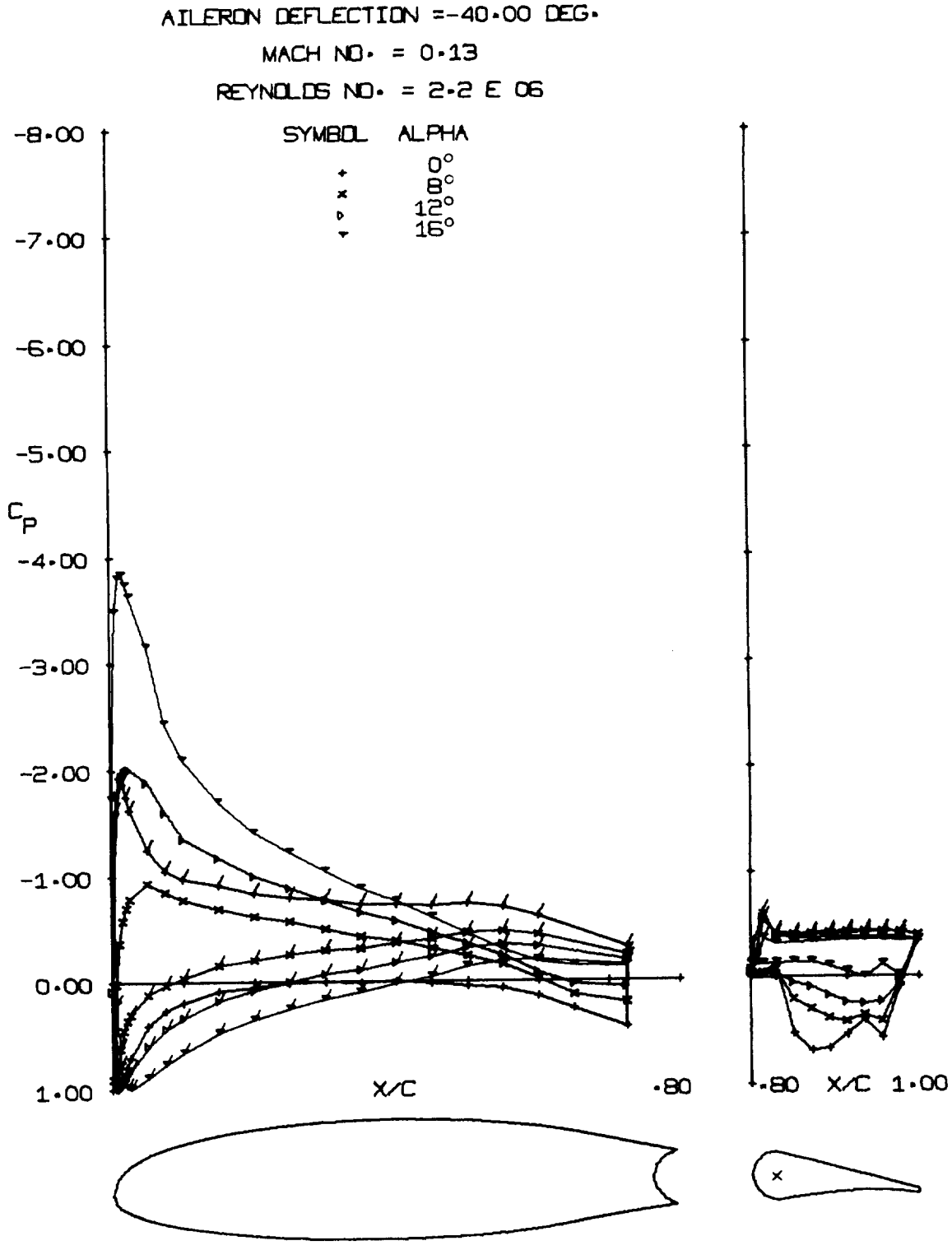

(d) -40° Aileron, Moderate α's.

Figure 9 - Continued.

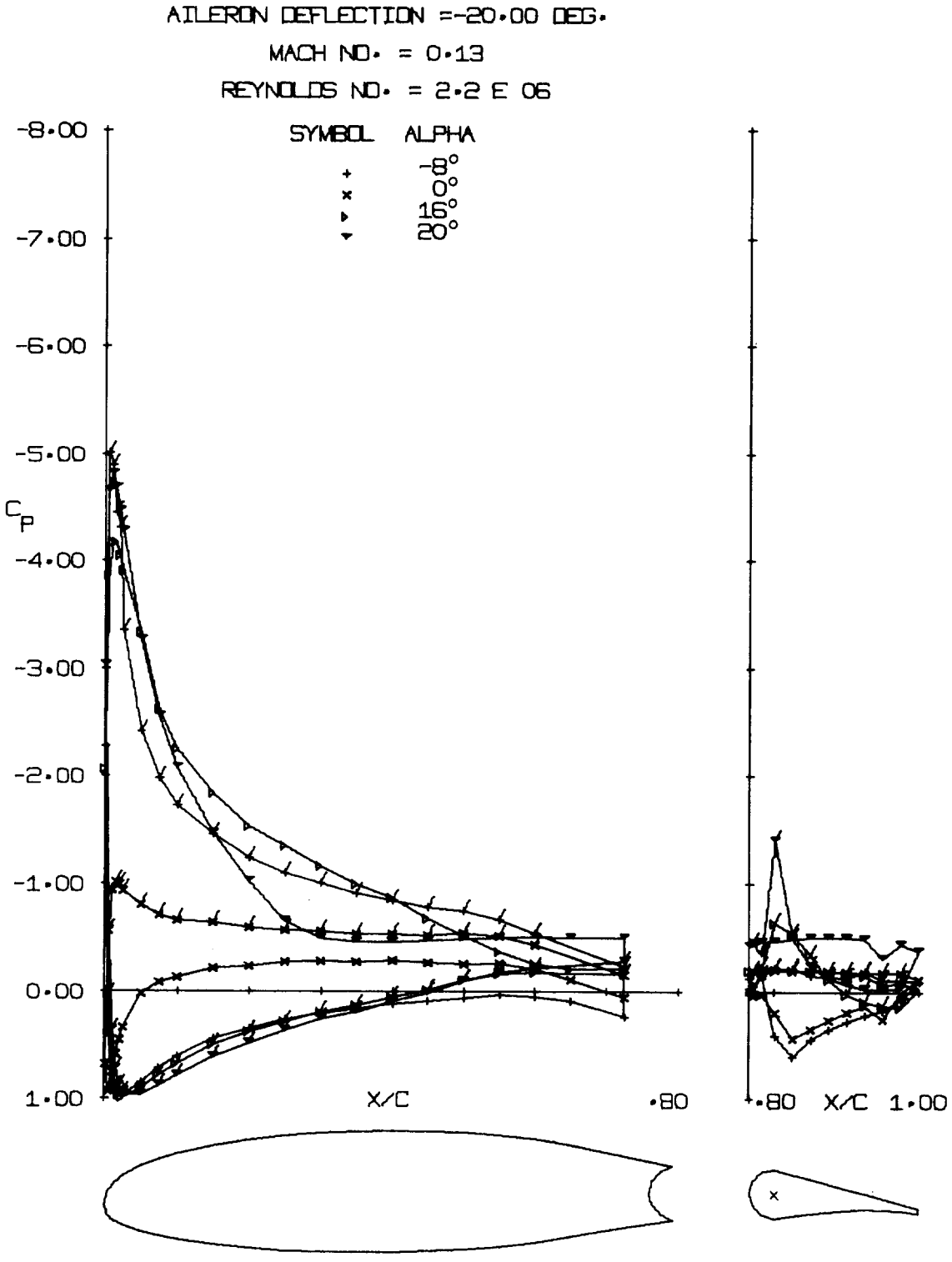

(e) -20° Aileron, Large α's.

Figure 9 - Continued.

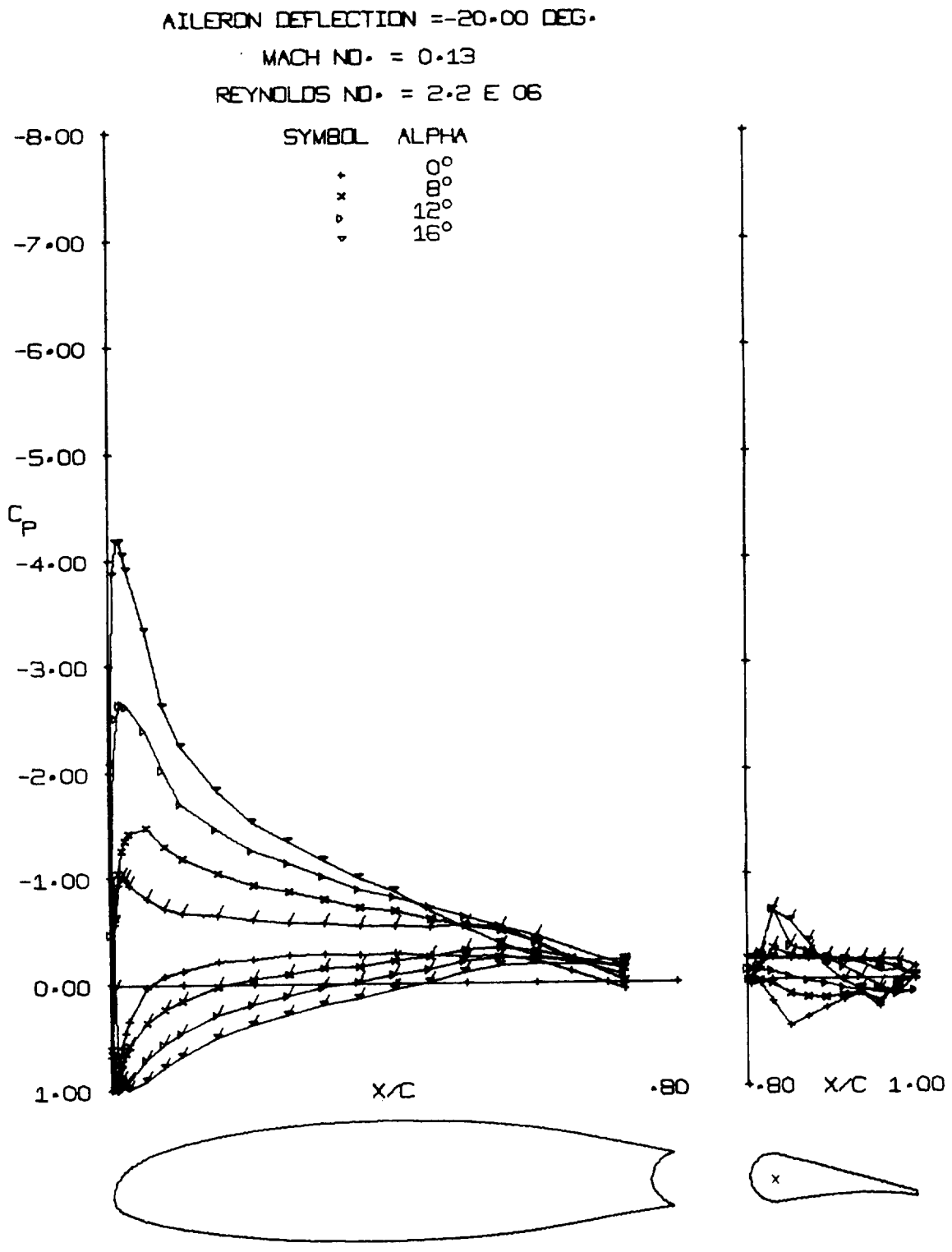

(f) -20° Aileron, Moderate α's.

Figure 9 - Continued.

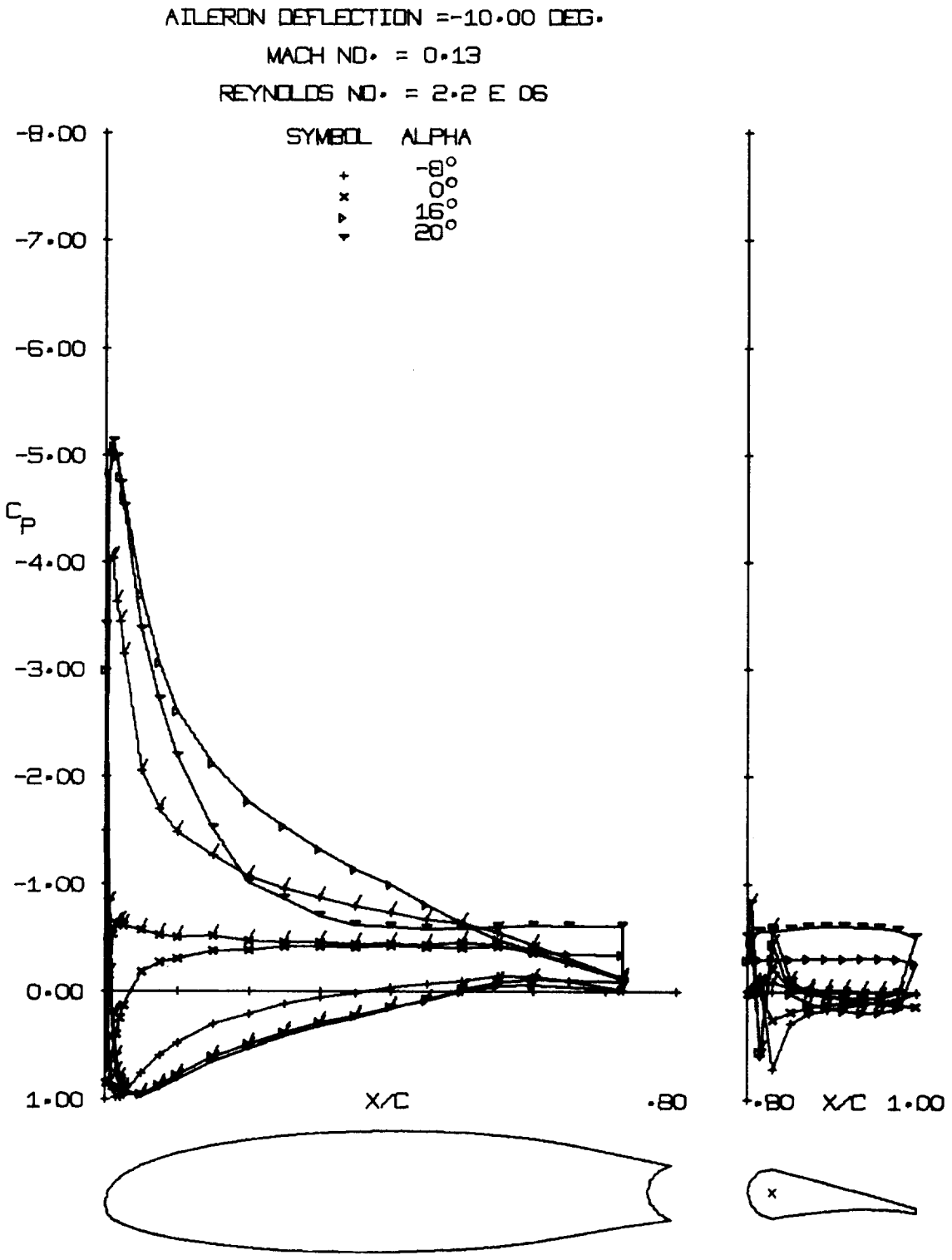

(g) -10° Aileron, Large α's.

Figure 9 - Continued.

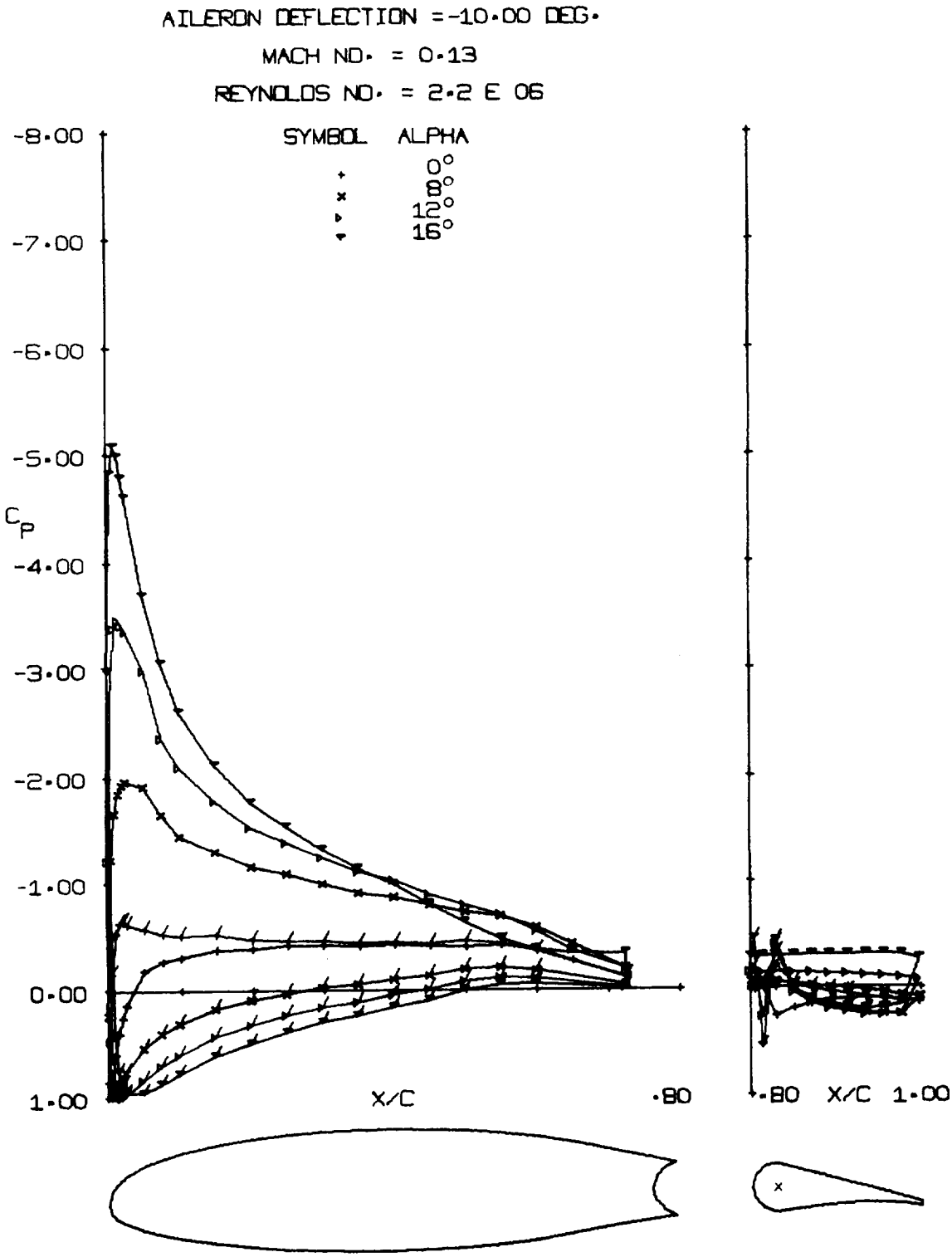

(h) -10° Aileron, Moderate α's.

Figure 9 - Continued.

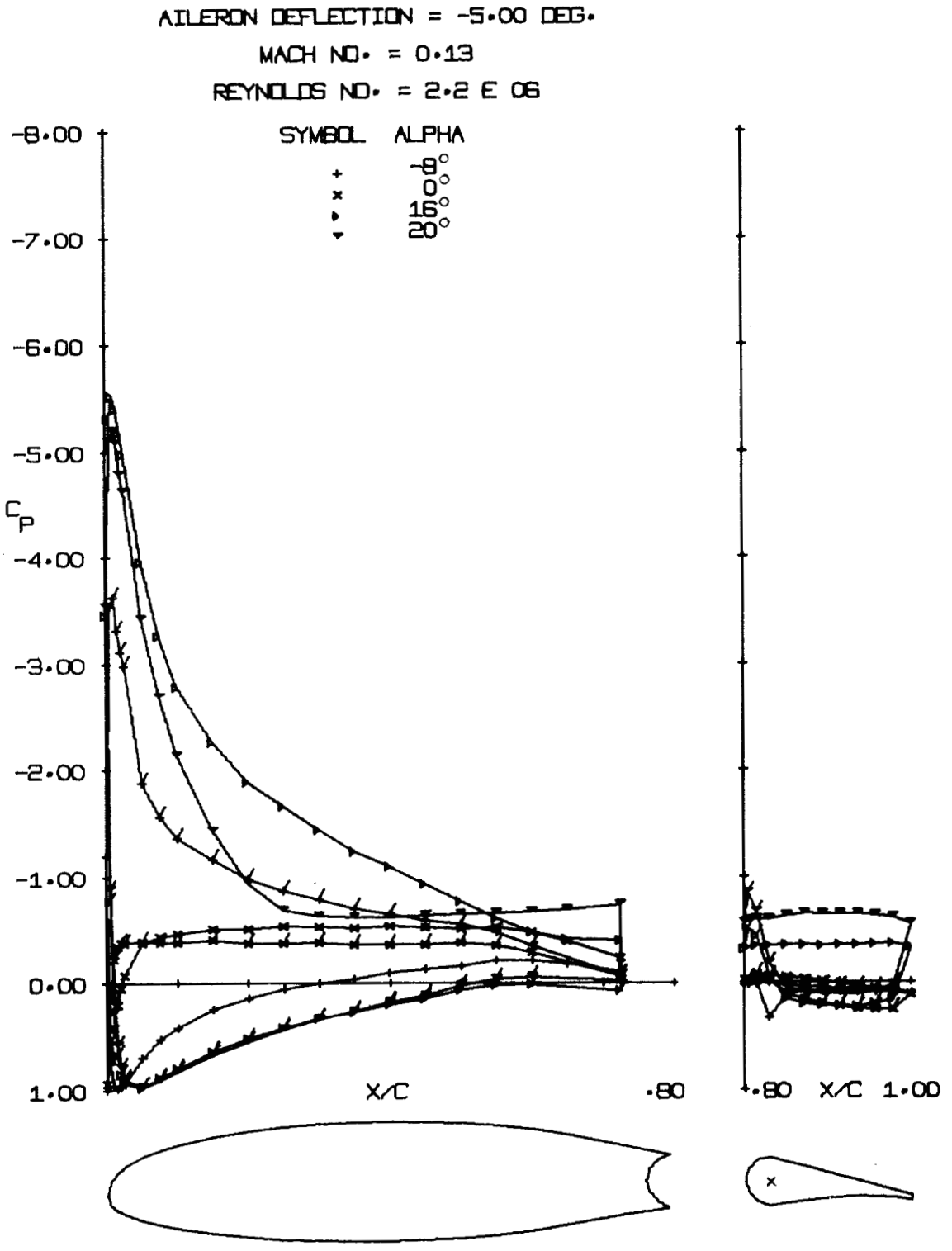

(i) -5° Aileron, Large α's.

Figure 9 - Continued.

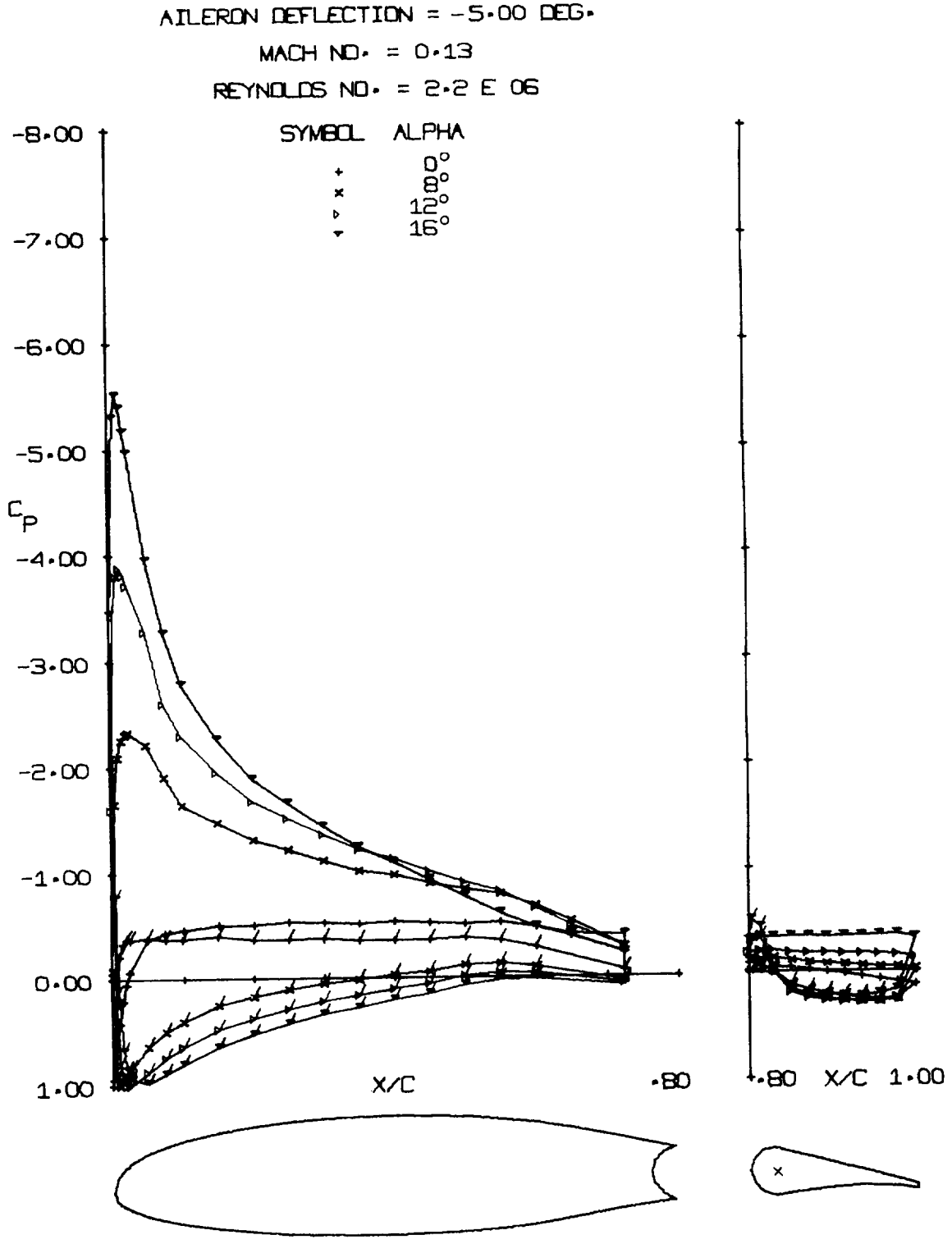

(j) -5° Aileron, Moderate α's.

Figure 9 - Continued.

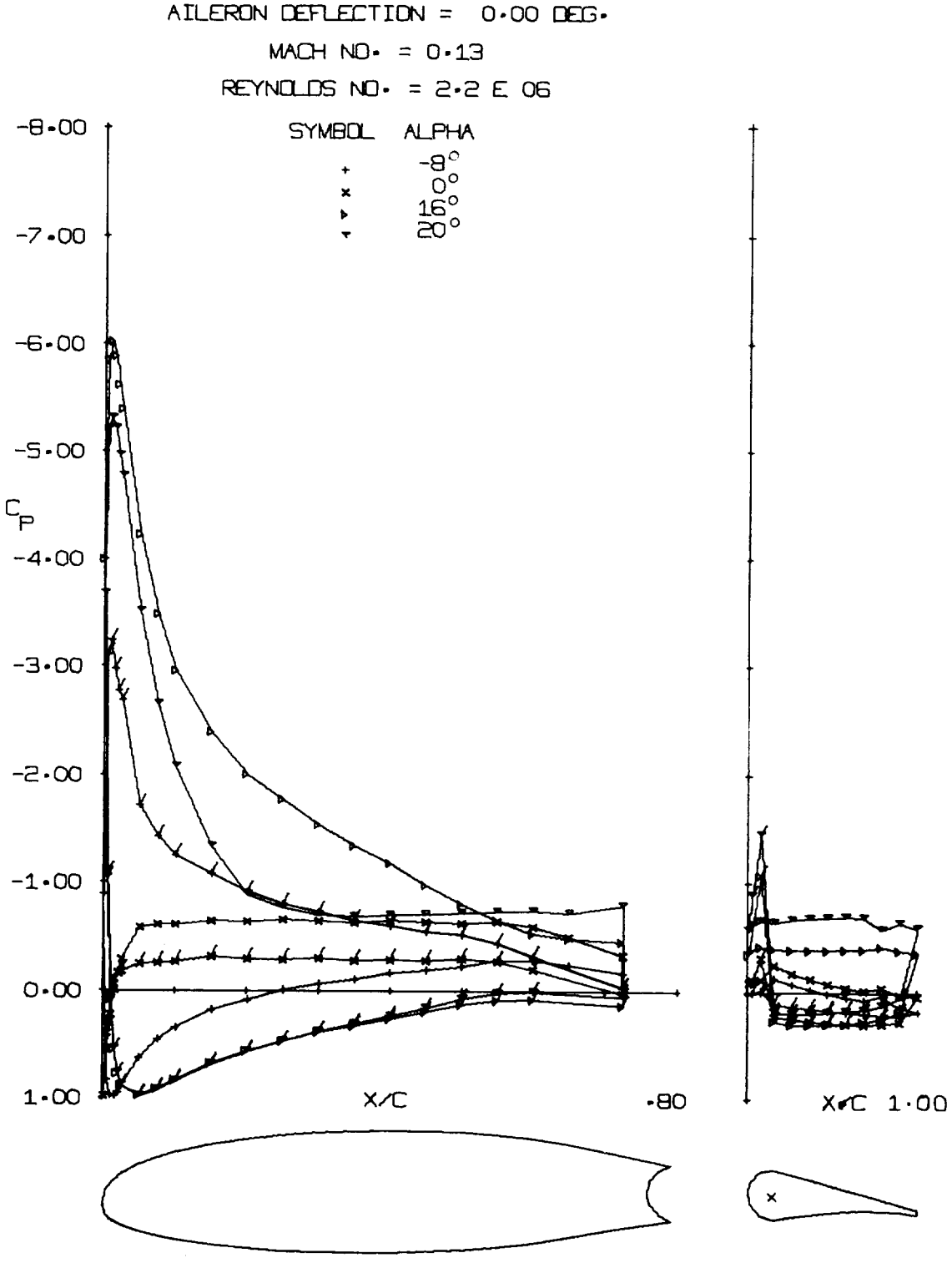

(k) 0° Aileron, Large α's.

Figure 9 - Continued.

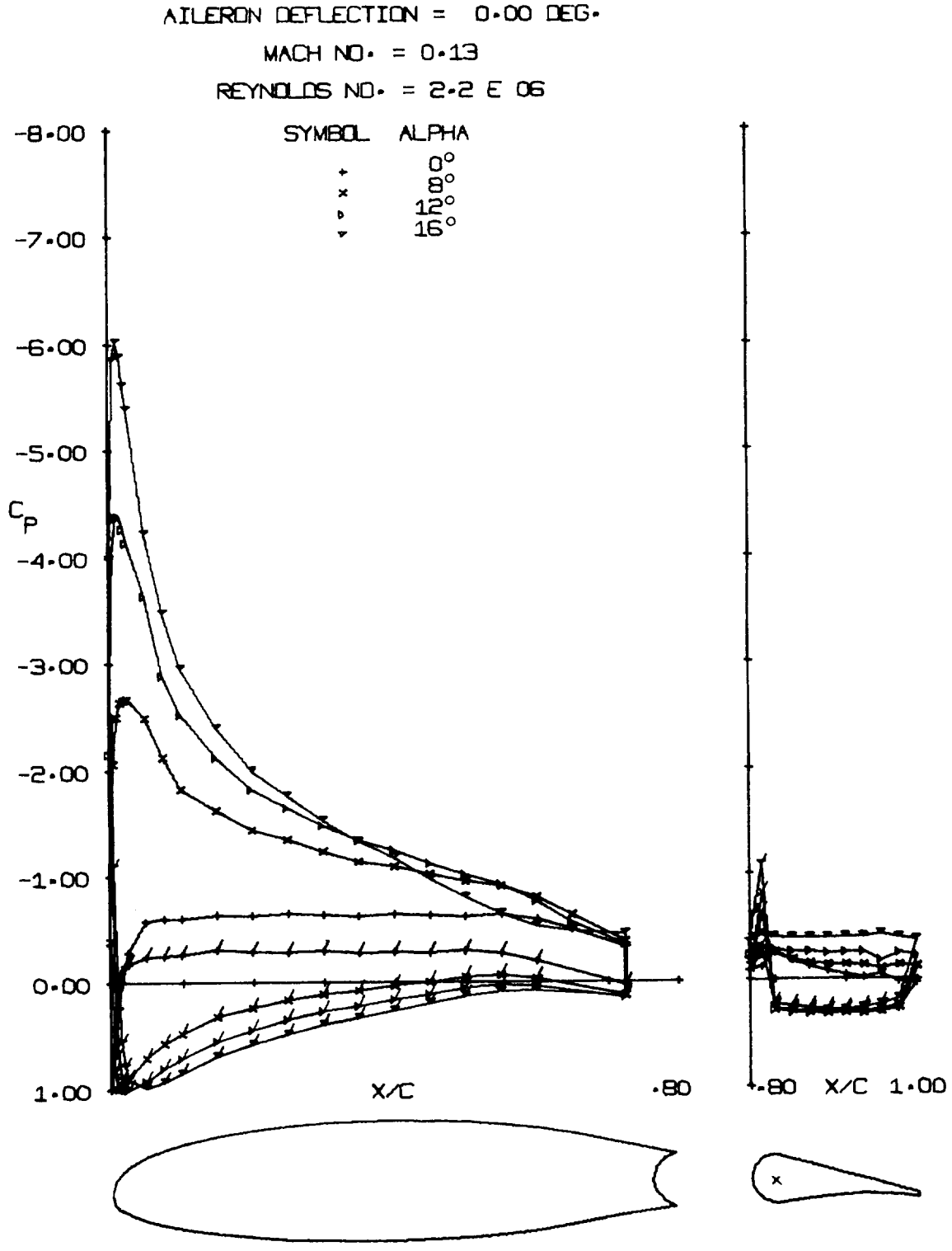

(1) 0° Aileron, Moderate α's.

Figure 9 - Continued.

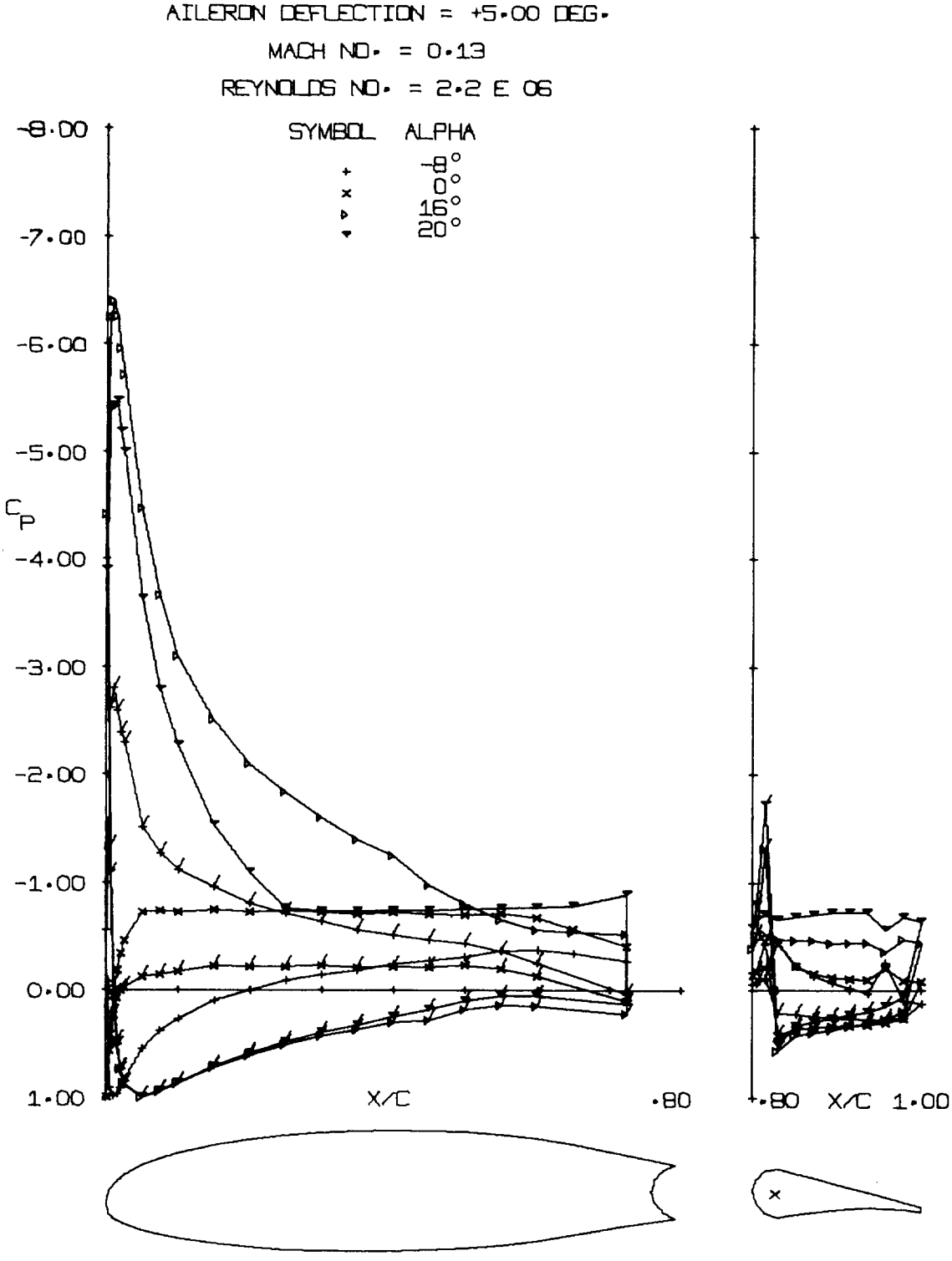

(m) 5° Aileron, Large α's.

Figure 9 - Continued.

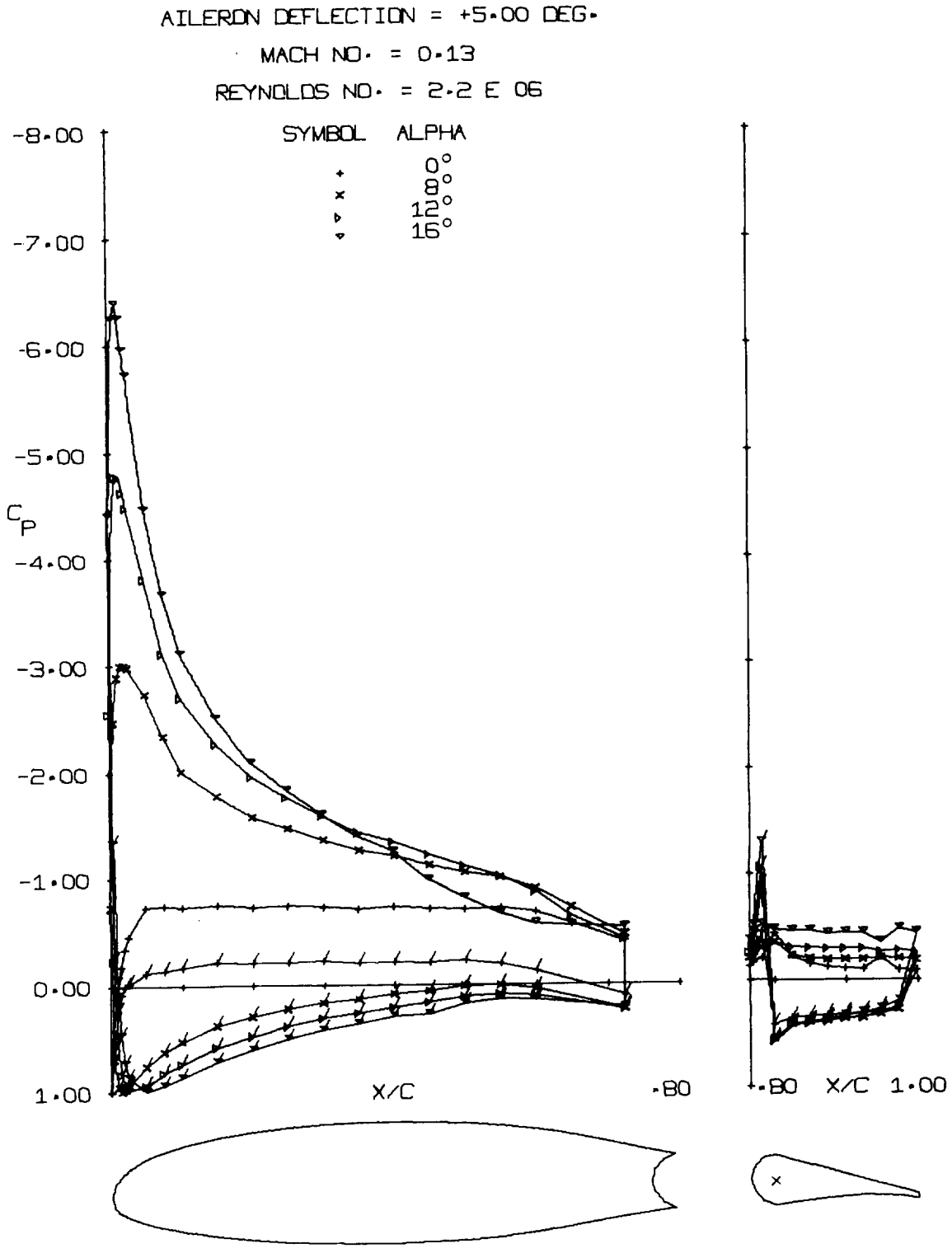

(n) 5° Aileron, Moderate α's.

Figure 9 - Continued.

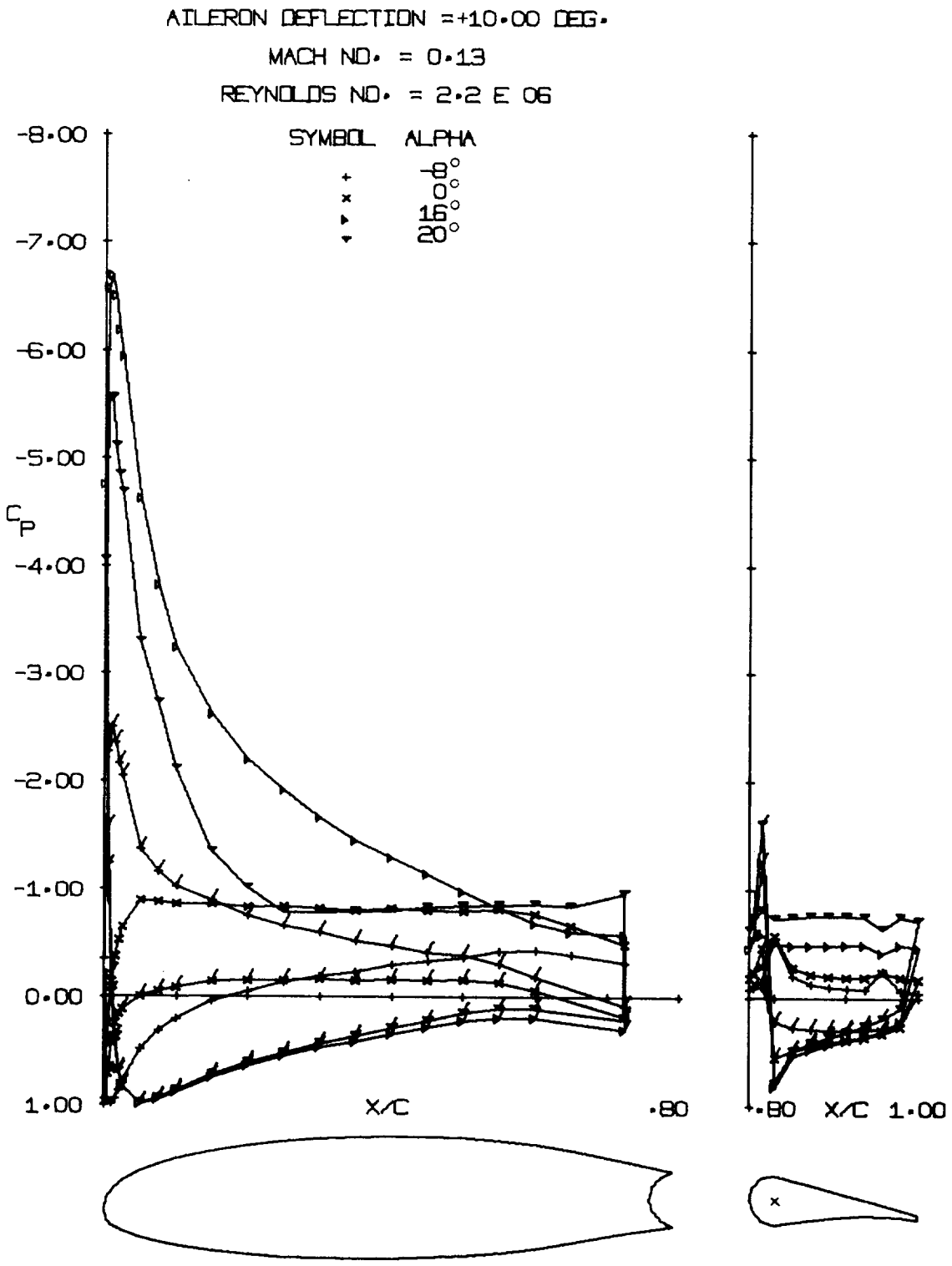

(o) 10° Aileron, Large α's.

Figure 9 - Continued.

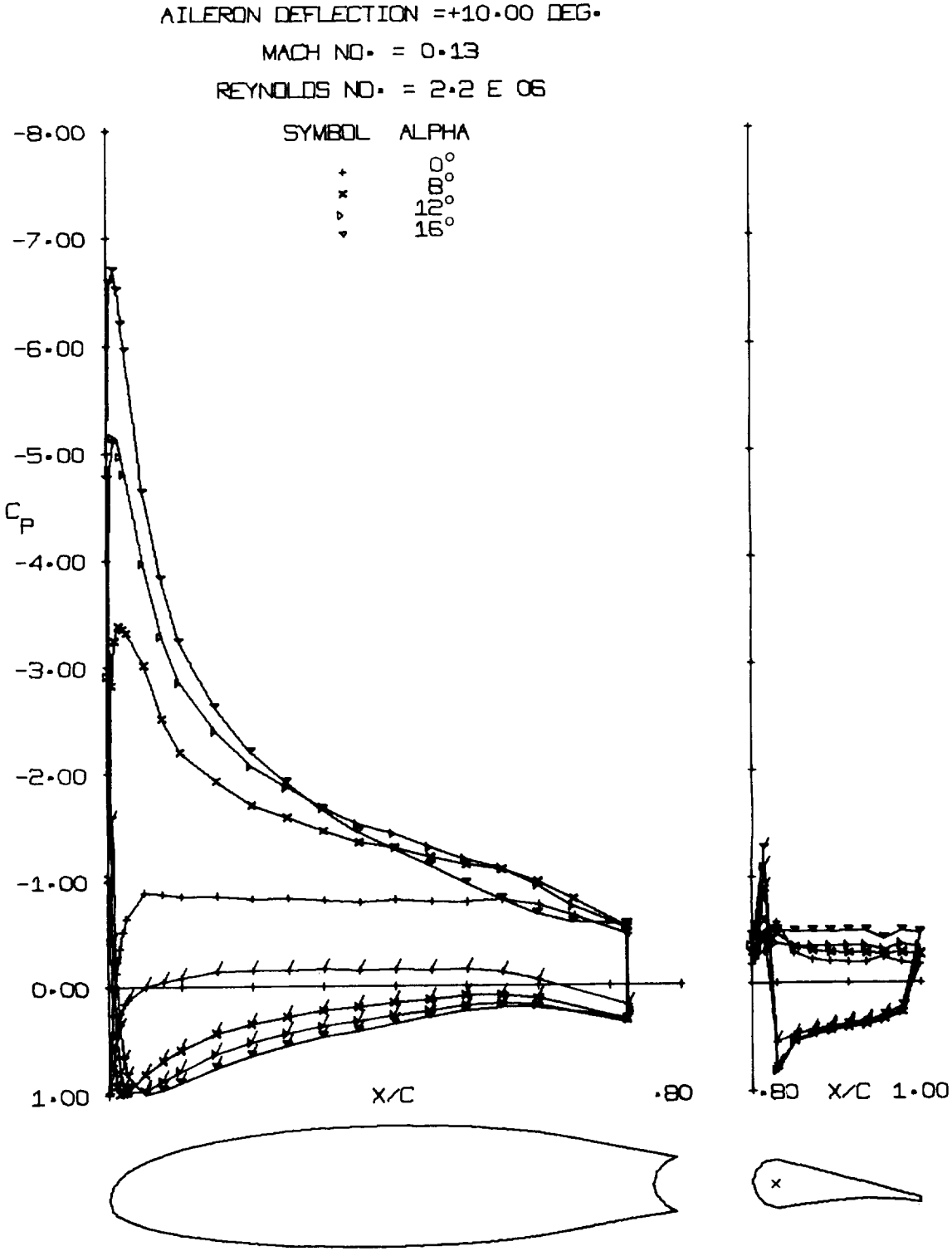

(p) 10° Aileron, Moderate α's.

Figure 9 - Continued.

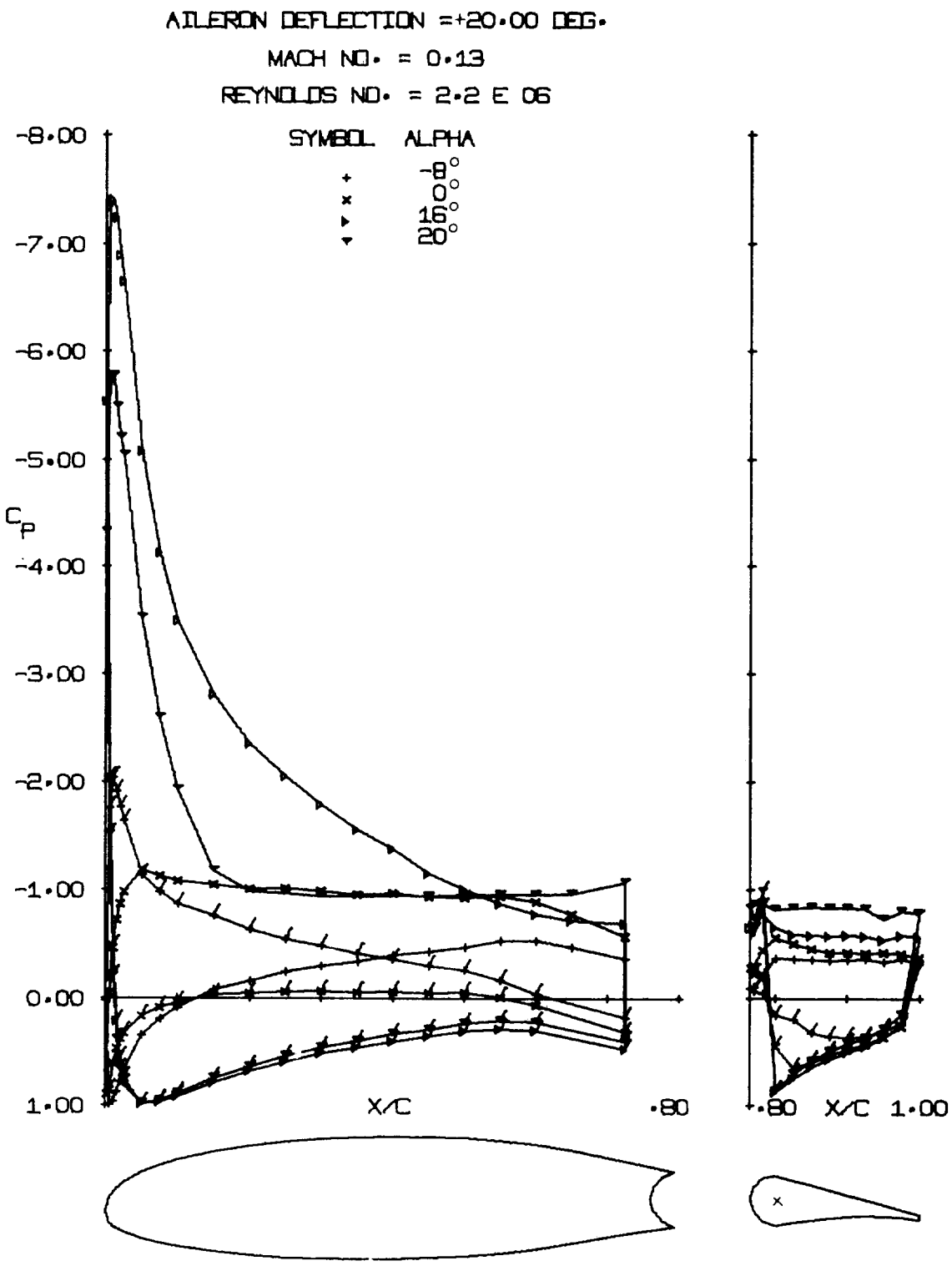

(q) 20° Aileron, Large α's.

Figure 9 - Continued.

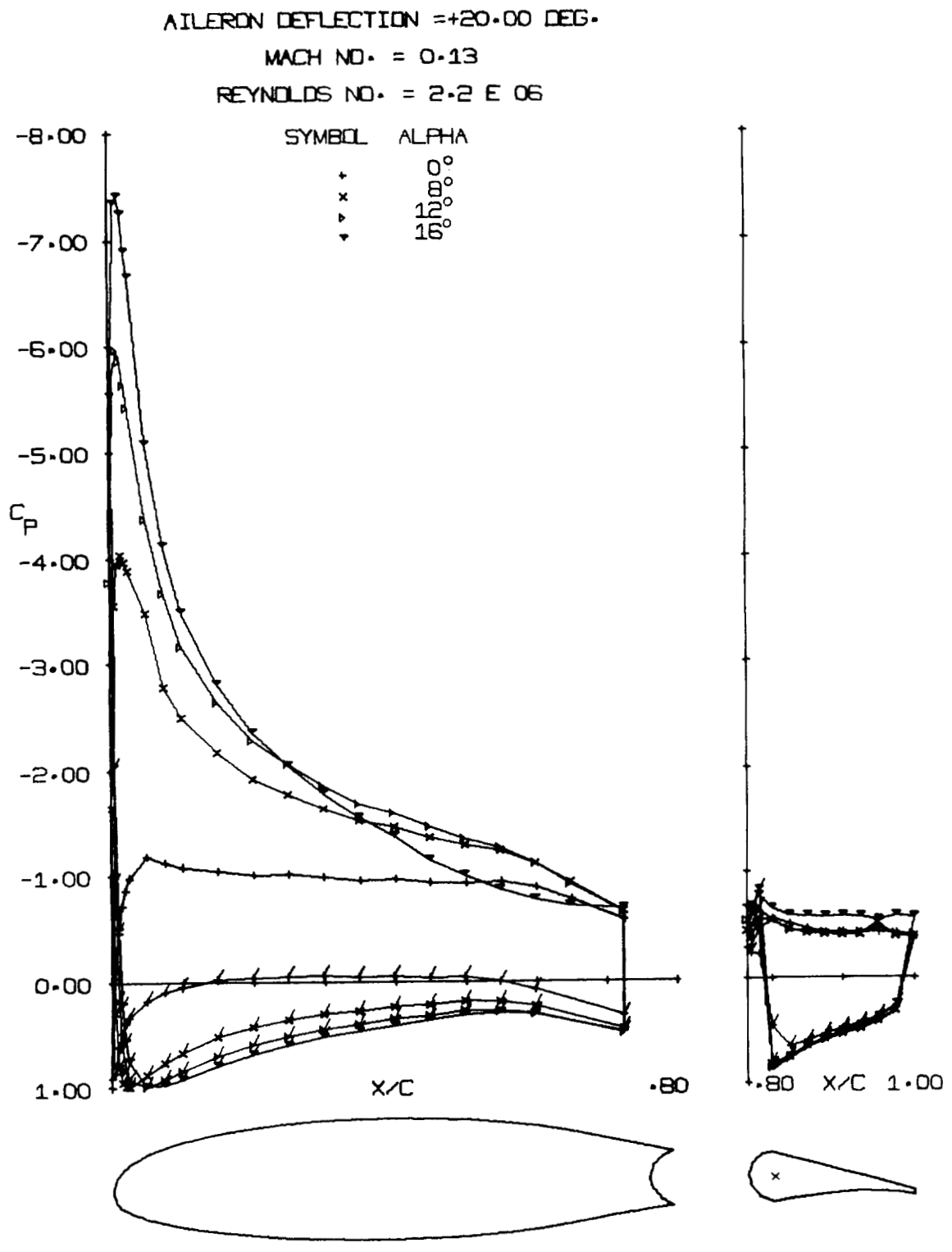

(r) 20° Aileron, Moderate α's.

Figure 9 - Continued.

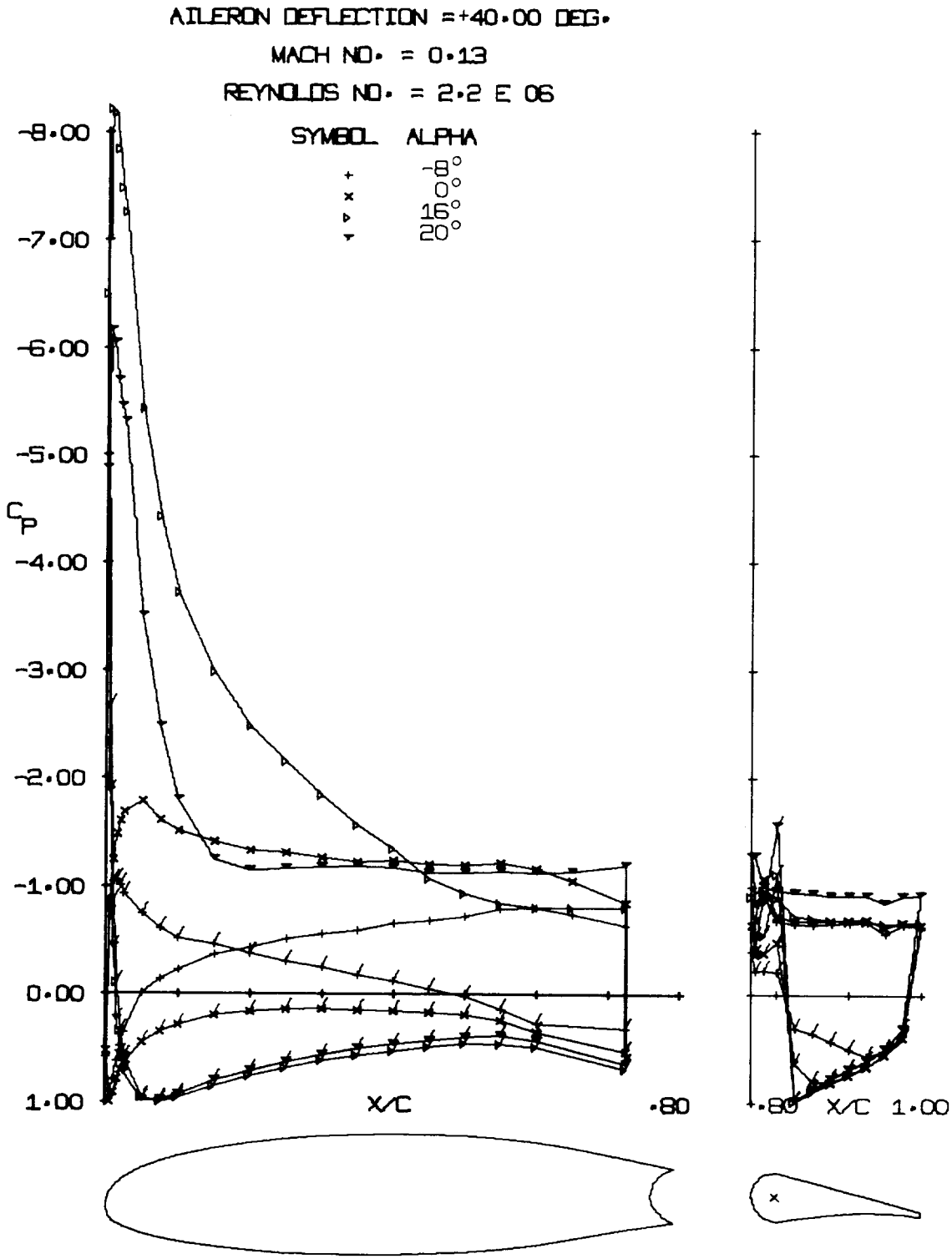

(s) 40° Aileron, Large α's.

Figure 9 - Continued.

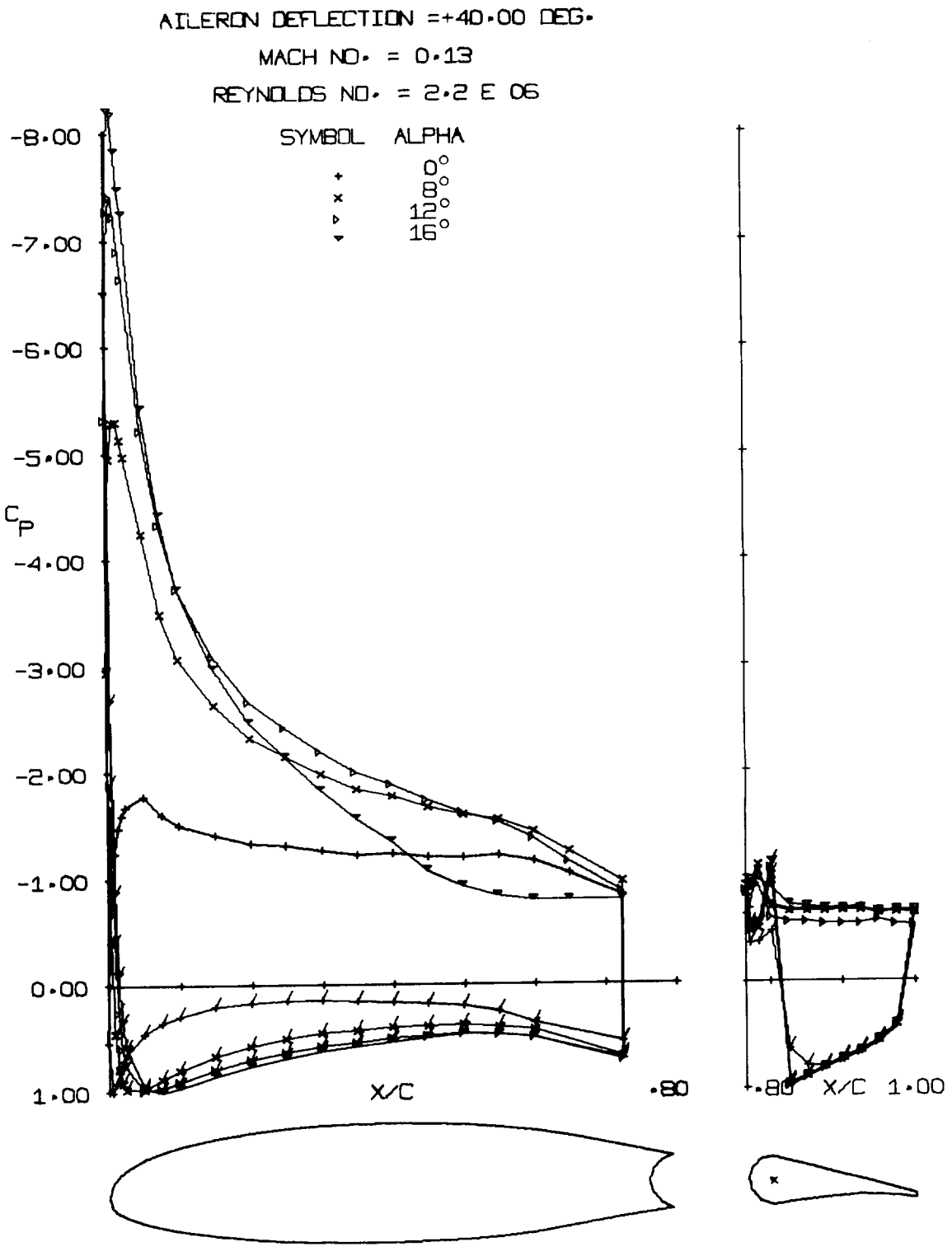

(t) 40° Aileron, Moderate α's.

Figure 9 - Continued.

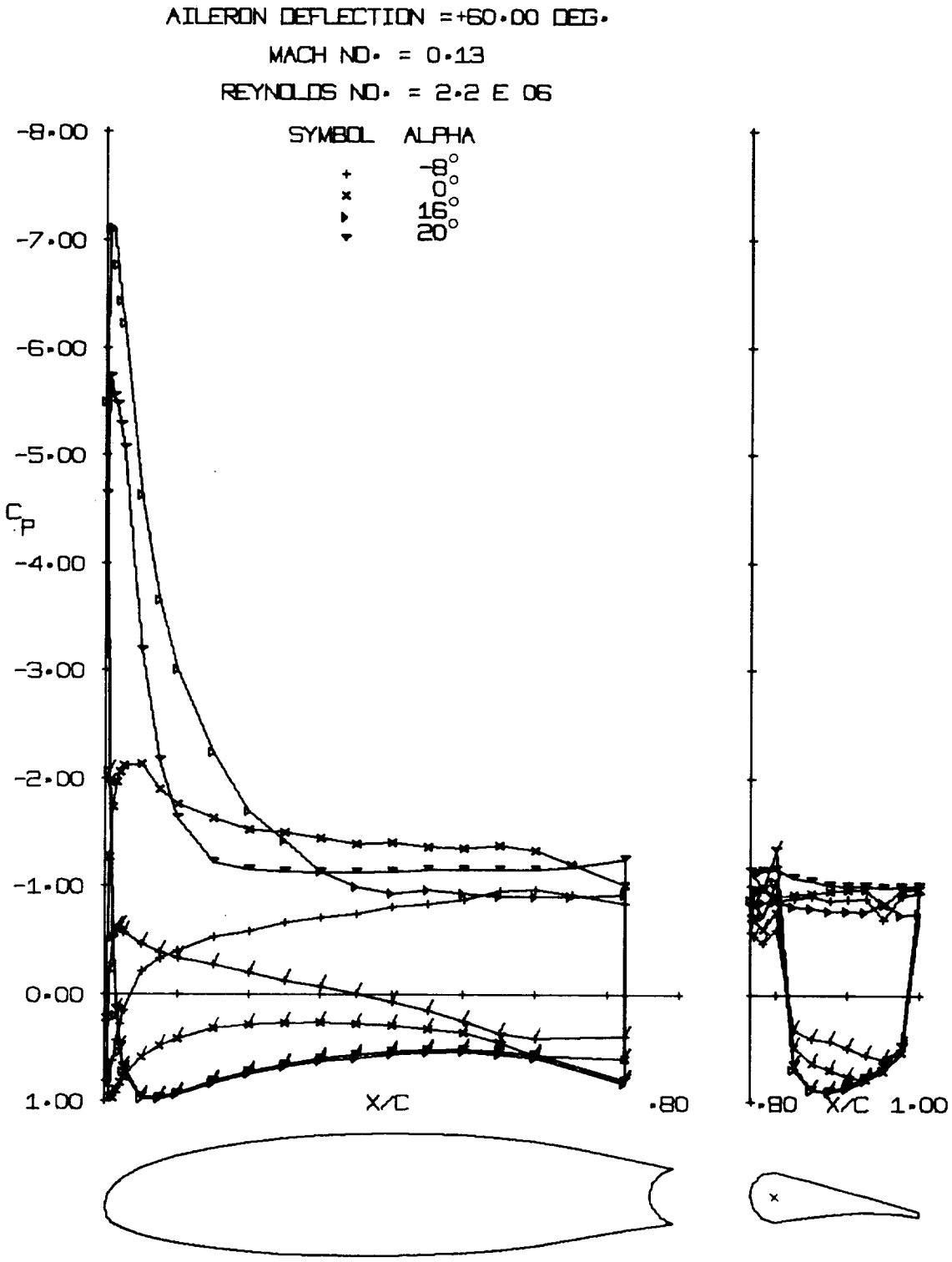

(u) 60° Aileron, Large α's.

Figure 9 - Continued.

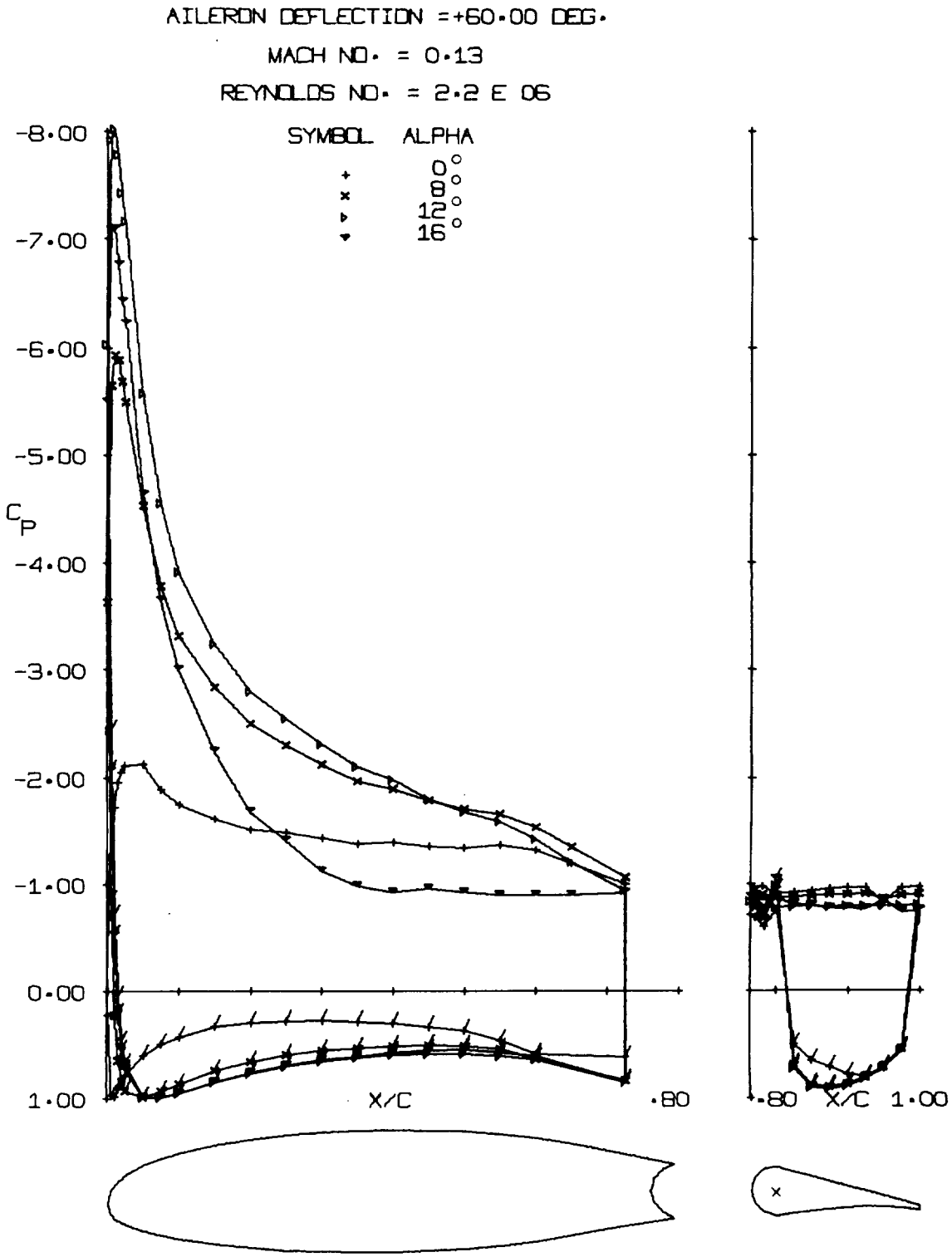

(v) 60° Aileron, Moderate α's.

Figure 9 - Concluded.

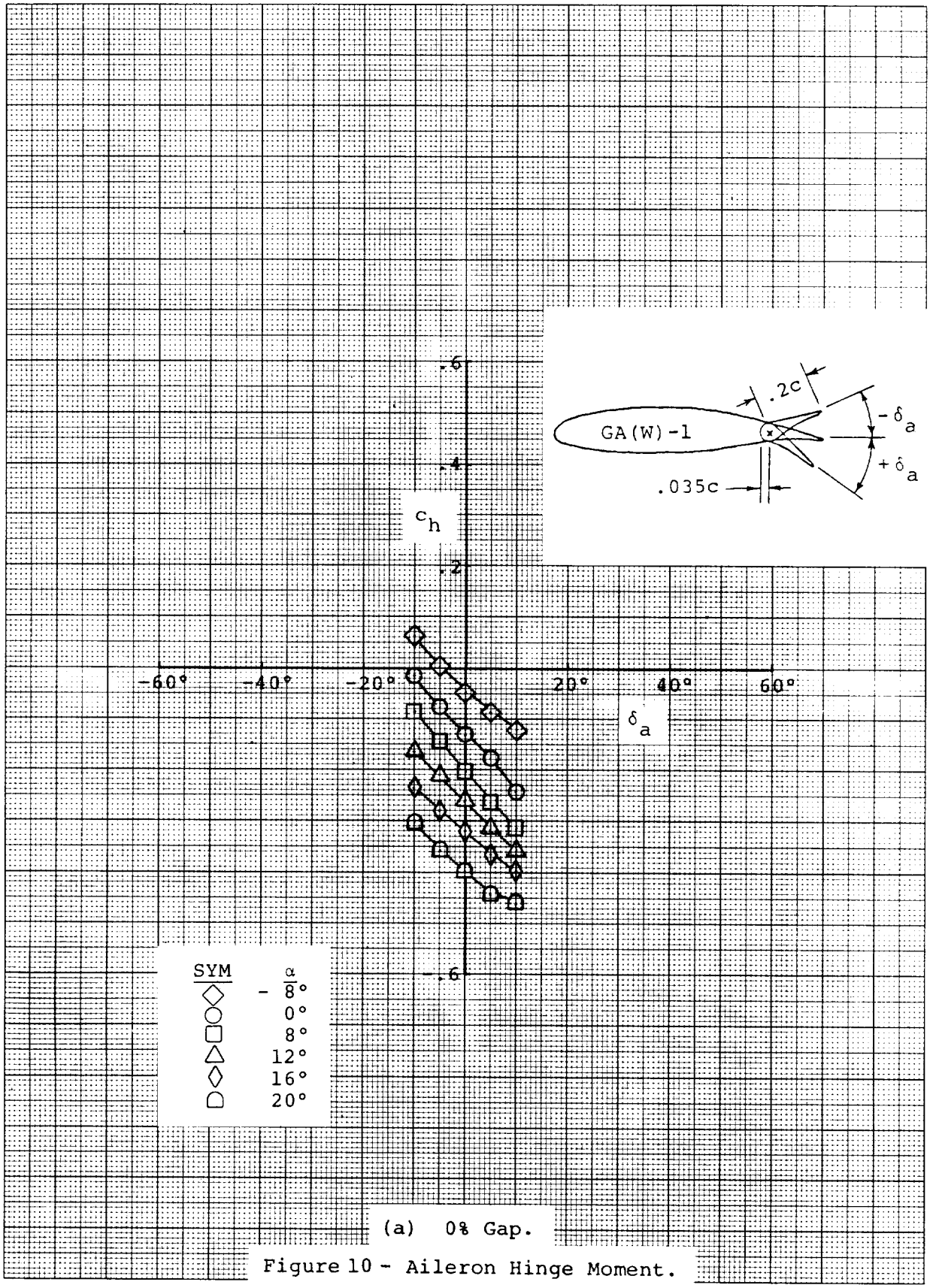

(a) 0% Gap.

Figure 10 - Aileron Hinge Moment.

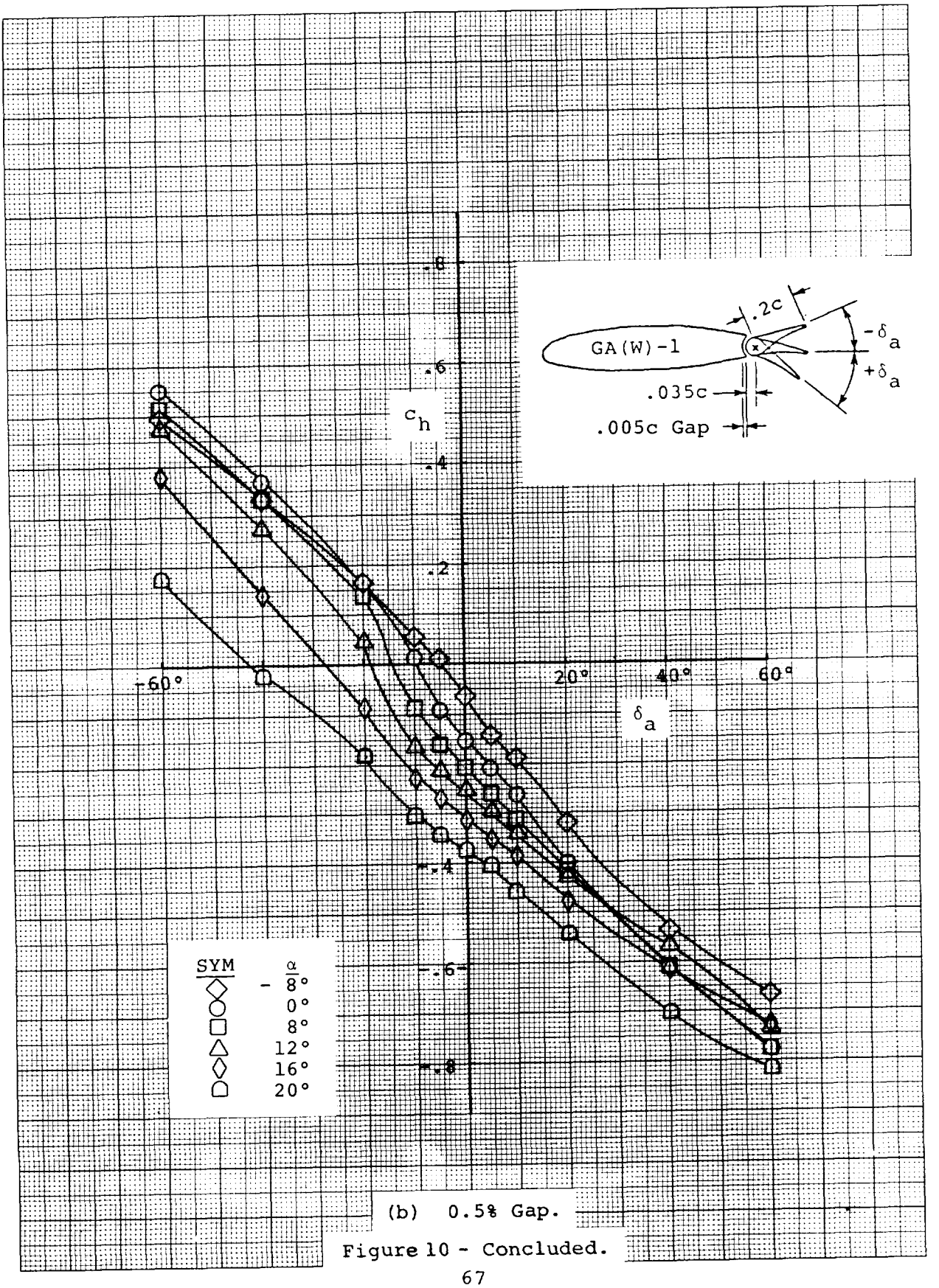

(b) 0.5% Gap.

Figure 10 - Concluded.

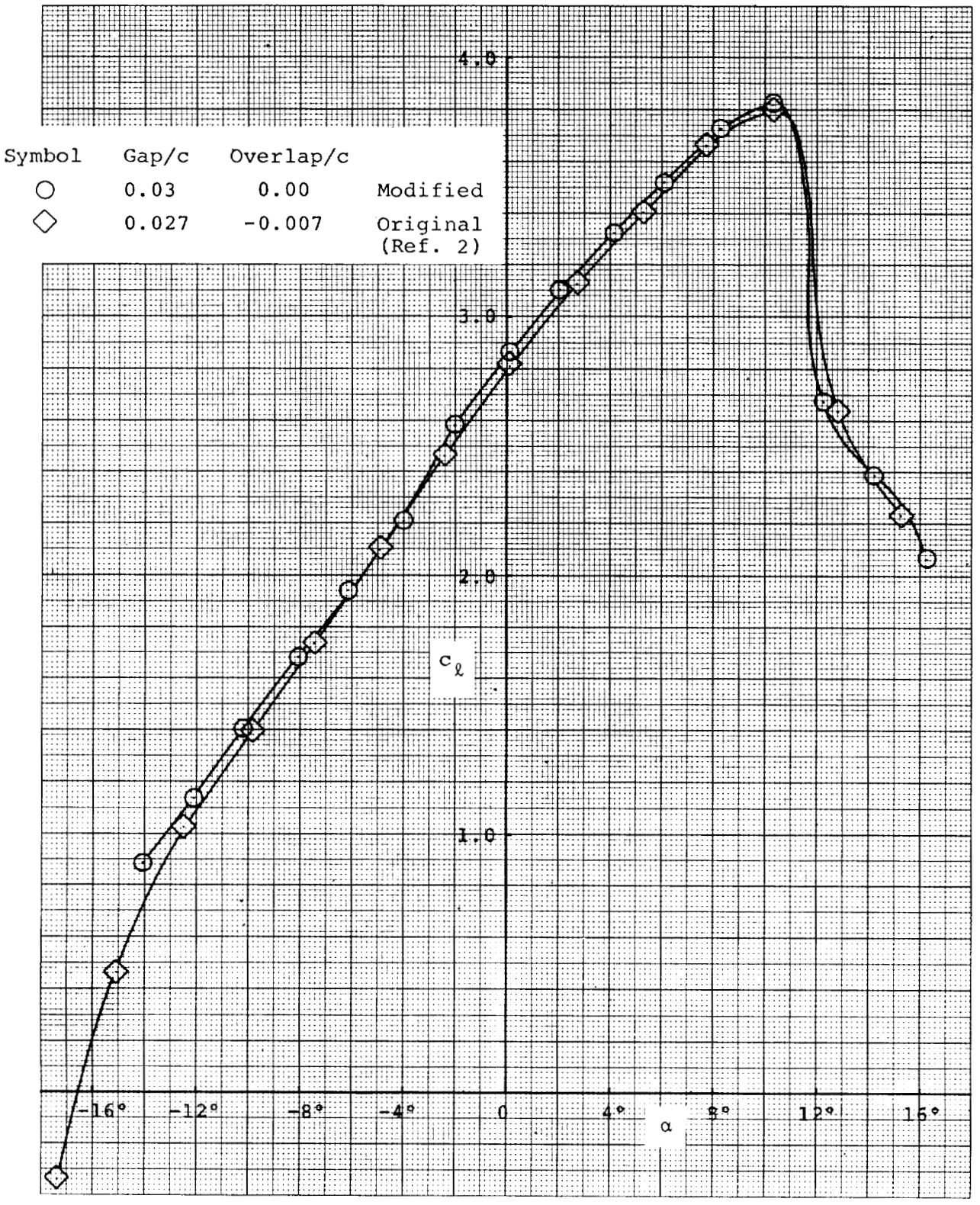

Figure 11 - Lift comparison between modified flap geometry and original flap geometry, $\delta_f = 40°$.

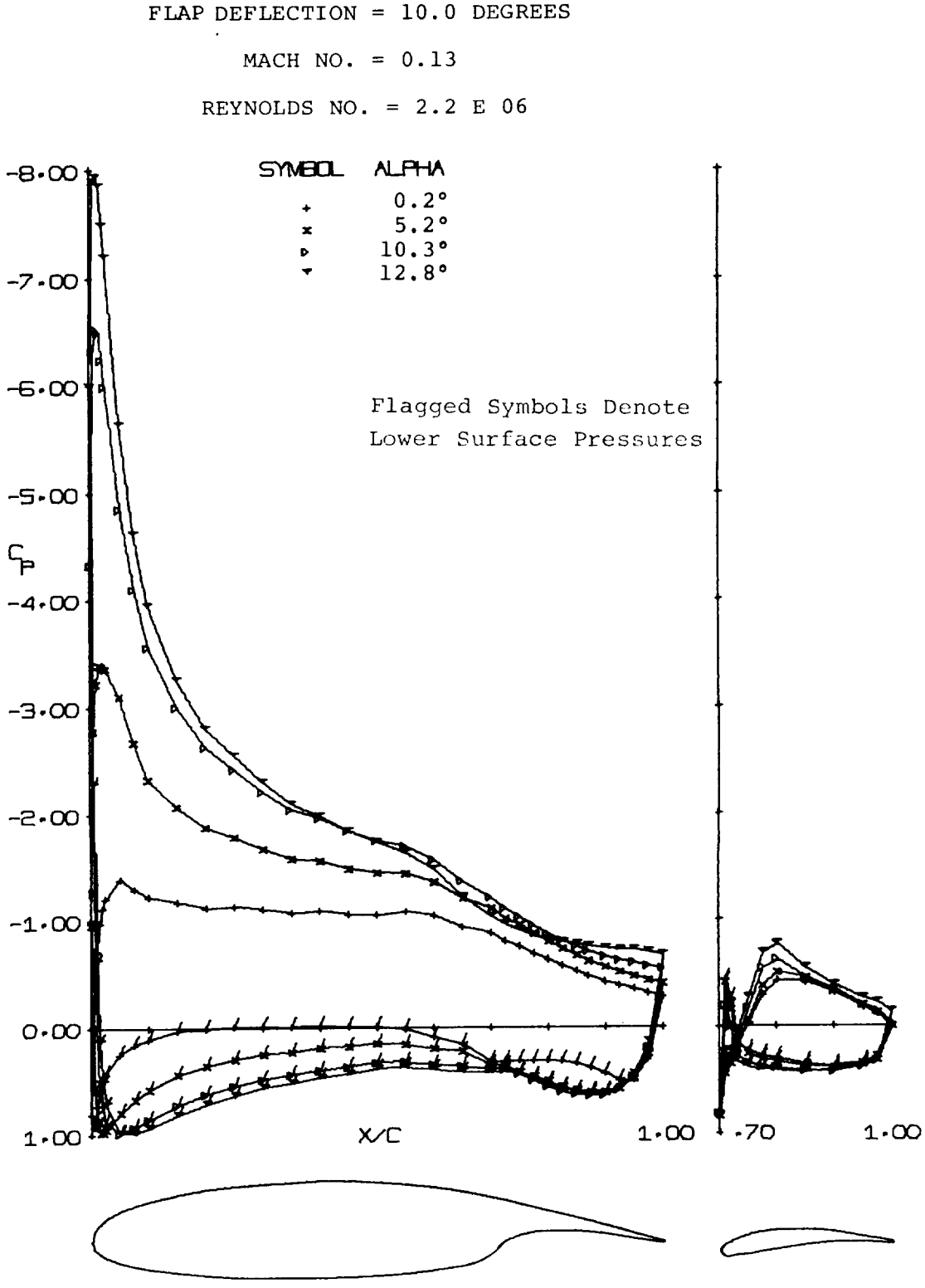

(a) 10° Flap.

Figure 12 - Experimental Pressure Distributions.

FLAP DEFLECTION = 20.0 DEGREES

MACH NO. = 0.13

REYNOLDS NO. = 2.2 E 06

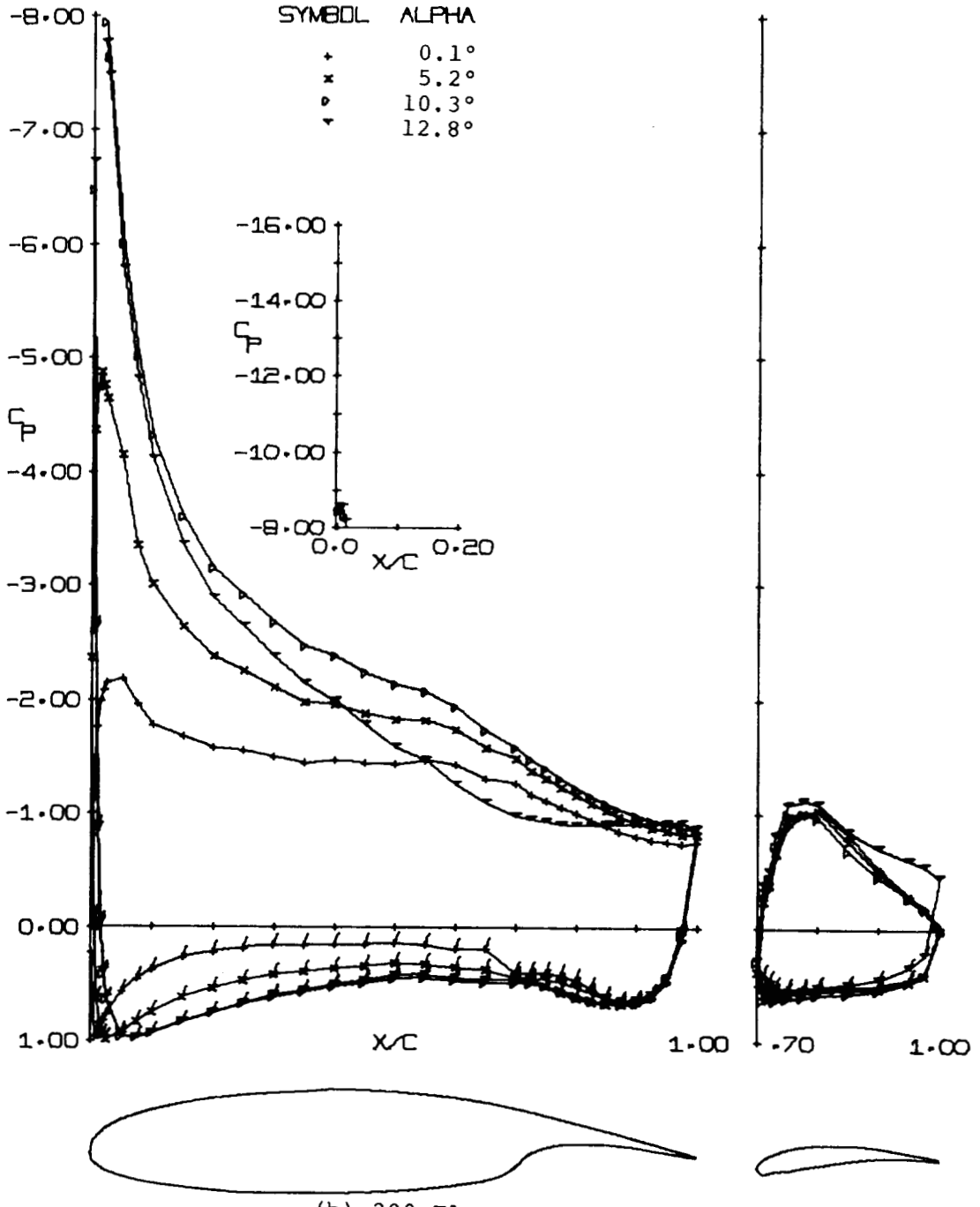

(b) 20° Flap.

Figure 12 - Continued.

FLAP DEFLECTION = 30.0 DEGREES

MACH NO. = 0.13

REYNOLDS NO. = 2.2 E 06

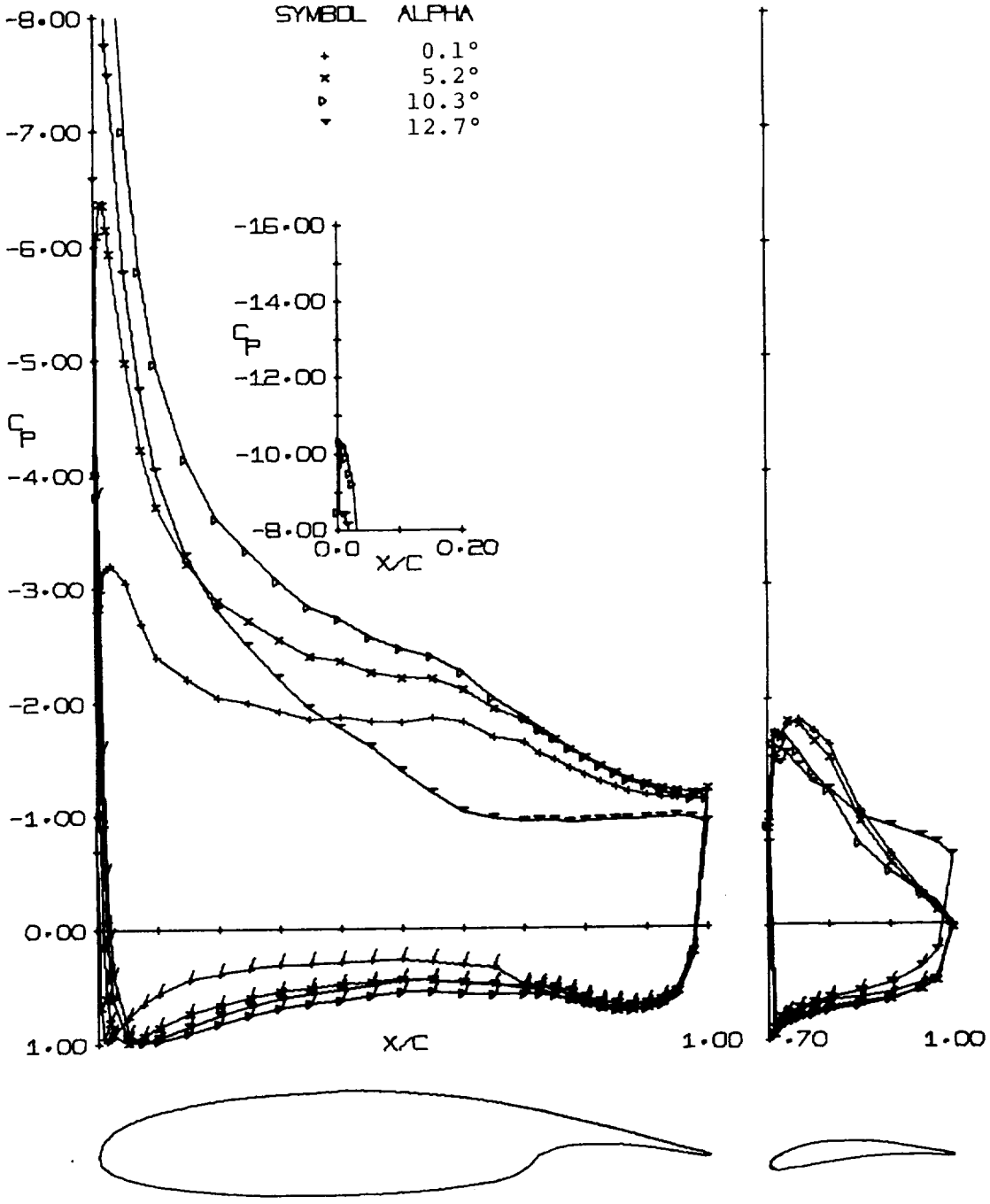

(c) 30° Flap.

Figure 12 - Continued.

FLAP DEFLECTION = 40.0 DEGREES

MACH NO. = 0.13

REYNOLDS NO. = 2.2 E 06

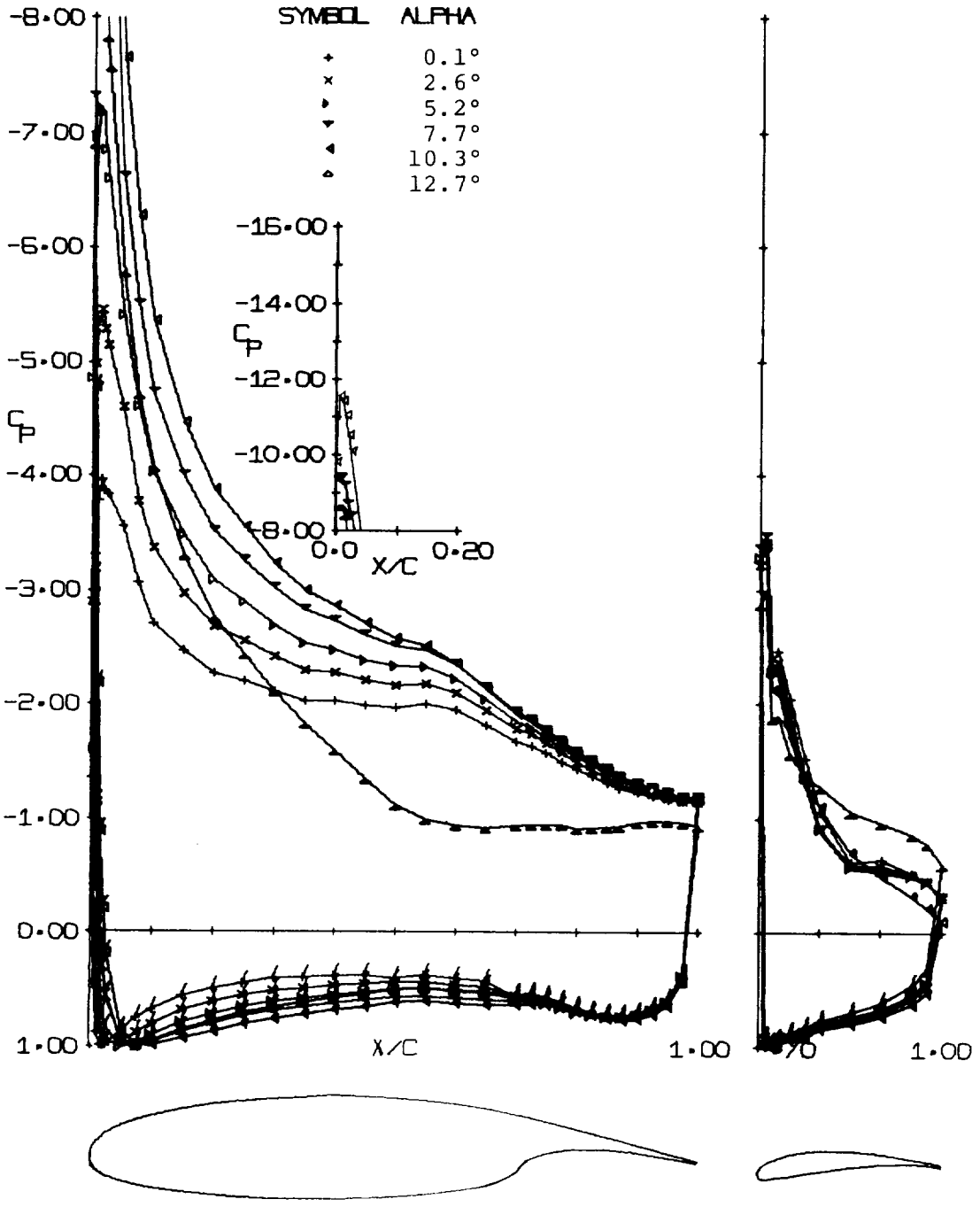

(d) 40° Flap.

Figure 12 - Concluded.

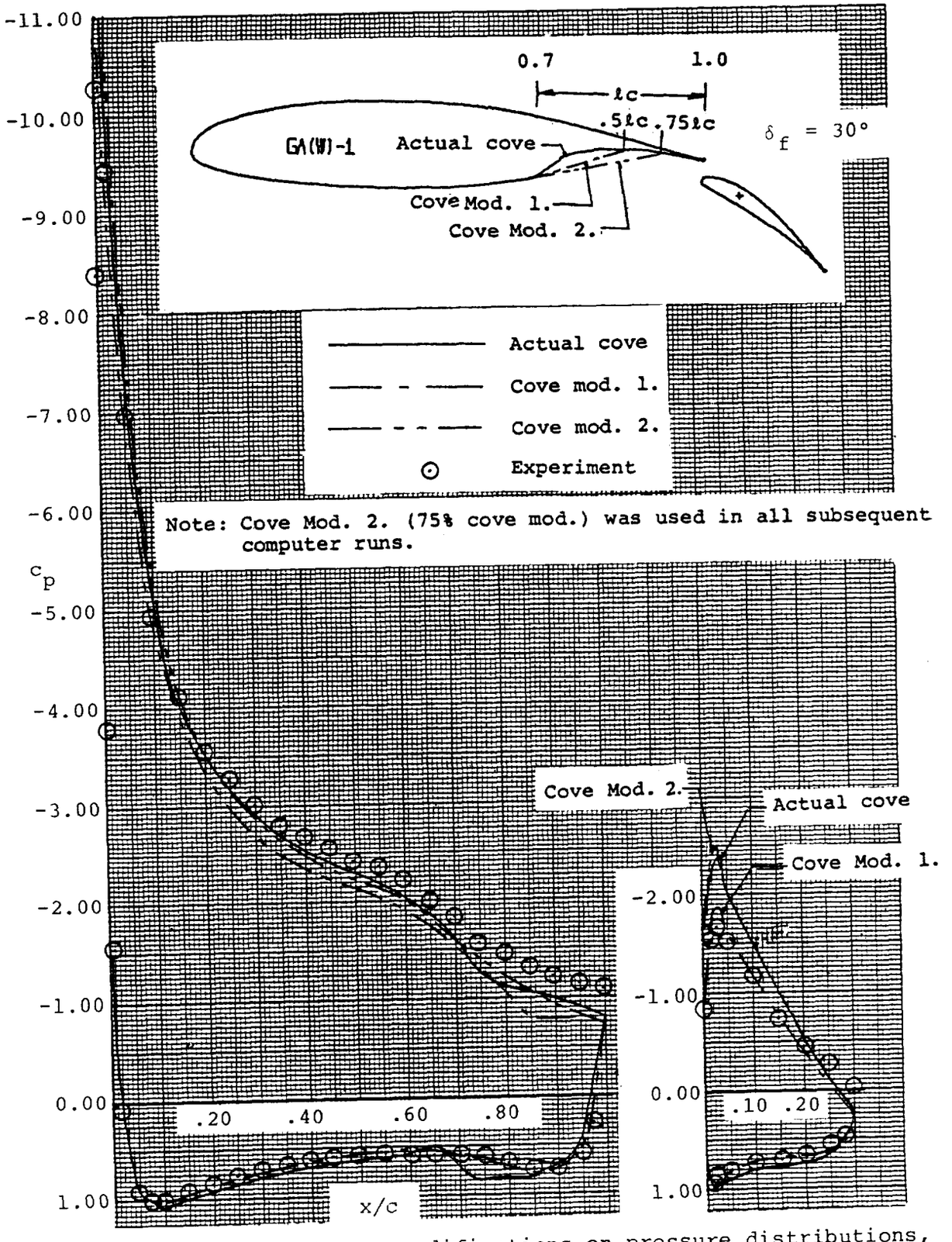

Figure 13 - Effects of cove modifications on pressure distributions, 30° flap, 10.3° angle of attack.

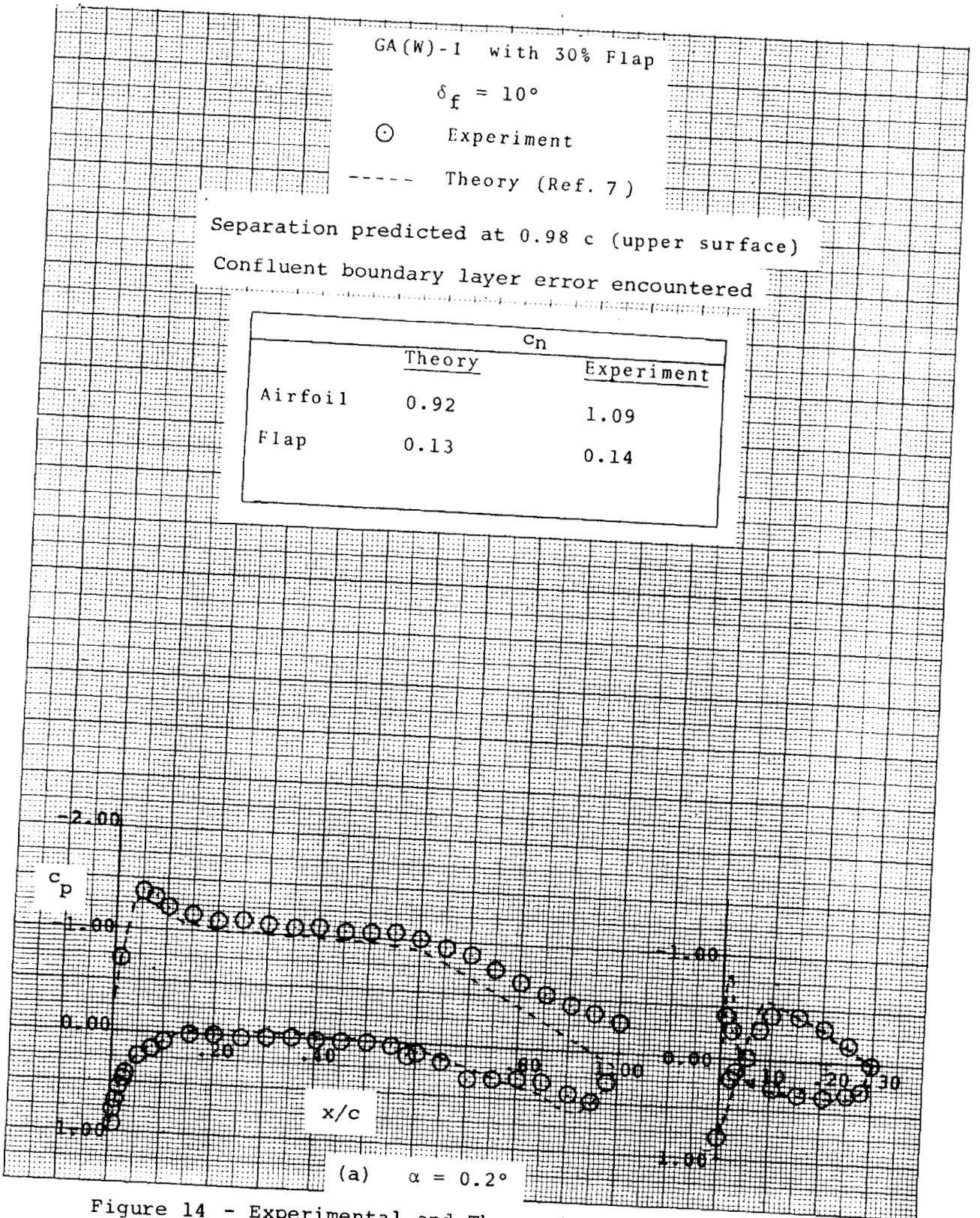

Figure 14 - Experimental and Theoretical Pressures, 10° Flap

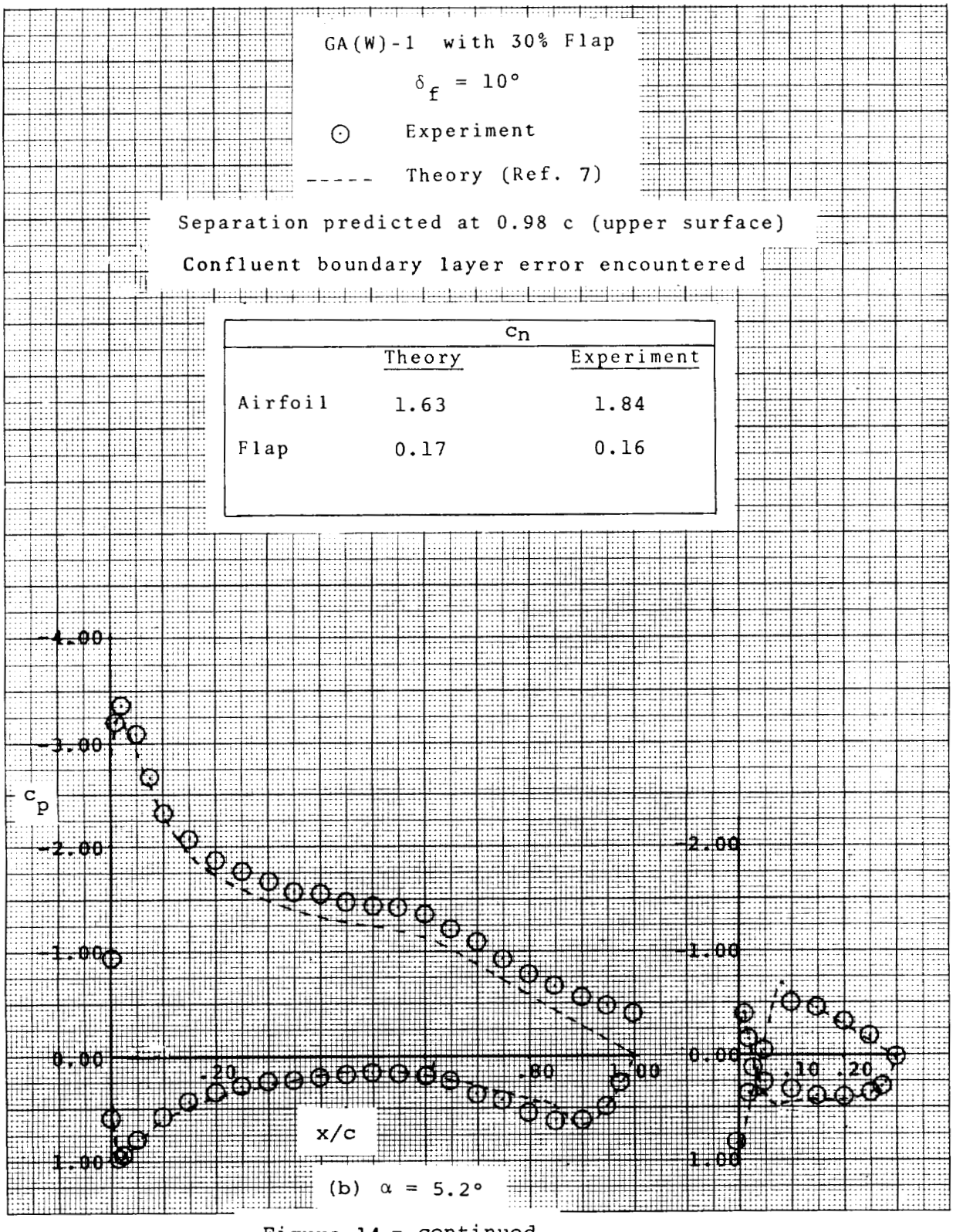

Figure 14 - continued

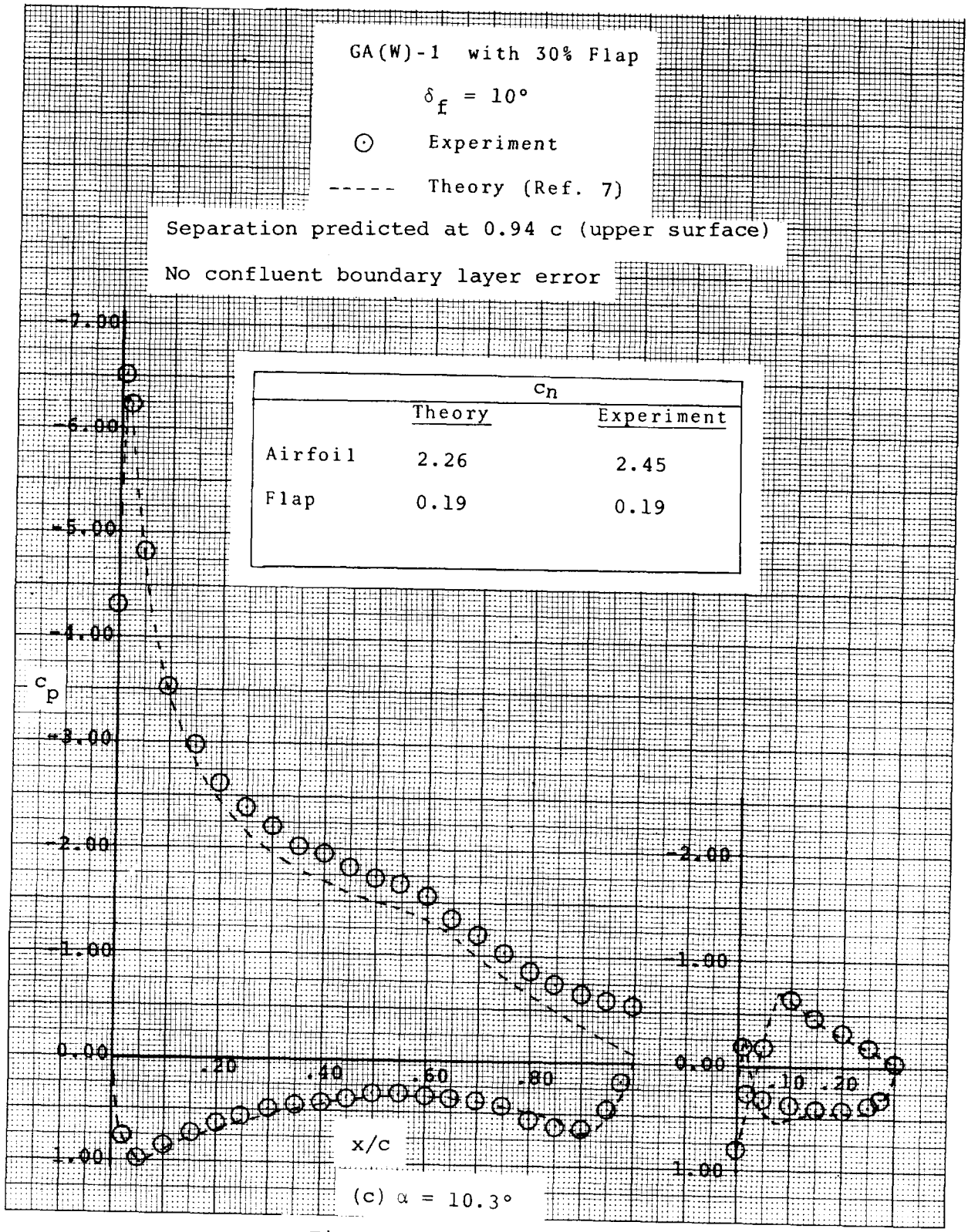

(c) α = 10.3°

Figure 14 - continued

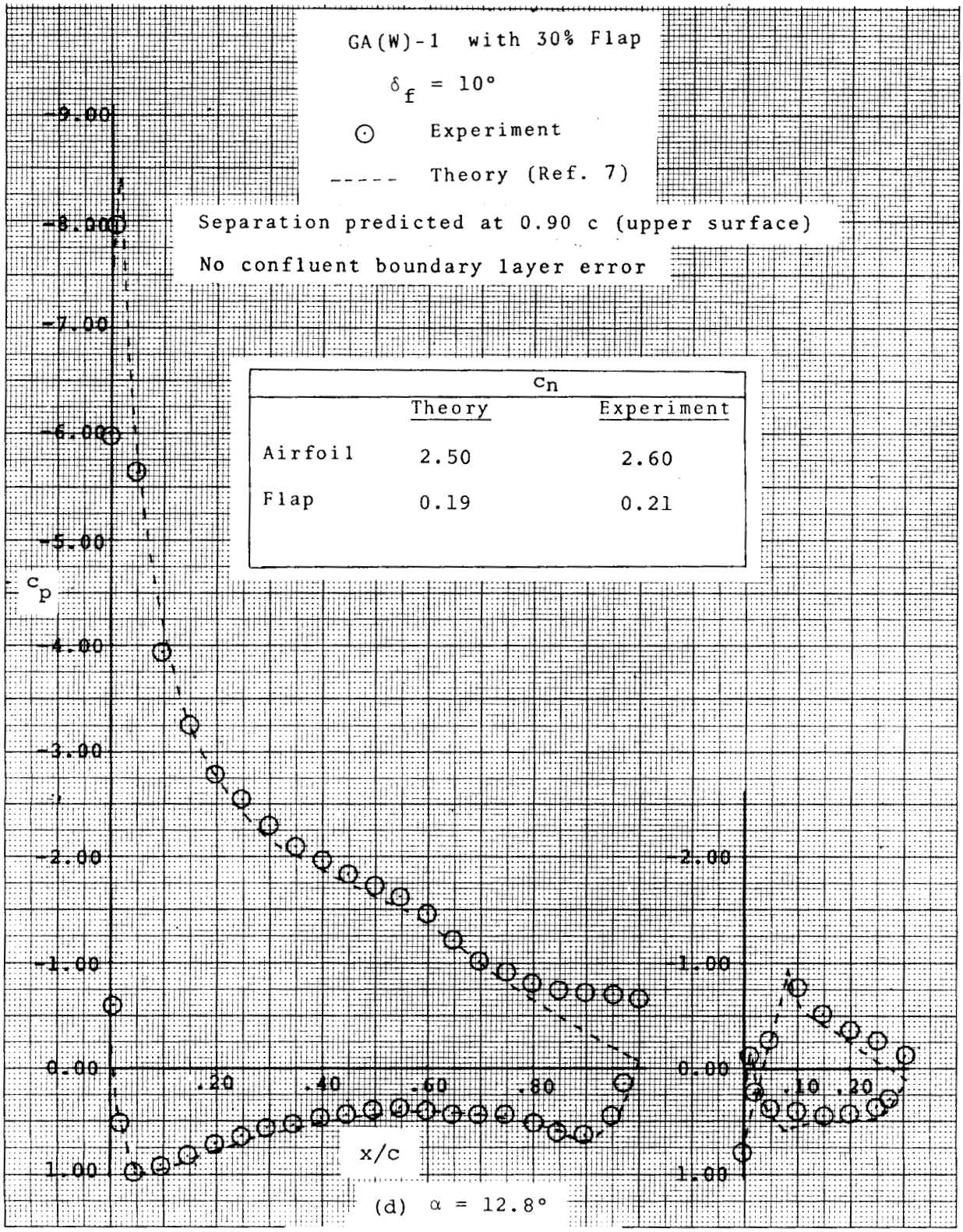

Figure 14 - concluded

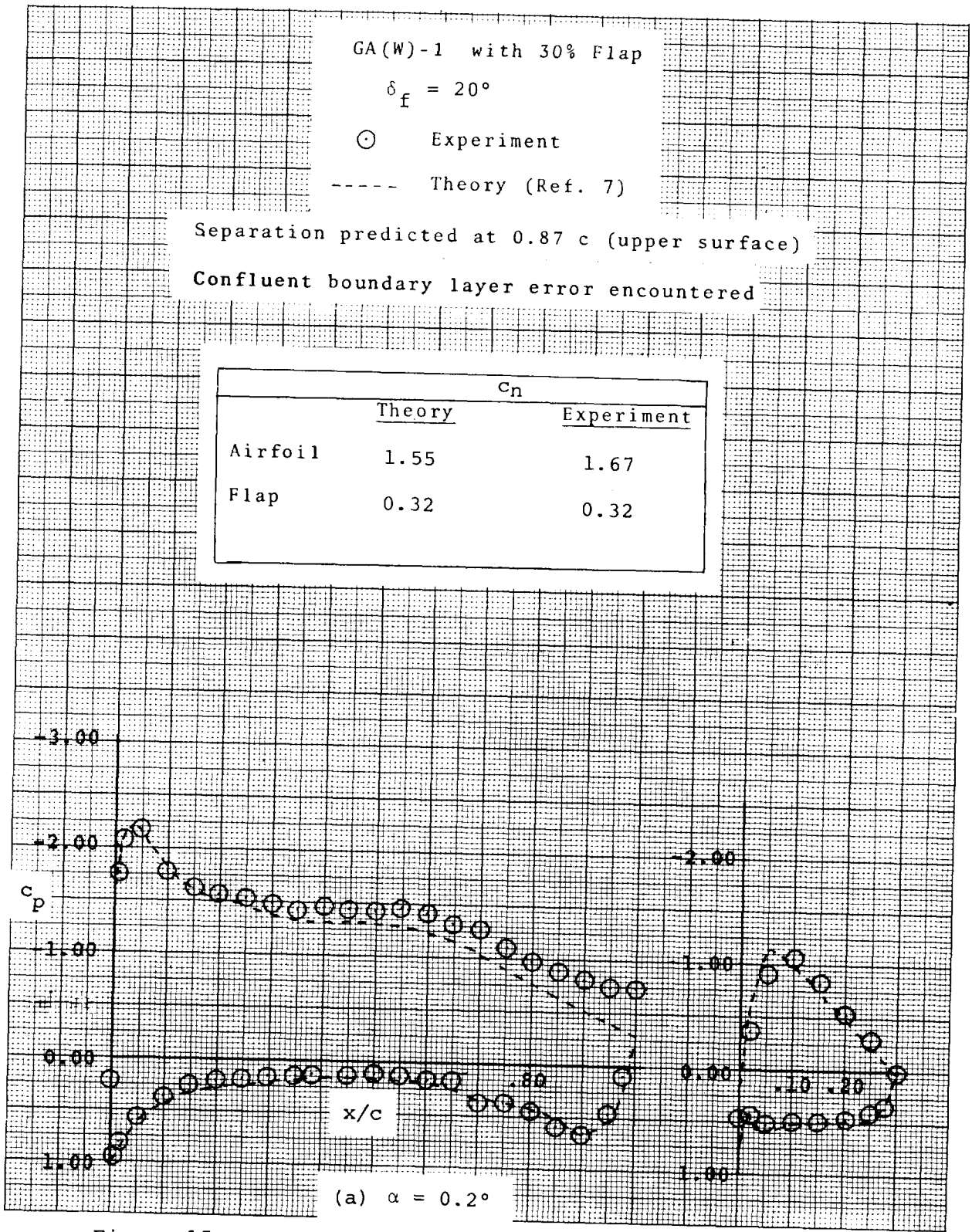

Figure 15 - Experimental and Theoretical Pressures, 20° Flap

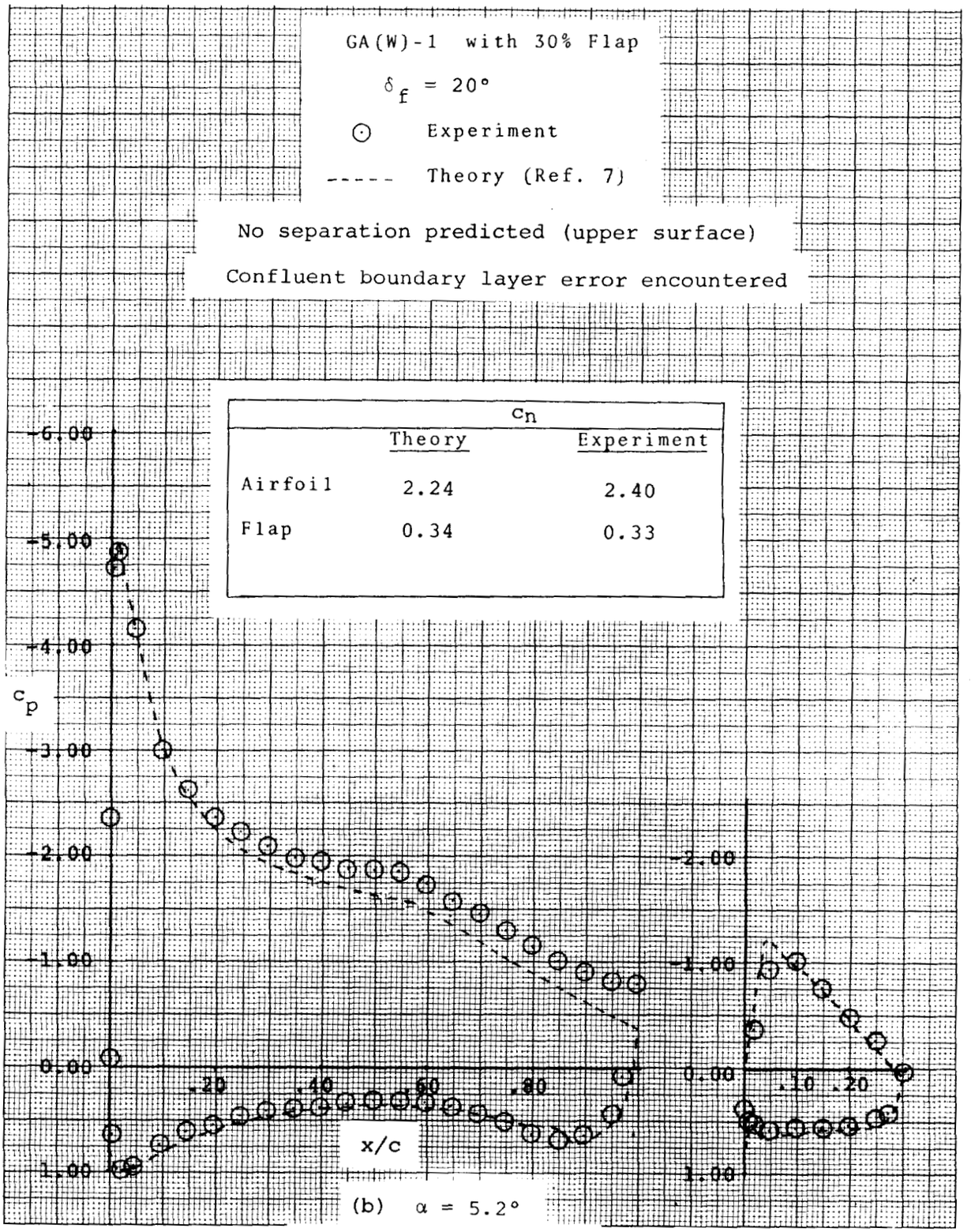

Figure 15 - continued

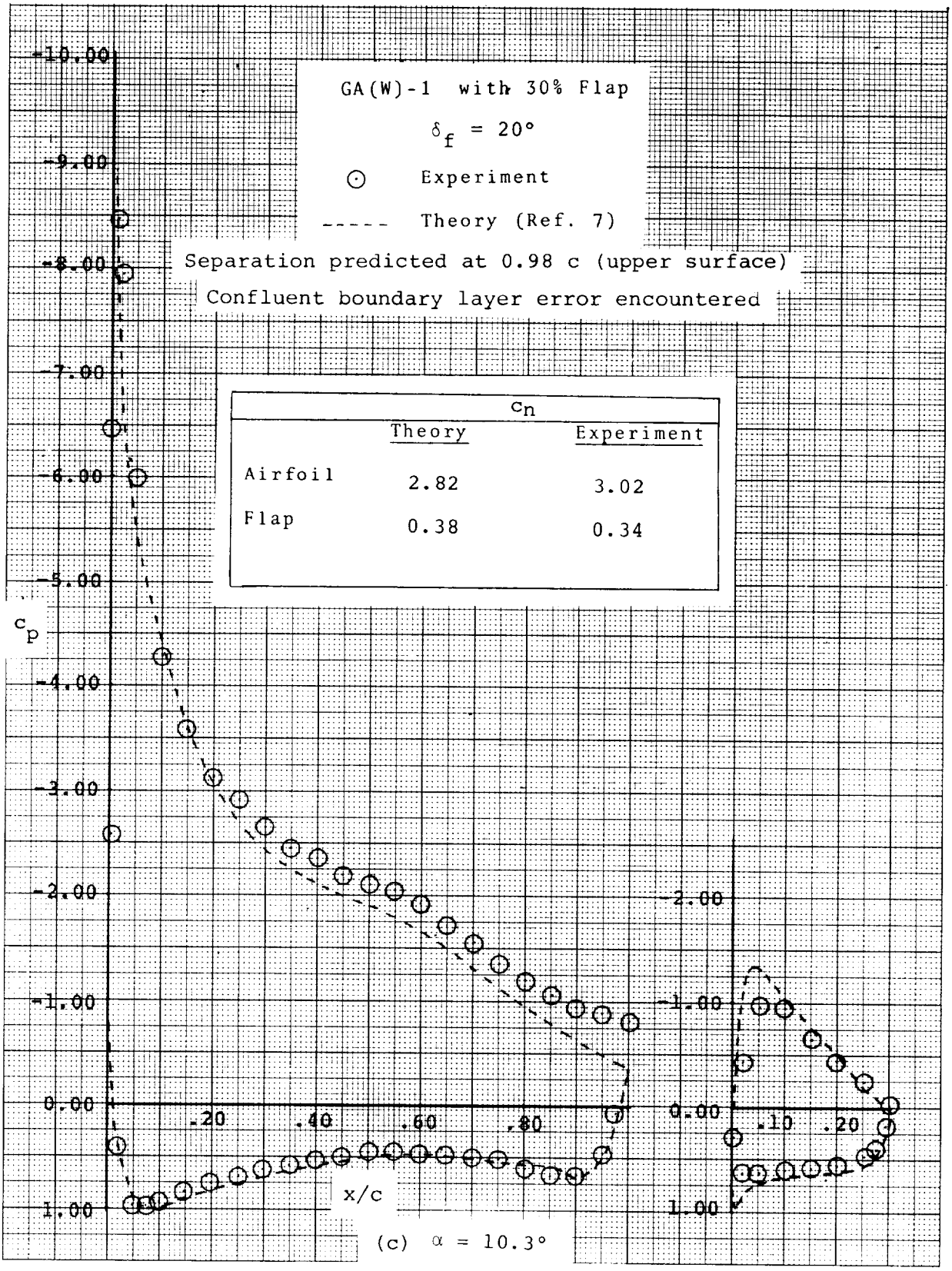

(c) α = 10.3°

Figure 15 - continued

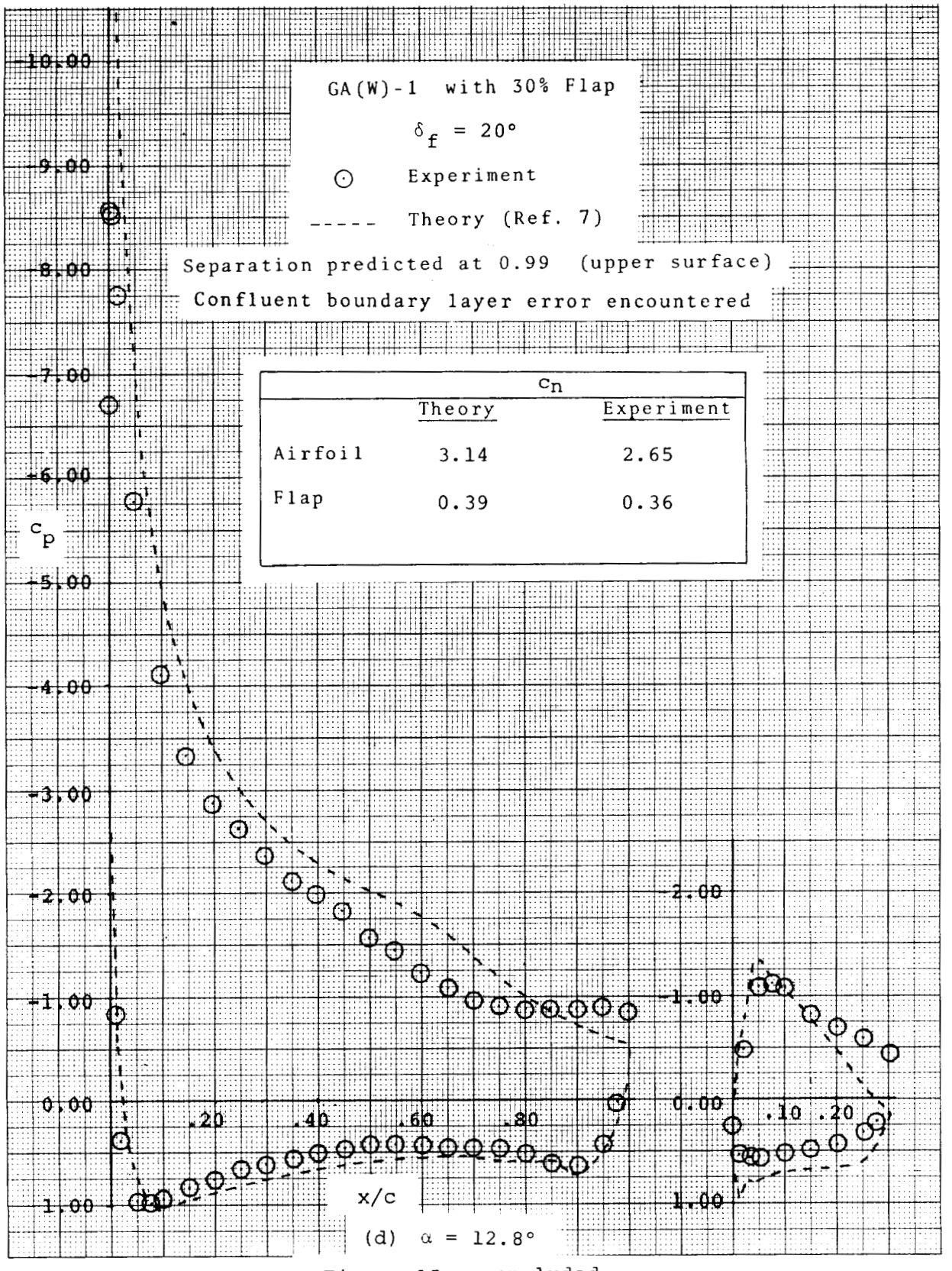

Figure 15 - concluded

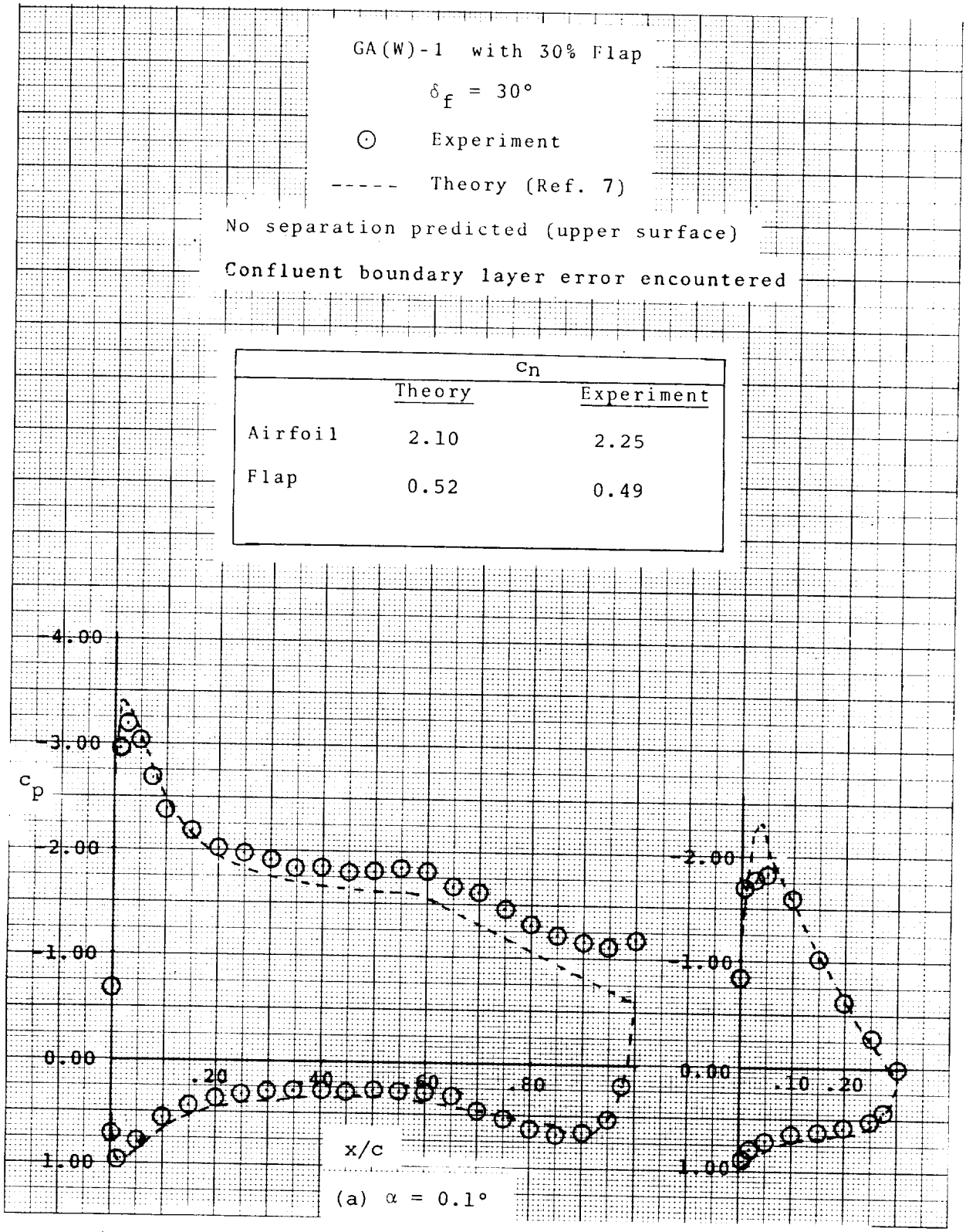

Figure 16 - Experimental and Theoretical Pressures, 30° Flap

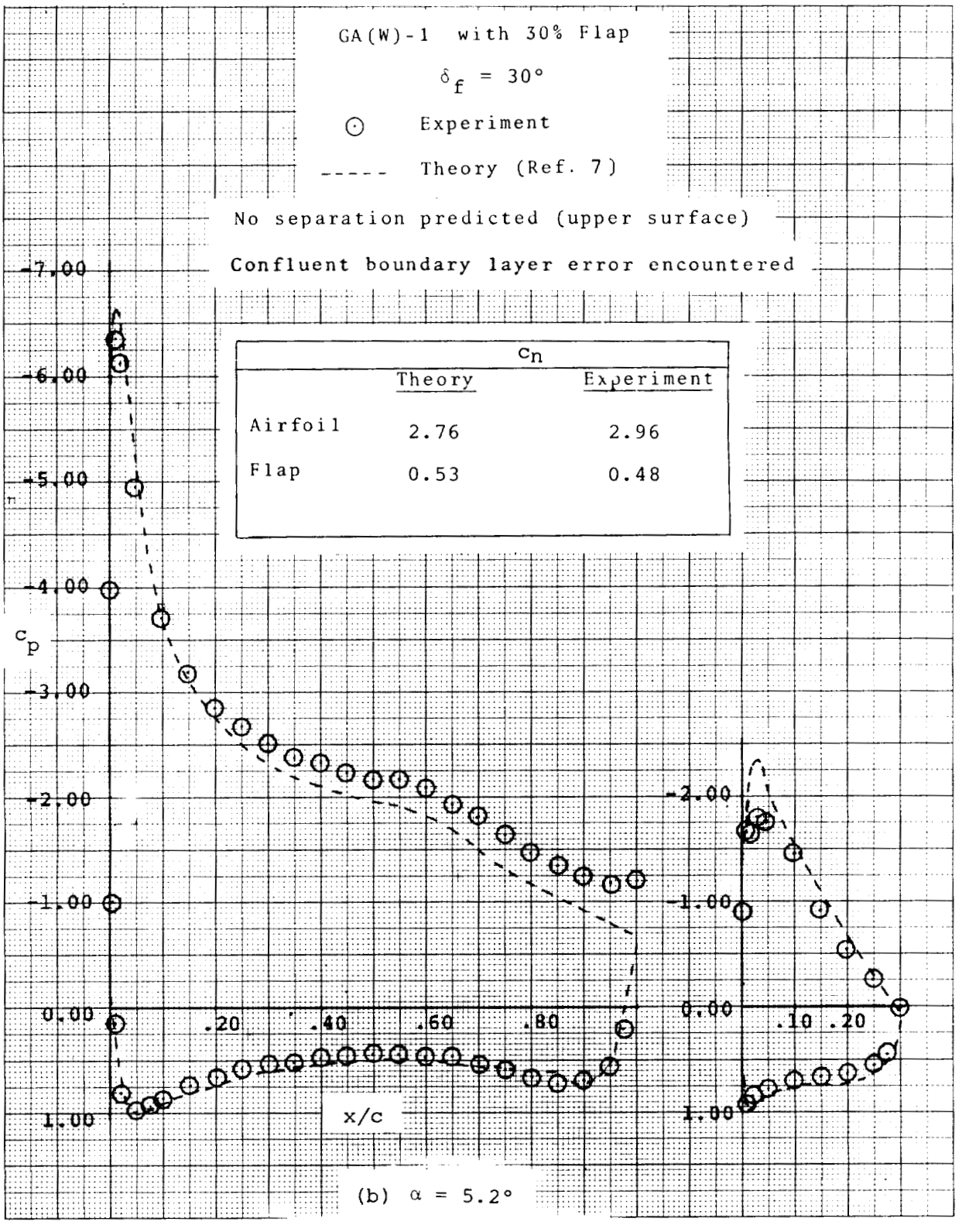

(b) α = 5.2°

Figure 16 - continued

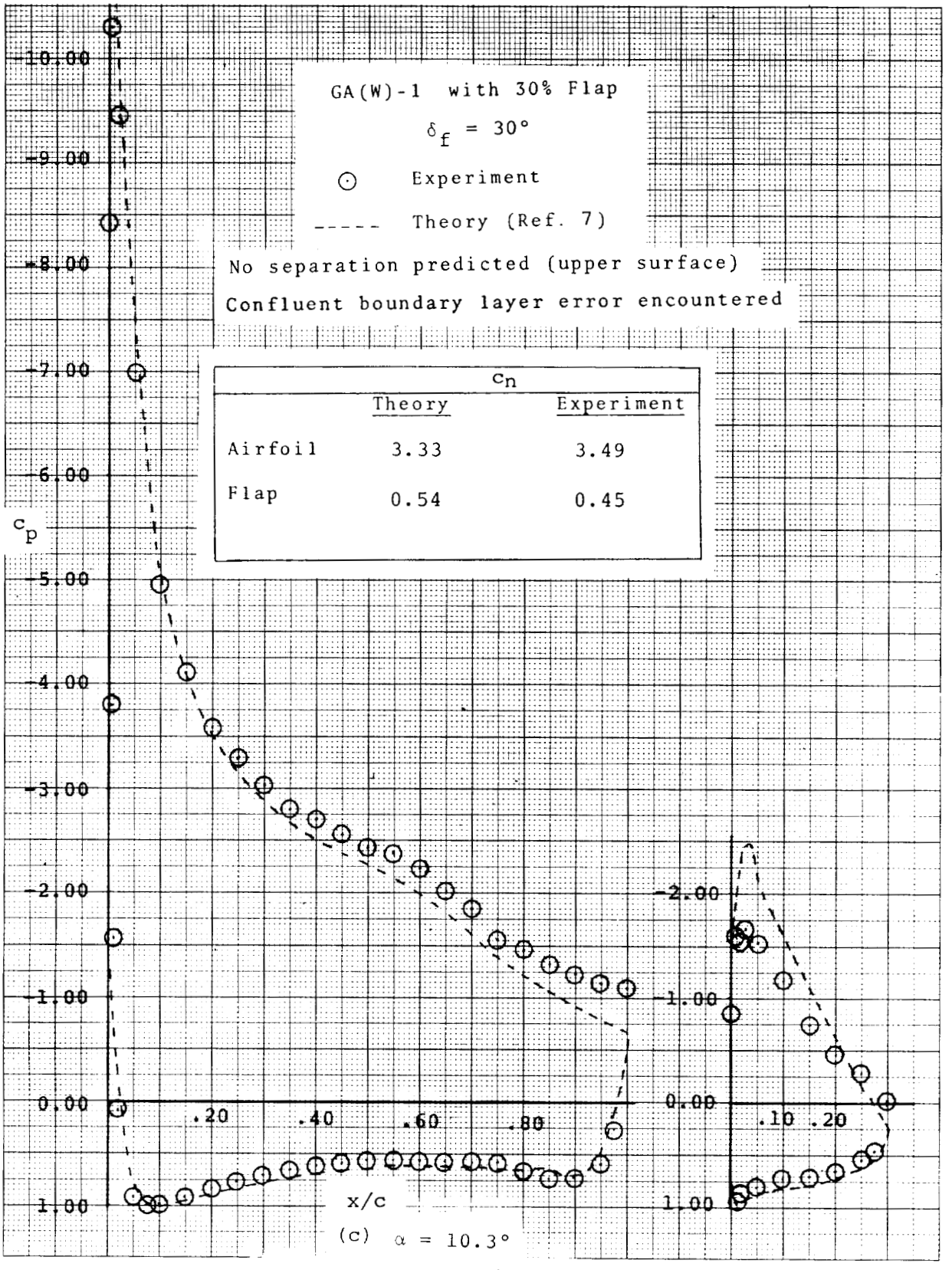

Figure 16 - continued

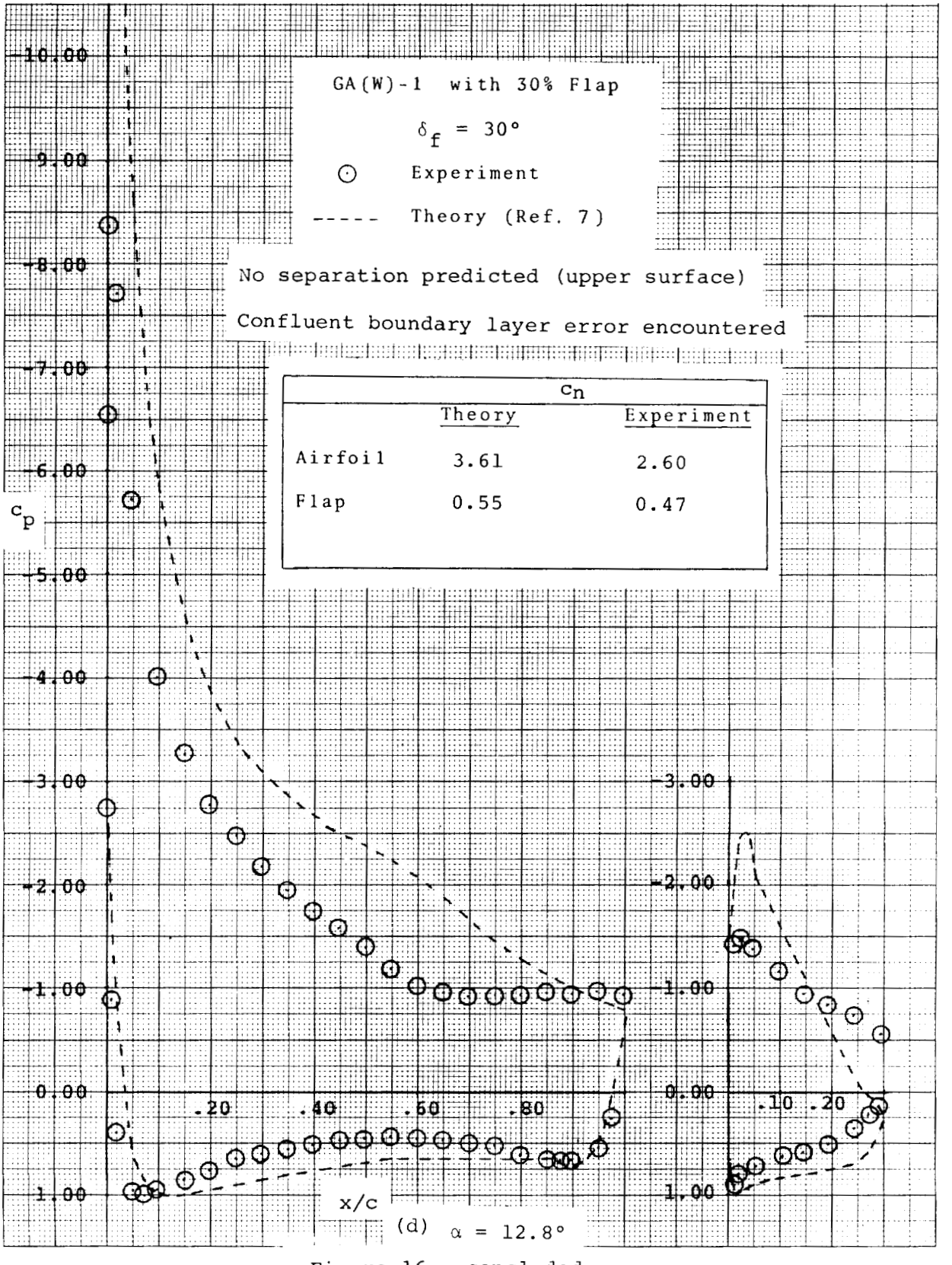

Figure 16 - concluded

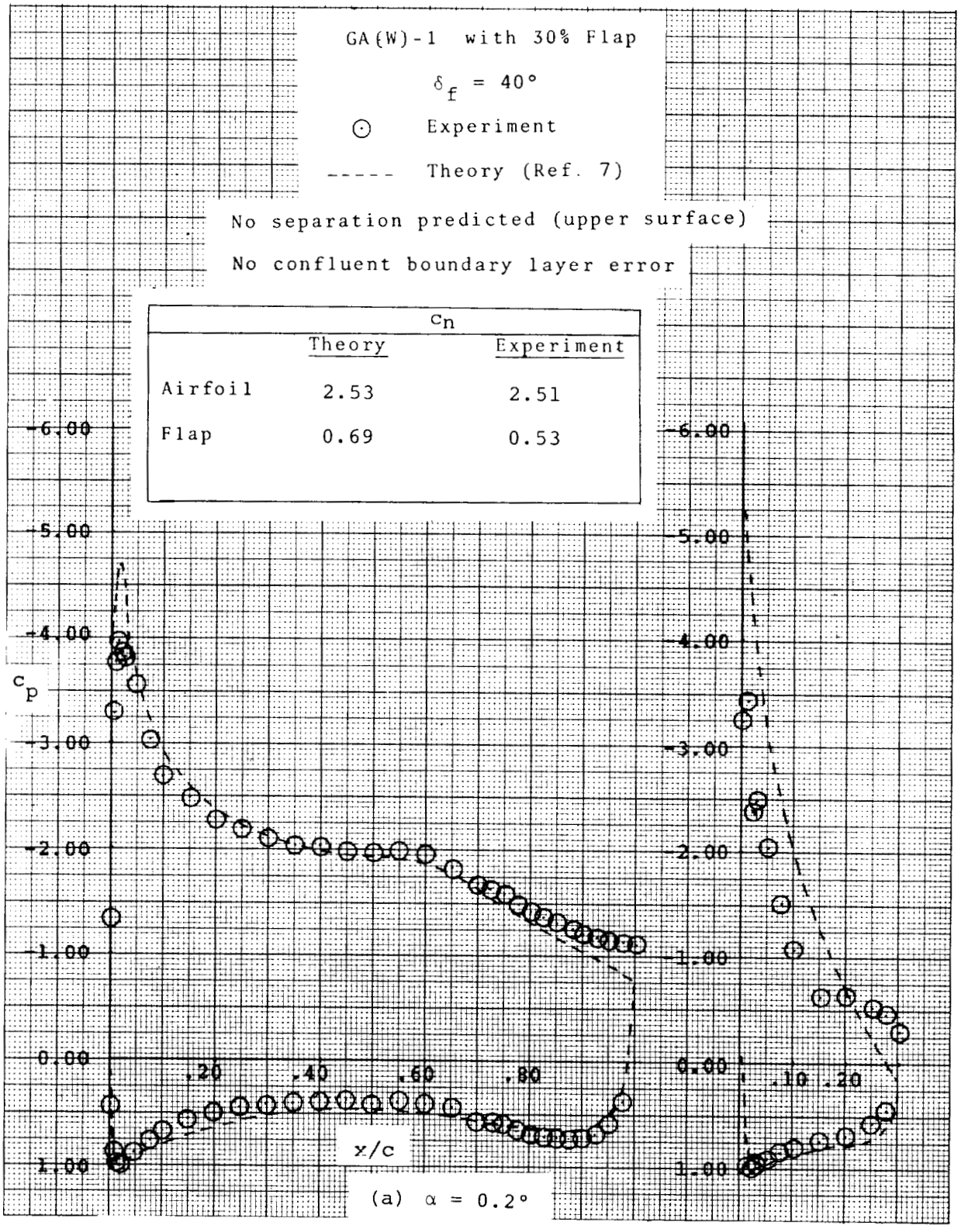

Figure 17 - Experimental and Theoretical Pressures,40° Flap

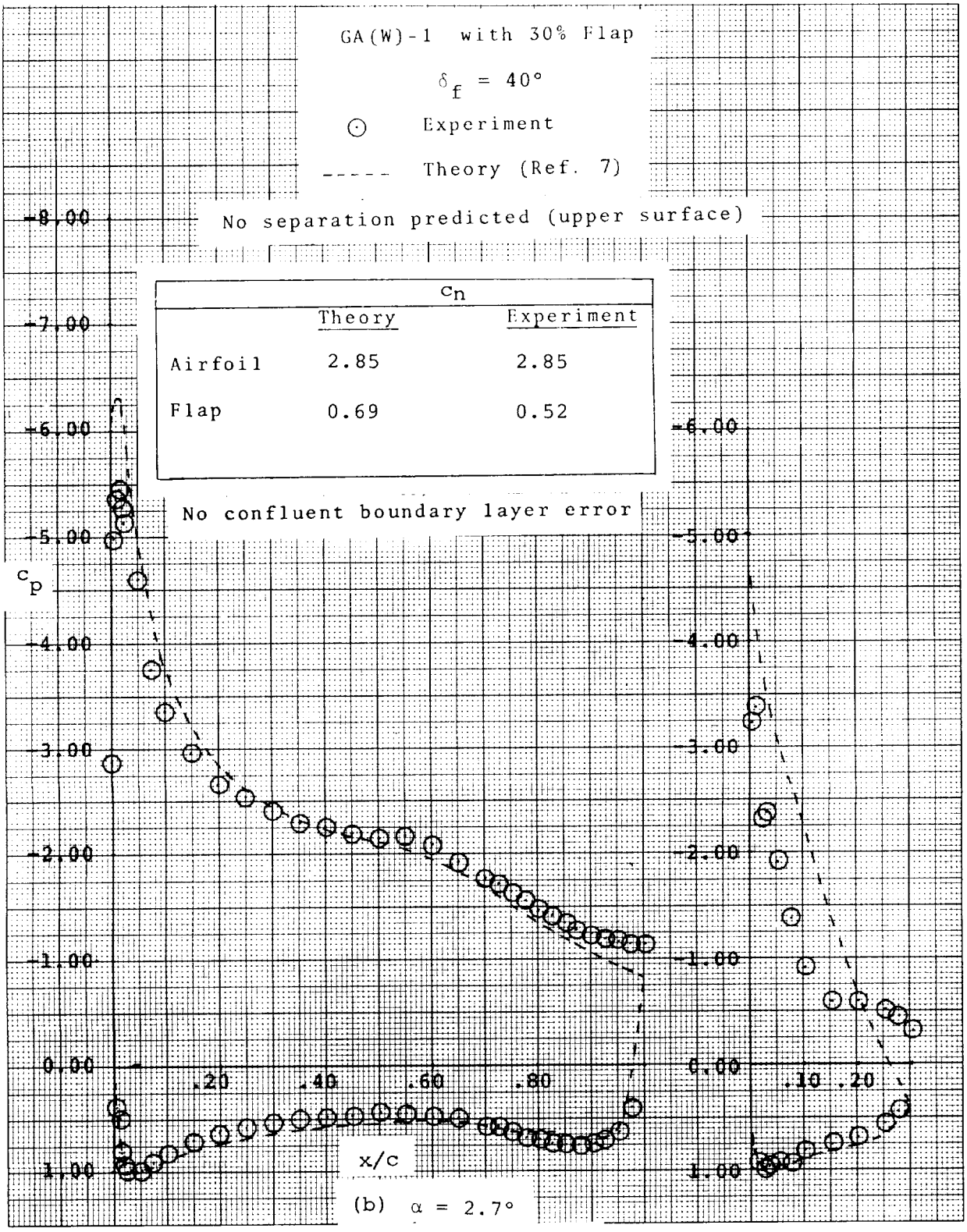

(b) α = 2.7°

Figure 17 - continued

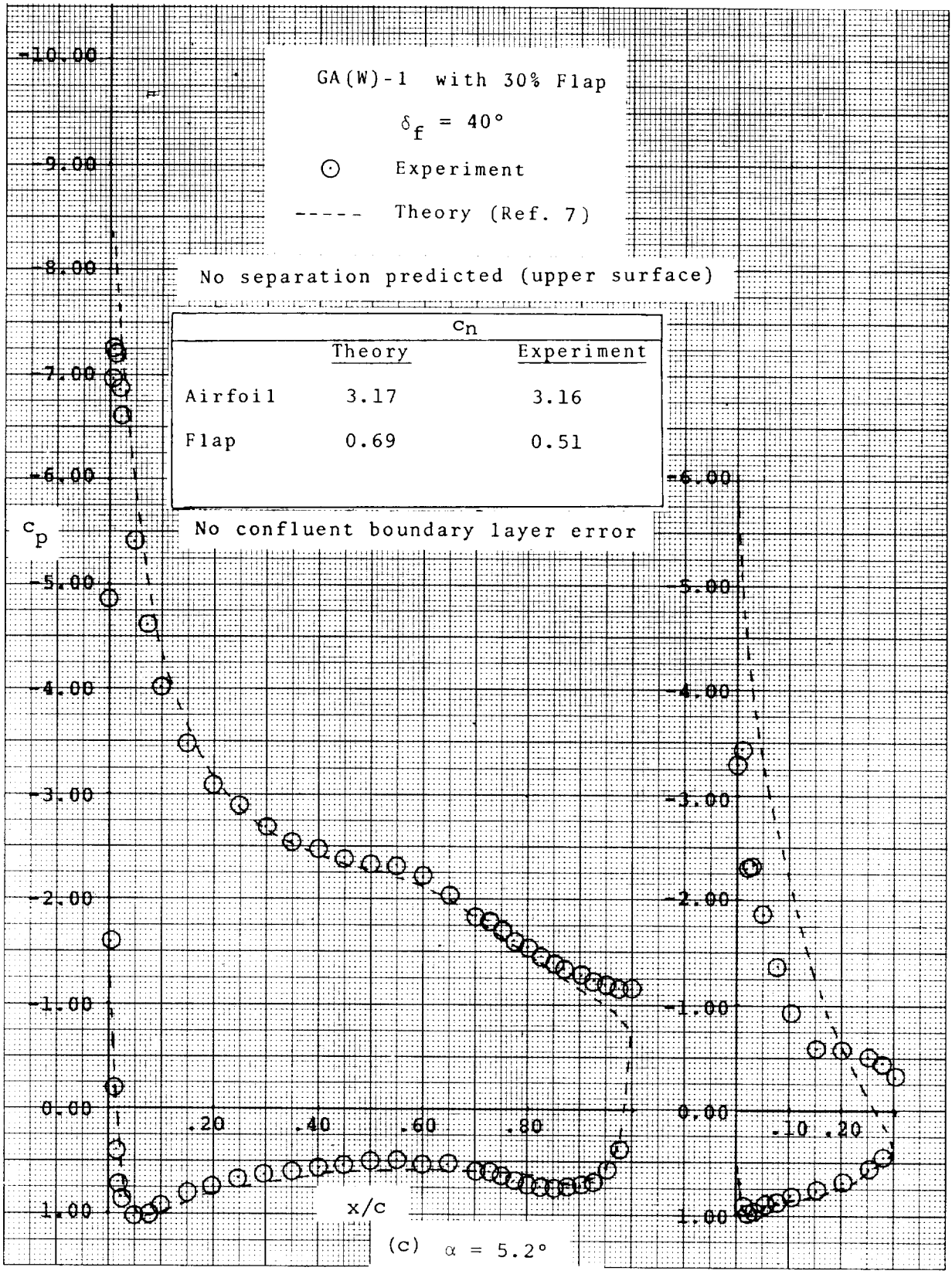

Figure 17 - continued

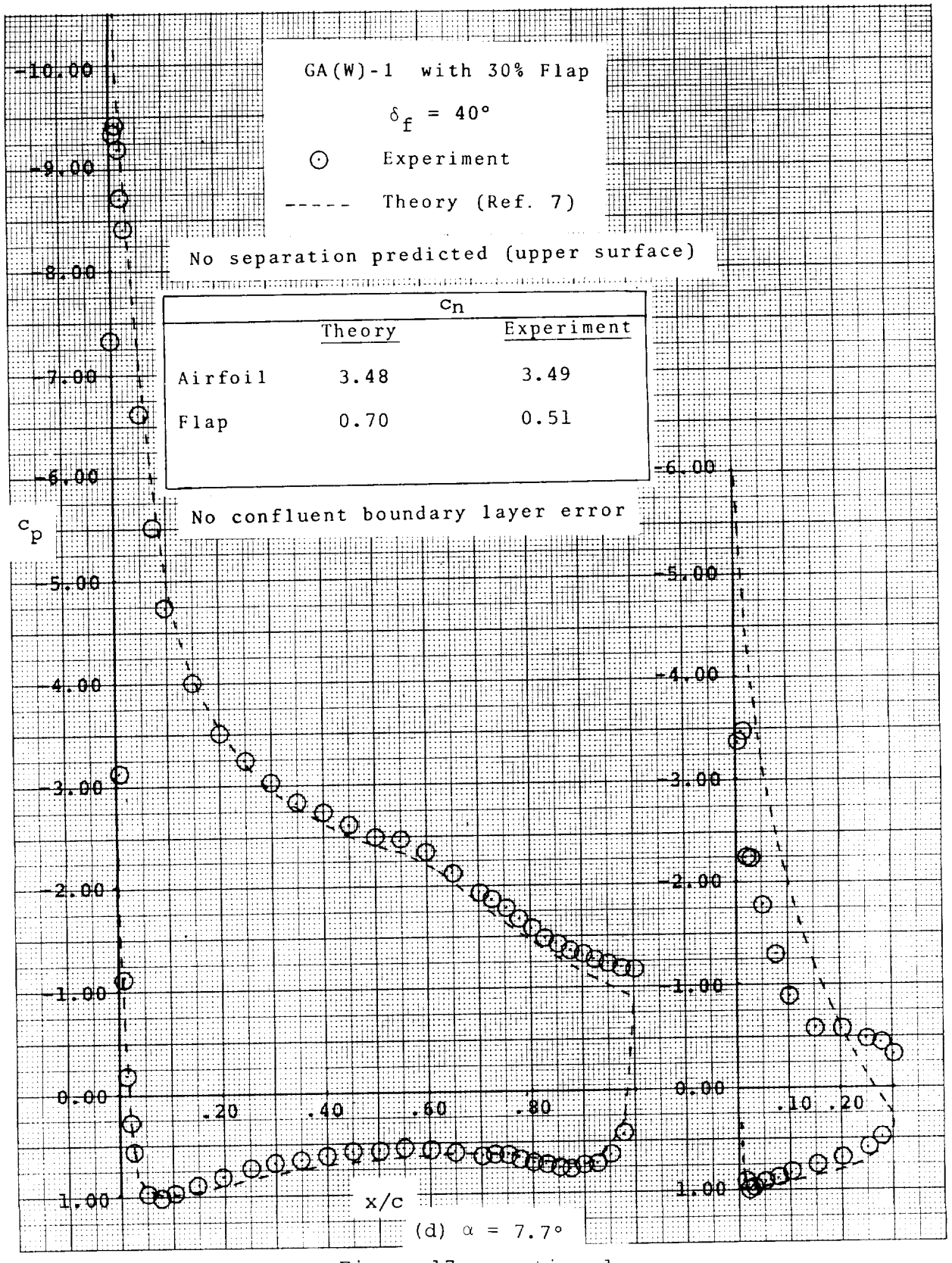

(d) α = 7.7°

Figure 17 - continued

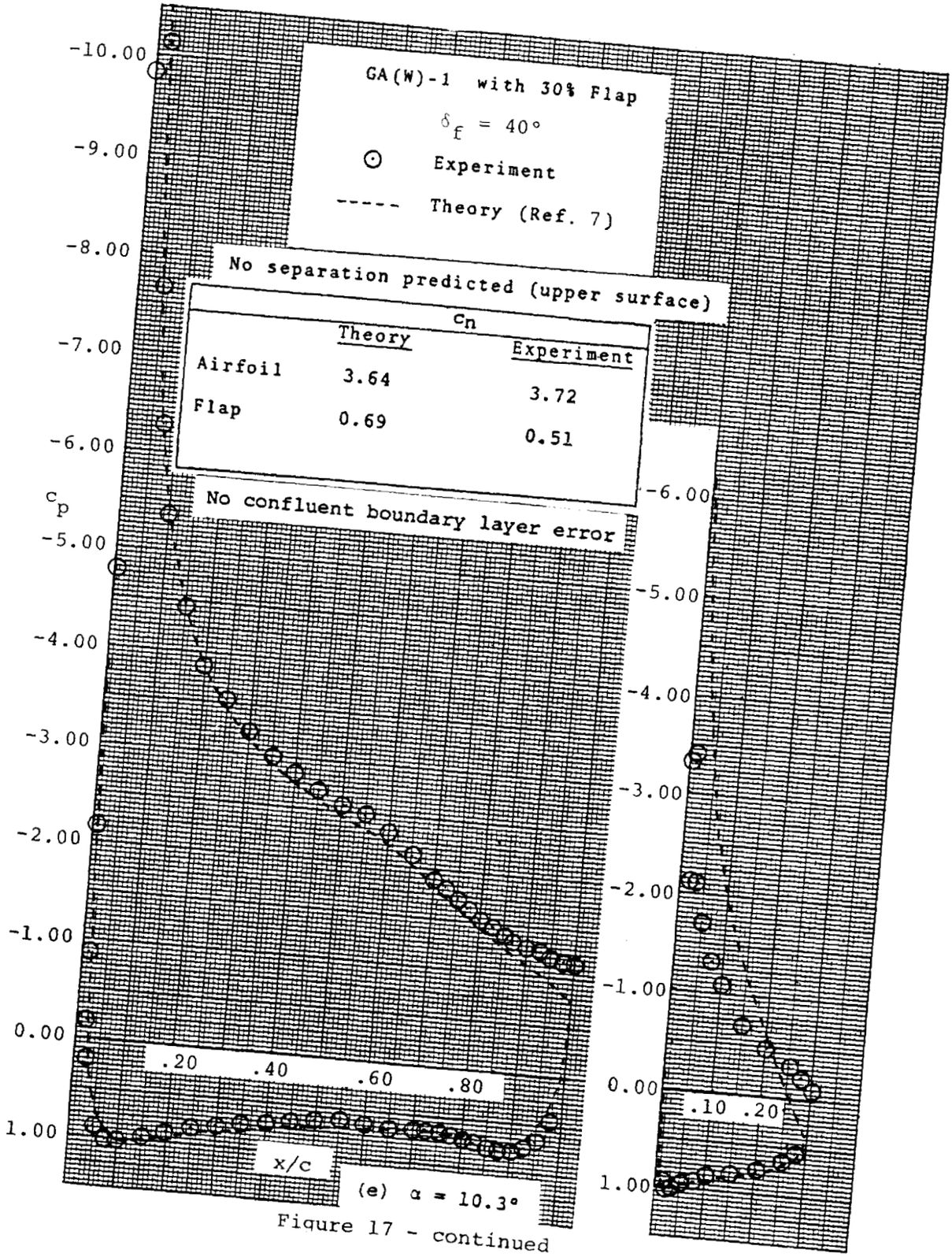

(e) $\alpha = 10.3°$

Figure 17 - continued

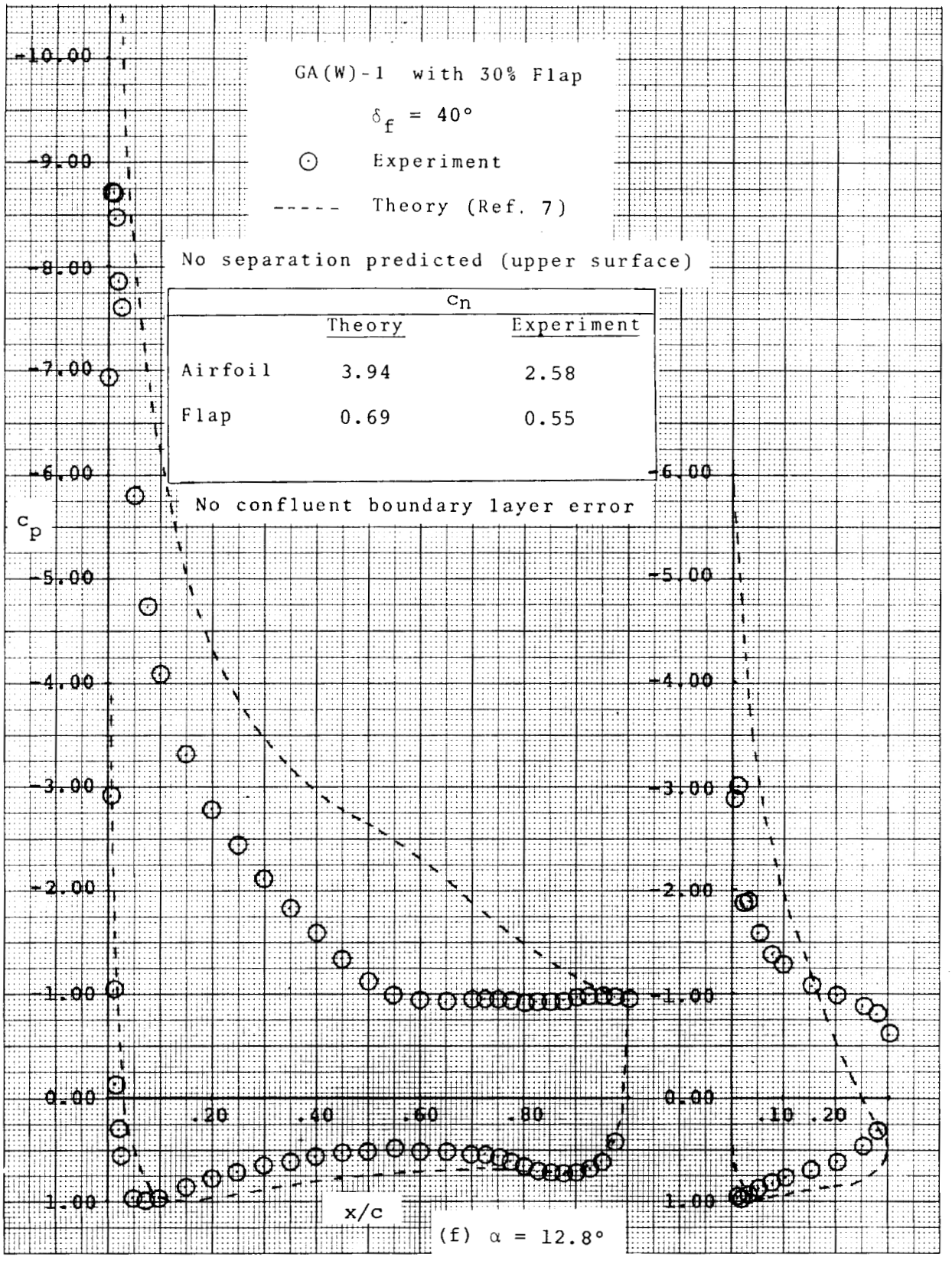

Figure 17 - concluded